REPORT DOCUMENTATION PAGE		READ INSTRUCTIONS BEFORE COMPLETING FORM
1. REPORT NUMBER 14150.7-P	2. GOVT ACCESSION NO. AD-A087480	3. RECIPIENT'S CATALOG NUMBER
4. TITLE (and Subtitle) MICROWAVE INVESTIGATIONS OF MATTER .		5. TYPE OF REPORT & PERIOD COVERED Final Report: 15 Oct 76 — 30 Nov 79
		6. PERFORMING ORG. REPORT NUMBER
7. AUTHOR(s) Frank C. De Lucia		8. CONTRACT OR GRANT NUMBER(s) DAAG29-77-G-0007
9. PERFORMING ORGANIZATION NAME AND ADDRESS Duke University Durham, NC 27706		10. PROGRAM ELEMENT, PROJECT, TASK AREA & WORK UNIT NUMBERS
11. CONTROLLING OFFICE NAME AND ADDRESS U. S. Army Research Office Post Office Box 12211 Research Triangle Park, NC 27709		12. REPORT DATE Jun 80
		13. NUMBER OF PAGES
14. MONITORING AGENCY NAME & ADDRESS(if different from Controlling Office)		15. SECURITY CLASS. (of this report) Unclassified
		15a. DECLASSIFICATION/DOWNGRADING SCHEDULE

16. DISTRIBUTION STATEMENT (of this Report)

Approved for public release; distribution unlimited. .

17. DISTRIBUTION STATEMENT (of the abstract entered in Block 20, if different from Report)

NA

18. SUPPLEMENTARY NOTES

19. KEY WORDS (Continue on reverse side if necessary and identify by block number)

microwaves	submillimeter waves
spectroscopy	silicon oxides
masers	molecular lasers
millimeter waves	

20. ABSTRACT (Continue on reverse side if necessary and identify by block number)

The project "Microwave Investigations of Matter" represented a broad attack on a wide variety of scientific topics and technological developments in the millimeter and submillimeter spectral region. Attached are the journal publications and a brief summary of our work. In addition to the cited journal publications, approximately an equal number of invited and contributed papers have been presented at scientific meetings. Because the material in these talks is highly correlated with journal articles, they will not be listed separately.

DD FORM 1473 1 JAN 73   EDITION OF 1 NOV 65 IS OBSOLETE

UNCLASSIFIED 118245

MICROWAVE INVESTIGATIONS OF MATTER

Frank C. De Lucia

Oct. 15, 1976 to Oct. 15, 1979

Department of Physics

Duke University

SUMMARY OF WORK UNDER ARO GRANT DAAG 29 77 G 0007

15 October 1976 through 15 October 1979

The project, "Microwave Investigations of Matter", 14150-P, represented a broad attack on a wide variety of scientific topics and technological developments in the millimeter and submillimeter spectral region.

Attached are the journal publications and a brief summary of our work. In addition to the cited journal publications, approximately an equal number of invited and contributed papers have been presented at scientific meetings. Because the material in these talks is highly correlated with the journal articles, they will not be listed separately.

Summary of Results

(keyed according to list of publications)

1. This paper represents the first operation of a molecular beam maser in the submillimeter spectral region. The extremely high resolution of this device makes it an especially powerful spectroscopic tool and presents the possibility of the construction of a primary frequency standard in the submillimeter.

2. This paper reports the first pressure broadening study on H_2S. Because of a paucity (none) of transitions at conventional microwave frequencies, this important species had not been previously studied. More importantly our theoretical calculations (Anderson theory) show that the theory was in fact generally valid (to $\sim 10\%$) and that previous inconsistencies ($\sim 100\%$) were due to inaccurate infrared data rather than theoretical shortcomings.

3. This paper reports the first observation of symmetric top forbidden transitions in the NMMW spectral region. The results lead to a substantially improved knowledge of the energy level structure of PH_3

4. This paper demonstrates the power of millimeter and submillimeter spectroscopy as a diagnostic probe of molecular lasers. Several conventional

wisdoms about the HCN laser were shown to be untrue. This project and its spin offs will become a major part of our effort in the next contract period.

5. This is a short note that relates centrifugal distortions to changes in molecular constants and is a spin off of paper 1.

6. This paper reports the results of a high temperature ($\sim 1500^{\circ}$C) study of SiO and represents the first laboratory observation of one of the interstellar masers.

7. This is an invited review of the applications and techniques of millimeter and submillimeter spectroscopy.

8. Molecular laser plasmas are rich sources of excited vibrational states. This paper reports the use of the HCN laser plasma as a source for these excited state studies. An interesting symbiosis between this project and that reported in 4) exists. So little is known about the excited states of molecules in the millimeter and submillimeter that one ordinarily must do the spectroscopic project first so that you know what you are diagnosing.

9. This paper represents an extension of the work reported in 3 to AsH_3.

10. Because of its extreme centrifugal distortion, water is the most difficult $^1\Sigma$ molecule to model. This paper reports a combined analysis of our millimeter and submillimeter microwave data, new FIR Fourier transform data, and energy levels derived from IR combination differences to upgrade the energy levels of AFGL spectral table.

11. This paper reports the results of an extensive project to model the HNO_3 spectrum from 0-300 GHz. The primary result is a model that predicts $\sim$ 5000 transitions in this region $\leqslant$ 1 MHz. I understand that this work is of some interest to BMD for their modeling of the "disturbed" atmosphere.

12. This work has been the subject of two papers delivered at the Columbus Meeting and is being finalized for inclusion in a thesis and journal publication. Again, I understand that this work (especially HO_2) relates to BMD interests.

13. This is a spectroscopic project on the millimeter and submillimeter spectrum of the extremely reactive and unstable mixed diatomic halides.

14. This is a paper that reports an interesting and potentially very valuable approach to the theoretical modeling of the absorptions of hot water vapor.

15. and 16. These papers represent the last papers from Professor Gordy's biophysics program.

With the exception of 12. (which has shared support with NASA) the work reported here was supported by no other federal agency than ARO.

Publication List

1. "Extension of High-resolution Beam Maser Spectroscopy into the Submillimeter Wave Region," Michael Garvey and Frank C. De Lucia, Canadian J. Phys. $\underline{55}$, 1115 (1977).

2. "Pressure Broadening of Hydrogen Sulfide," Paul Helminger and Frank C. De Lucia, J. Quant. Spectrosc. Radiat. Transfer $\underline{17}$, 751 (1977).

3. "'Forbidden' Rotational Spectra of Symmetric-top Molecules: PH_3 and PD_3," David A. Helms and Walter Gordy, J. Mol. Spectrosc. $\underline{66}$, 206 (1977).

4. "The Study of Laser Processes by Millimeter and Submillimeter Microwave Spectroscopy," Applied Physics Letter $\underline{31}$, 606 (1977).

5. "Centrifugal Distortion in Water and Hydrogen Sulfide," R. Michael Garvey, J. Mol. Spectrosc. $\underline{65}$, 330 (1977).

6. "Millimeter Spectrum and Molecular Constants of Silicon Monoxide," E. Lowry Manson, Jr., William W. Clark, Frank C. De Lucia, and Walter Gordy, Phys. Rev. A $\underline{15}$, 223 (1977).

7. "Millimeter and Submillimeter-wave Spectroscopy," Frank C. De Lucia in <u>Molecular Spectroscopy: Modern Research</u>, Vol. II, Academic Press (1976).

8. "Millimeterwave Spectroscopy of Active Laser Plasmas: The Excited Vibrational States of HCN," Paul A. Helminger and Frank C. De Lucia, J. Chem. Phys. $\underline{67}$, 4262 (1977).

9. "'Forbidden' Millimeter-wave Transitions in Arsine," David Helms and Walter Gordy, J. Mol. Spectrosc. $\underline{69}$, 473 (1978).

10. "Centrifugal Distortion Analysis of the Ground Vibrational States of $H_2^{17}O$ and $H_2^{18}O$," Paul A. Helminger and Frank C. De Lucia, J. Mol. Spectrosc. $\underline{70}$, 263 (1978).

11. "Millimeter-wave Spectrum, Centrifugal Distortion Analysis, and Energy Levels of HNO_3," Gabriele Cazzoli and Frank C. De Lucia, J. Mol. Spectrosc. $\underline{76}$, 131 (1979).

12. "Millimeter-wave Studies of Unstable Molecular Species," Arthur Charo and Frank C. De Lucia (presented in part at the 1977 Ohio State Symposium).

13. "Millimeter Wave Measurements of the Rotational Spectra of ClF, BrF, BrCl, ICl, and IBr," Robert E. Willis and William W. Clark, J. Chem. Physics $\underline{72}$, 4946 (1980).

14. "A Modified Centrifugal Distortion Hamiltonian for Light Asymmetric Rotors," John Kolena and Frank C. De Lucia (presented at AAS San Francisco, January, 1980).

15. "Nuclear Coupling of ^{33}S and the Nature of Free Radicals in Irradiated Crystals of N-Acetyl-L-Cysteine," J. H. Hadley and W. Gordy, Proc. Natl. Acad. Sci. $\underline{74}$, 216 (1977).

16. "Electron Spin Resonance of ^{17}O-labeled Protein-Peroxide Radicals: Zein and Edestin," Louis J. Dimmey and Walter Gordy, Proc. Natl. Acad. Sci. USA $\underline{77}$, 343 (1980).

Participating Scientific Personnel

(1) Walter Gordy, James B. Duke Professor of Physics: Principal Investigator

(2) Frank C. De Lucia, Associate Professor of Physics: Co-principal Investigator

(3) John Kolena, Visiting Assistant Professor

(4) Paul A. Helminger, Senior Visiting Scientist

(5) R. Michael Garvey, Research Assistant, Ph. D. , Instructor/Research Associate

(6) William W. Clark, Research Assistant, Ph. D. , Instructor/Research Associate

(7) Gabriele Cazzoli , Nato Senior Postdoctoral Fellow

(8) David A. Helms, Research Assistant, Ph. D.

(9) Robert E. Willis, Research Assistant, Ph. D.

(10) Arthur Charo, Research Assistant

(11) William Matteson, Research Assistant

Extension of high resolution beam maser
spectroscopy into the submillimetre wave region

R. Michael Garvey and Frank C. De Lucia

Extension of high resolution beam maser spectroscopy into the submillimetre wave region[1]

R. Michael Garvey[2] and Frank C. De Lucia

Department of Physics, Duke University, Durham, NC 27706, U.S.A.

Received December 20, 1976

High resolution molecular beam maser spectroscopy has been extended into the submillimetre wave region of the spectrum. The maser spectrometer consists of a multiple beam source, stacked quadrupole state selector, and Fabry–Perot cavity. The submillimetre wave stimulating signal is produced by harmonic generation from a millimetre-wave klystron, directly referenced to WWVB. The maser signal is detected in a cryogenic photodetector. Linewidths 50–100 times narrower than the Doppler width and good signal-to-noise ratios were obtained. This system has been used to resolve the small deuterium hyperfine splittings of both the $1_{10} \rightarrow 1_{01}$ transition of D_2O at 317 GHz and the $J = 1 \rightarrow 0$ transition of ND_3 at 309 GHz. The relevance of the D_2O quadrupole interaction data to the electric field gradient in water is discussed. The spectroscopic constants in kilohertz for D_2O in the states 1_{10} and 1_{01} are, respectively, $(eQq_J)_D = 34.81 \pm 0.32$, $C_D = -2.661$, and $(eQq_J)_D = -29.60 \pm 0.55$, $C_D = -2.532$. The constants for ND_3 are, in kilohertz: $(eQq_J)_N = 816.2 \pm 1.1$, $C_N = 2.0 \pm 1.5$, $(eQq_J)_D = 19.9 \pm 0.8$, and $C_D = -2.2 \pm 0.8$.

La spectroscopie à haute résolution par maser et faisceau moléculaire a été étendue à la région des longueurs d'onde inframillimétriques. Le spectromètre maser est constitué par une source à multiples faisceaux, un sélecteur d'états quadrupolaire et une cavité Fabry–Pérot. Le signal stimulant les ondes inframillimétriques est produit, par génération d'harmoniques, à partir d'un klystron fonctionnant dans la région millimétrique, avec référence directe aux signaux WWVB. Le signal maser est détecté dans un photodétecteur cryogénique. On a obtenu des raies ayant des largeurs de 50 à 100 fois inférieures à la largeur Doppler et de bonnes valeurs du rapport signal-bruit. Le système a été utilisé pour résoudre les faibles séparations de structure hyperfine du deutérium dans les deux transitions $1_{10} \rightarrow 1_{01}$ de D_2O, à 317 GHz, et $J = 1 \rightarrow 0$ de ND_3, à 309 GHz. La portée des données concernant l'interaction quadrupolaire de D_2O sur la question du gradient du champ électrique dans l'eau est discutée. Les valeurs en kilohertz des constantes spectroscopiques de D_2O, pour les états 1_{10} et 1_{01}, sont respectivement $(eQq_J)_D = 34.81 \pm 0.32$, $C_D = -2.661$ et $(eQq_J)_D = -29.60 \pm 0.55$, $C_D = -2.532$. Les constantes pour ND_3 sont, en kilohertz: $(eQq_J)_N = 816.2 \pm 1.1$, $C_N = 2.0 \pm 1.5$, $(eQq_J)_D = 19.9 \pm 0.8$ et $C_D = -2.2 \pm 0.8$.

[Traduit par le journal]

I. Introduction

Molecular beam maser spectroscopy was first reported by Gordon (1955) in the centimetre microwave region and the high resolution capabilities of this technique have now been used to study numerous molecular species in this spectral region. A number of proposals have been made to extend beam maser spectroscopy into the submillimetre wavelength region and beam absorption spectroscopy has been reported in this region by van Dijk and Dymanus (1970). These proposals have been motivated by the general desire to extend the capabilities of these devices as well as by the need for studies of specific transitions. For many of the fundamental and interesting molecules, these submillimetre transitions are either the only ones available or are more advantageous to study than the higher J transitions which fall at longer wavelengths. Low J transitions exhibit the largest hyperfine splittings and are least affected by centrifugal distortion. In this paper we report the extension of high resolution molecular beam maser spectroscopy into the submillimetre region and the study of the $J = 1 \rightarrow 0$ transition of ND_3 at 309 GHz and the $1_{10} \rightarrow 1_{01}$ transition of D_2O at 317 GHz.

II. Experimental

Numerous articles which describe centimetre wave molecular beam maser spectrometers have appeared in the literature (Gordon *et al.* 1955;
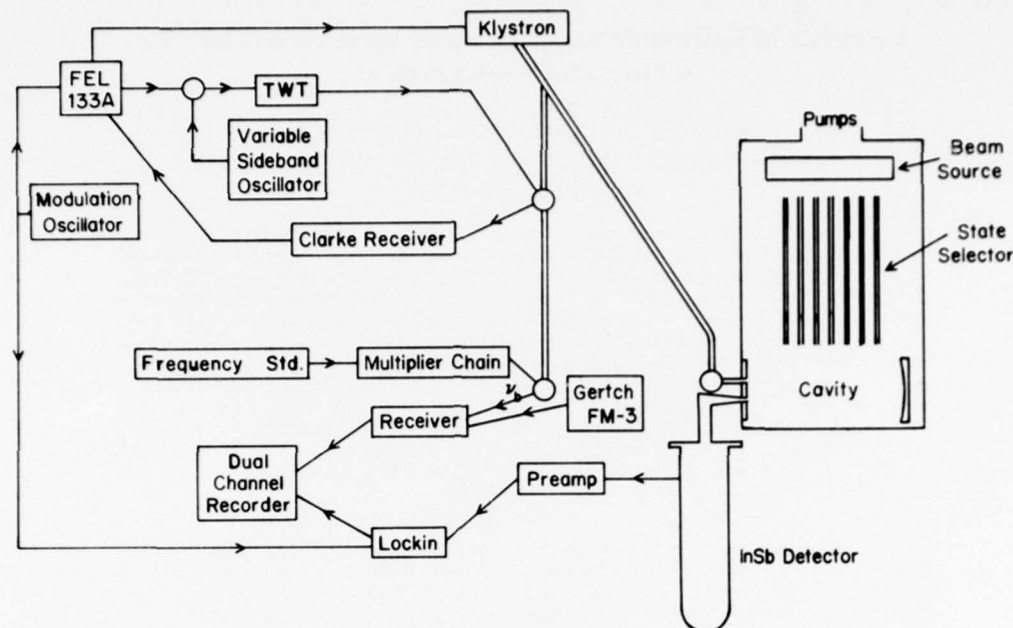
FIG. 1. Submillimetre beam maser spectrometer.

Thaddeus *et al.* 1964). In addition, molecular beam masers for 88 GHz (Marcuse 1961), 72 GHz (Krupnov *et al.* 1964), and various frequencies between 50 and 200 GHz (De Lucia and Gordy 1969; De Lucia and Cederberg 1971; Garvey and De Lucia 1974; Garvey *et al.* 1976) have been described. Because of the difference in wavelength between the more common centimetre wave devices and the one described here, a simple scaling down of dimensions is not a satisfactory design approach. The operation of a molecular beam maser may be divided as follows: (*1*) beam formation, (*2*) state selection, (*3*) microwave cavity, (*4*) generation and detection of submillimetre-wave energy, (*5*) frequency measurement. Figure 1 shows a diagram of the experimental apparatus. Multiple molecular beams are formed in the beam source, pass through a stacked quadrupole electrostatic state selector, and interact with the microwave field of a tunable Fabry–Perot cavity. The microwave field in this cavity is produced by harmonic generation from a millimetre wave klystron. The maser output signal is detected by a helium temperature (1.6 K) InSb photoconducting detector.

A. Beam Formation

Molecular beam masers have ordinarily used effusive beam sources. Kantrowitz and Grey

(1951) proposed the use of supersonic jets to obtain beams with greater forward directivity and intensity. Until recently these sources have not been used in beam masers. These supersonic nozzles produce increased forward beam intensities compared to effusive sources, but for beam spectroscopy the greatest gains result from the cooling effects of the supersonic expansion (Dyke *et al.* 1972). Rotational cooling results in partition functions which are substantially smaller than can be obtained in a bulk gas sample before condensation. The increase in population which results is largest for low J transitions. This is fortuitous because of the previously discussed spectroscopic advantages of low J transitions.

Because of the large frontal area of Fabry–Perot cavities, it is advantageous to employ multiple beams to increase the filling factor of the cavity. We have used a seven by nine array of nozzles, each beam having its own electrostatic quadrupole state selector. Collimation of each beam is accomplished by an arrangement of cryogenically cooled channels. It has been found that the complex and precise nozzle geometries originally used in studies of supersonic jet phenomena may be replaced by small holes in a thin metal sheet. To take full advantage of the nozzle source, it is desirable to expand the molecules into the maser vacuum chamber from

as high a source pressure as is feasible. Ultimately, the gas load presented to the collimation structure limits the maximum source pressure that may be used. With holes of 0.34 mm diameter, approximately 10 Torr source pressure was found to be appropriate in our experiment. Although this design is an order of magnitude from the source pressures used in single beam systems, we have realized gains of approximately five over a similar effusive source.

B. State Selection

Population inversion may produce intensity gains of the order of $kT/h\nu$ for transitions of frequency ν. Although this factor is inversely proportional to the frequency, gains of 20 may be realized at 300 GHz. The process of state selection with inhomogeneous electric fields has been the subject of extensive discussion (Becker and Angew 1963; Mednikov and Parygin 1963). A number of different state selectors have been successfully employed, but the multiple beam arrangement allowed by the submillimetre wave Fabry–Perot cavity places constraints upon the state selector geometries which can be used efficiently. Figure 2 shows an end view (beam flow perpendicular to figure) of the state selector used for this experiment (De Lucia and Gordy 1969). The poles of the quadrupole are fabricated from copper rods of 3/16-in. diameter, spaced 3/8-in. on centers. The structure is 12 in. long and is cryogenically pumped from within by cooled
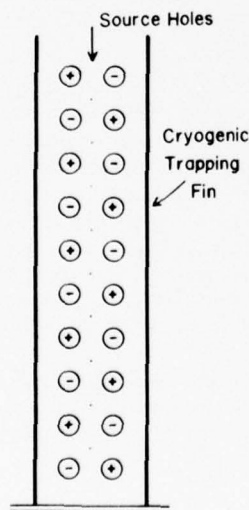
copper fins. Arcing within the state selector places an upper limit on the applied voltage of about 35 kV.

C. Cavity

At millimetre and submillimetre wavelengths the closed cylindrical cavities used as resonant structures for centimetre wave masers become significantly less advantageous than quasi-optical Fabry–Perot cavities. Because the molecular time-of-flight in the microwave field is the ultimate limit to maser resolution, the diameter of the microwave mode in the cavity should be maximized. For Fabry–Perot cavities made with the usual spherical mirrors, large mode diameters are difficult to obtain at submillimetre wavelengths and the modes themselves are sensitive to imperfections in the long focal length mirrors which are required.

We have developed a Fabry–Perot mirror, shown in Fig. 3, which overcomes the submillimetre-wave mode size problem. The center of the mirror is flat; the edges are curved to confine the microwave mode in a manner analogous to that of conventional spherical mirrors. This mirror may be cut in a stepwise fashion and polished to the final curve as illustrated in Fig. 3. The cavity is formed from this curved mirror and an opposing plane mirror, both fabricated from copper. Diffraction losses are insignificant, Q's approaching the limit imposed by copper losses are attainable, and high order modes are effectively suppressed. This new mirror design has the added advantage that the mode diameter is only a very slow function of wavelength (essentially filling the cavity to the curved edges) and is thereby usable over a wide wavelength range. Power is coupled into and out of the cavity through small holes in the plane mirror. Tuning is accomplished by translation of one of the mirrors.

For the cavity used in this work (the mirror of Fig. 3 and a plane mirror separated by about 20 cm) a mode of approximately 10 cm diameter results. The Q is approximately proportional to $\nu^{1/2}$ and at 1 mm, $Q \approx 500\,000$.
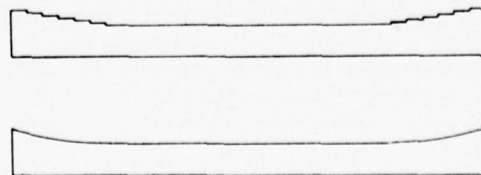
FIG. 2. End view of one vertical bay of state selector with beam source holes indicated.

FIG. 3. Fabry–Perot mirror fabrication.

D. Generation and Detection of Submillimetre Radiation

Harmonic generation (King and Gordy 1953) is a proven technique for production of modest amounts of submillimetre radiation and is particularly attractive for beam maser spectroscopy; relaxation rates in a molecular beam are slow and saturation occurs at relatively low power levels. With the high Q cavity used, we have found it possible to generate enough power to saturate the $1_{10} \rightarrow 1_{01}$ transition of D_2O at 317 GHz from a 300 mW 53 GHz klystron (OKI-55V11).

Since the observed linewidth depends upon spectral purity of the stimulating source, it is important that this source be as stable as possible. Free running klystron oscillators are too unstable and it is necessary to lock the signal source to a stable crystal oscillator. A diagram of this stabilization system is included in Fig. 1. The Frequency Engineering Labs 133A Synchronizer contains a variable crystal oscillator and multiplier–amplifier chain which produces a 48 MHz frequency comb extending to several gigahertz. A variable sideband is added and the comb with sidebands is amplified in a traveling wave tube and applied to a crystal mixer (1N26) coupled to the klystron. One of the resulting beat frequencies is down-converted to 27 MHz in a modified Clarke Instruments receiver. This 27 MHz signal is returned to the synchronizer where it is phase compared to a crystal reference oscillator. An error signal is generated and used to stabilize the klystron. The klystron is swept in frequency by means of the variable sideband oscillator.

The very low power levels at which saturation of maser levels occur make superheterodyne linear detectors, which are almost universally used in centimetre wave masers, more attractive than square-law detectors. However, at submillimetre wavelengths, local oscillators and mixers for superheterodyne detection are either unavailable or prohibitively expensive. We have found that the square-law InSb photodetector cooled to 1.6 K has adequate sensitivity for these experiments in the submillimetre region (Helminger et al. 1971). This results partly from the increased power output and saturation threshold of submillimetre masers compared to centimetre masers and partly from the increased sensitivity of the cryogenic detector compared to the room temperature detectors more commonly employed. This detector is broadbanded, requires no local oscillator, and is extremely reliable; it has proven to be very satisfactory for our experiments. The output signals are recovered by means of phase sensitive detection (at 3 kHz) of the signal produced as a result of the demodulation by the maser line of a small 1.5 kHz frequency modulation of the klystron.

E. Frequency Measurement

A frequency measurement system, separate from the frequency stabilization system, is used to avoid errors that might be introduced either by inexact loop locks or by instabilities or inaccuracies in the several oscillators. For the frequency measurement system, a 5 MHz crystal oscillator (General Radio 1115-B), phase compared to WWVB (HP117A), generates a standard reference signal which is amplified and multiplied to provide a 60 MHz comb extending to several GHz. This comb is mixed with a sampled portion of the stabilized klystron signal and the beat frequency v_b is amplified and mixed with a counted reference oscillator (Gertch FM-3) in a communications receiver. As v_b is swept (as the stabilized klystron is swept) the resulting zero beat is recorded simultaneously with the spectra on a dual channel chart recorder. Ten kilohertz sidebands may be added to the reference oscillator signal to provide a lattice of zero beats which serves as a frequency dispersion calibration on the chart paper.

III. Theory

The theory of molecular hyperfine structure has been extensively discussed in the literature (Thaddeus et al. 1964; Garvey et al. 1976; Cook and De Lucia 1971; Cederberg 1972). Powerful techniques have been developed which make the calculation of transition frequencies and intensities straightforward. We use the results and notation of Garvey et al. (1976) and Cook and De Lucia (1971).

The two identical deuterium nuclei of D_2O make the only contributions to the nuclear hyperfine structure. The Hamiltonian for the relevant interactions is:

$$[1] \qquad \mathcal{H} = \sum_{i=1}^{2} \frac{1}{6} V(D_i) \cdot Q(D_i) + I(D_i) \cdot C(D_i) \cdot J + I(D_1) \cdot D(D_1 D_2) \cdot I(D_2)$$

where the terms included represent the electric quadrupole, magnetic dipole, and spin–spin interactions, respectively. This problem is identical in form to the D_2S investigation reported by De Lucia and Cederberg (1971) and the matrix elements for the D_2O hyperfine interactions may be found in that work.

Analysis of the hyperfine structure of ND_3 is considerably more complex, partially because of the increased number of interactions but more significantly because of the three identical particle problem. Application of the techniques of Cederberg (1972) circumvents ambiguities which may occur in such an analysis. The appropriate Hamiltonian for the spectrum observed is:

$$[2] \quad \mathscr{H} = \frac{1}{6} V(N) \cdot Q(N) + I(N) \cdot C(N) \cdot J + \sum_{i=1}^{3} \left[\frac{1}{6} V(D_i) \cdot Q(D_i) + I(D_i) \cdot C(D_i) \cdot J \right.$$
$$\left. + I(N) \cdot D(ND_i) \cdot I(D_i) \right] + \frac{1}{2} \sum_{\substack{i,j=1 \\ i \neq j}}^{3} [I(D_i) \cdot D(D_iD_j) \cdot I(D_j)]$$

where the terms included represent the nitrogen electric quadrupole and magnetic dipole interactions, the deuterium electric quadrupole and magnetic dipole interactions, the nitrogen–deuterium spin–spin interaction, and the deuterium–deuterium spin–spin interaction, respectively. The matrix elements of these terms are included in the Appendix of this paper. The expressions which result lend themselves to machine computation and the energy levels and transition frequencies are obtained by numerical diagonalization of the resulting Hamiltonian matrix.

IV. Results

The experimental beam maser spectrum of the $1_{10} \rightarrow 1_{01}$ transition of D_2O is shown in Fig. 4 along with a theoretical spectrum calculated from the hyperfine constants of Table 1. Table 2 shows both the observed and calculated transition frequencies. The spin–spin interaction constant may be calculated from the molecular geometry. Because of the small size of the nuclear g-factor for deuterium compared to that of hydrogen, the spin rotation constants $C_{1_{10}}$ and $C_{1_{01}}$ can be calculated from previous beam maser work on H_2O and HDO (Bluyssen et al. 1967a,b) with higher accuracy than they can be determined from the D_2O spectrum. The deuterium quadrupole constants of Table 1 were calculated from the observed spectrum. Comparison of the experimental and theoretical data shows agreement well within the experimental error.

The large nitrogen quadrupole interaction in ND_3 produces a triplet which may be resolved in a conventional absorption spectrometer, but the much smaller splittings which result from the deuterium quadrupole interaction are obscured by the Doppler broadening. Figures 5–7 show

the resolution of this structure obtained in this experiment. As in the case of D_2O, the spin–spin interactions may be calculated from the molecular geometry. The remaining hyperfine constants have been evaluated from the beam maser spectrum and appear in Table 3. Table 4 shows a com-
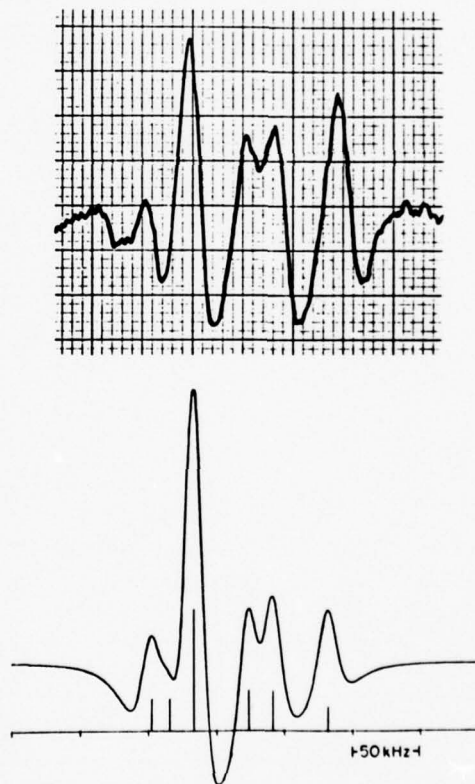

FIG. 4. Experimental and theoretical spectra of the $1_{10} \rightarrow 1_{01}$ transition in D_2O.

TABLE 1. Hyperfine constants of
D_2O for $1_{10} \rightarrow 1_{01}$

	Constant	Value (kHz)
1_{10}	$(eQq_J)_D$	34.81 ± 0.32[a]
	C_D	-2.661[b]
	$\langle 11|D_{zz}|11\rangle$	-0.163[c]
1_{01}	$(eQq_J)_D$	-29.60 ± 0.55
	C_D	-2.532[b]
	$\langle 11|D_{zz}|11\rangle$	0.325[c]

[a]Uncertainties represent one standard deviation of the experimental data.
[b]Calculated from Bluyssen *et al.* (1967*a*).
[c]Calculated from molecular geometry.

TABLE 2. Hyperfine spectrum of D_2O for $1_{10} \rightarrow 1_{01}$

F	Measured[a] (kHz)	Calculated (kHz)	Difference (kHz)
$0 \rightarrow 1$			
$1 \rightarrow 0$	-46.6 ± 1.8	-46.9	0.3
$2 \rightarrow 2$	-16.3 ± 1.4	-16.5	0.2
$2 \rightarrow 1$	23.3 ± 1.2	24.4	-1.1
$1 \rightarrow 2$	41.5 ± 1.2	41.5	0.0
$1 \rightarrow 1$	82.4 ± 1.2	82.1	0.3

[a]Measured relative to 316 799 845 kHz. Uncertainties represent one standard deviation of the experimental data.
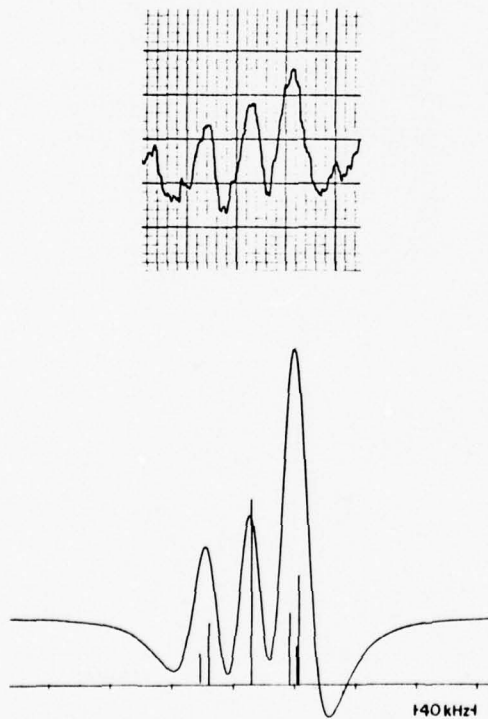

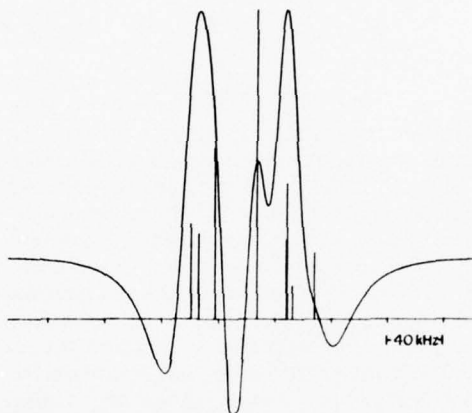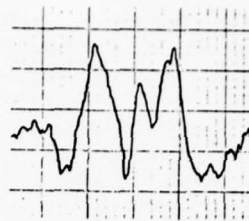FIG. 6. Experimental and theoretical spectra of the $J = 1 \rightarrow 0$, $F_N = 2$ transition in ND_3.

FIG. 5. Experimental and theoretical spectra of the $J = 1 \rightarrow 0$, $F_N = 1$ transition in ND_3.

parison between the experimental hyperfine frequencies and those calculated from the constants of Table 3.

Although there has been considerable experimental and theoretical work on the hyperfine spectra of the isotopic species of ammonia, numerous uncertainties and inconsistencies remain. These problems and the relation of new experimental work to them have been discussed recently by Garvey *et al.* (1976). The submillimetre capabilities of the spectrometer discussed in this paper allow the observation of the $J = 1 \rightarrow 0$ transition, which is less complex than the spectra which fall at longer wavelengths.

V. Discussion

The deuterium quadrupole interaction in the water molecule may be employed to investigate the electric field gradient tensor at the deuterium site. Specifically,

$$[3] \qquad q_J = \frac{2J}{2J + 3} \sum_g \frac{\langle P_g^2 \rangle}{J(J + 1)} V_{gg}$$

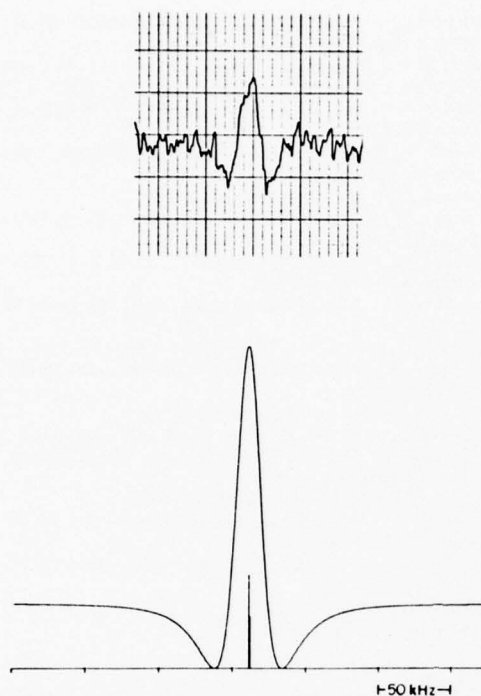where q_J is the spectral quadrupole constant, g

FIG. 7. Experimental and theoretical spectra of the $J = 1 \rightarrow 0$, $F_N = 0$ transition in ND_3.

TABLE 3. Hyperfine constants of $J = 1 \rightarrow 0$ of ND_3

Constant	Value (kHz)
$(eQq_J)_N$	816.2 ± 1.1 [a]
C_N	2.0 ± 1.5
$(eQq_J)_D$	19.9 ± 0.8
C_D	-2.2 ± 0.8
$\langle 11|D_{zz}(DD)|11\rangle$	-0.13 [b]
$\langle 11|D_{zz}(ND)|11\rangle$	-0.15 [b]

[a] Uncertainties represent one standard deviation of the experimental data.
[b] Calculated from molecular geometry.

TABLE 4. Hyperfine spectrum of ND_3 for $J = 1 \rightarrow 0$

Upper state	Observed[a] (kHz)	Calculated (kHz)	Difference (kHz)
$F_N = 0$	2037.7 ± 0.8	2037.7	0.0
	235.3 ± 2.9	235.4	-0.1
$F_N = 2$	214.3 ± 1.9	213.2	1.1
	181.7 ± 3.0	182.2	-0.5
	-1002.9 ± 1.3	-1002.9	0.0
$F_N = 1$	-1032.4 ± 1.4	-1032.5	-0.1
	-1060.8 ± 1.4	-1060.7	0.1

[a] Measured relative to 309 909 388 kHz. Uncertainties represent one standard deviation of the experimental data.

refers to the molecular principal inertial axes, P_g is the rotational angular momentum along g, and V_{gg} are components of the electric field gradient tensor. Combination of spectroscopic data from HDO and D_2O allow complete solution of V due to the rotation of the molecular inertial axes from one isotopic form of water to the other. As a result of Laplace's equation and molecular symmetry, the tensor may be described by values of two of its components and by the location of its principal axes in the molecular plane. Posener (1960) first performed such an evaluation of the electric field gradient tensor in water. Using beam maser techniques, Bluyssen et al. (1967a,b) were able to significantly improve this analysis. As was pointed out by Bluyssen et al. (1967a,b), Posener erroneously attributed the wrong direction to the angle of rotation from the O—D bond to the principal axis system of the tensor V. The direction of the angle of rotation has more recently been incorrectly reported in the literature (De Lucia et al. 1974) because of an erroneous communication to the authors. Posener's data, as well as that of Bluyssen et al. and the present experiment, indicate that the principal axes of the quadrupole tensor are rotated from the O—D bond direction by approximately $1°$ clockwise about Posener's positive ζ axis.

Figure 8 shows the correct geometry for the location of the quadrupole tensor relative to the direction of the molecular bond, and Table 5 gives the components of V in its own principal axis system. These results are calculated from all available data except that from the 7_{44} and 7_{34} states which Verhoeven et al. (1968) have shown to be contaminated by centrifugal distortion effects. The uncertainties shown in Table 5 include contributions from both experimental uncertainties and model errors. The model errors
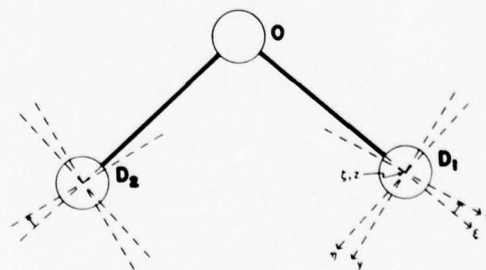

FIG. 8. Rotation of the quadrupole tensor from the OD bond direction. The positive ζ, z axes point into the paper for D_1. Different sign conventions and (or) axis assignments would be required for D_2.

TABLE 5. Components of the quadrupole coupling tensor in its principal axis system

	D_2O	D_2S
V_{xx}	307.5 ± 0.6	149.0
V_{yy}	-132.6 ± 0.6	-59.8
V_{zz}	-174.9 ± 0.6	-89.2
a	$-1° 16' \pm 3'$	$-1° 35'$

arise principally from neglect of centrifugal distortion and isotope effects. These errors were not included in the earlier calculation of Bluyssen *et al.* (1967*a,b*) because their smaller data set did not provide adequate redundancy for their evaluation.

Also included in Table 5 are similar results for D_2S (De Lucia and Cederberg (1971). It is interesting and reassuring to note the similarity both in the rotation of the principal axis of the V tensor from the bond direction and the deviation from cylindrical symmetry for both molecules.

Acknowledgements

BECKER, G. and ANGEW, Z. 1963. Phys. 15, 281.
BLUYSSEN, H., VERHOEVEN, J., and DYMANUS, A. 1967*a*. Phys. Lett. A, 25, 214.
BLUYSSEN, H., DYMANUS, A., REUSS, J., and VERHOEVEN, J. 1967*b*. Phys. Lett. A, 25, 584.
CEDERBERG, J. W. 1972. Am. J. Phys. 40, 159.
COOK, R. L. and DE LUCIA, F. C. 1971. Am. J. Phys. 39, 1433.
DE LUCIA, F. C. and CEDERBERG, J. W. 1971. J. Mol. Spectrosc. 40, 52.
DE LUCIA, F. C. and GORDY, W. 1969. Phys. Rev. 187, 58.

DE LUCIA, F. C., HELMINGER, P., and KIRCHHOFF, W. H. 1974. J. Phys. Chem. Ref. Data, 3, 211.
DYKE, T. R., TOMASEVICH, G. R., KLEMPERER, W., and FALCONER, W. E. 1972. J. Chem. Phys. 57, 2277.
GARVEY, R. M. and DE LUCIA, F. C. 1974. J. Mol. Spectrosc. 50, 38.
GARVEY, R. M., DE LUCIA, F. C., and CEDERBERG, J. W. 1976. Mol. Phys. 31, 265.
GORDON, J. P. 1955. Phys. Rev. 99, 1253.
GORDON, J. P., ZEIGER, H. J., and TOWNES, C. H. 1955. Phys. Rev. 99, 1264.
HELMINGER, P., COOK, R. L., and DE LUCIA, F. C. 1971. J. Mol. Spectrosc. 40, 125.
KANTROWITZ, A. and GREY, J. 1951. Rev. Sci. Instrum. 22, 328.
KING, W. C. and GORDY, W. 1953. Phys. Rev. 90, 319.
KRUPNOV, A. F. and SKVORTSOV, V. A. 1964. Sov. Phys. JETP, 18, 74.
MARCUSE, D. 1961. J. Appl. Phys. 32, 743.
MEDNIKOV, O. I. and PARYGIN, V. H. 1963. Radiotekh. Elektron. 8, 653; *Engl. transl.* Radio Eng. Electron. Phys. USSR, 8, 685.
POSENER, D. W. 1960. Aust. J. Phys. 13, 168.
THADDEUS, P., KRISHER, L. C., and LOUBSER, J. H. N. 1964. J. Chem. Phys. 40, 257.
VAN DIJK, F. A. and DYMANUS, A. 1970. Chem. Phys. Lett. 5, 387.
VERHOEVEN, J., BLUYSSEN, H., and DYMANUS, A. 1968. Phys. Lett. A, 26, 424.

Appendix

The matrix elements of the various Hamiltonian terms for the nuclear hyperfine interactions in ND_3 may be conveniently evaluated in the coupling scheme:

$$J + I_N = F_N$$
$$[A.1] \quad I(D_1) + I(D_2) + I(D_3) = I_D$$
$$F_N + I_D = F$$

In the equations to follow the states are designated by specific cases of the general form $\langle KJI_N F_N I_D FM|$. For brevity, the Hamiltonian is retained in Cartesian form.

$$[A.2] \quad \left\langle 011\, F_N I_D FM \left| \frac{1}{6} V(N) \cdot Q(N) \right| 011\, F_N I_D FM \right\rangle = (-1)^{F_N} \begin{Bmatrix} 1 & 1 & 2 \\ 1 & 1 & F_N \end{Bmatrix} (15/2)(eQq_J)_N$$

$$[A.3] \quad \langle 011\, F_N I_D FM | I(N) \cdot C(N) \cdot J | 011\, F_N I_D FM \rangle = (-1)^{F_N} \begin{Bmatrix} 1 & 1 & 1 \\ 1 & 1 & F_N \end{Bmatrix} (6)(C_J)_N$$

The relationship between C_J and C is considered by Cook and De Lucia (1971)

$$[A.4] \quad \left\langle 011\, F_N' I_D' FM \left| \frac{1}{6} \sum_{i=1}^{3} Q(D_i) \cdot V(D_i) \right| 011\, F_N I_D FM \right\rangle =$$

for $I_D' = I_D = 3$:

$$(-1)^{2F_N + 1 + F} [(2F_N' + 1)(2F_N + 1)]^{1/2} \begin{Bmatrix} F_N' & F_N & 2 \\ 3 & 3 & F \end{Bmatrix} \begin{Bmatrix} 1 & F_N' & 1 \\ F_N & 1 & 2 \end{Bmatrix} \left(9 \sqrt{\frac{7}{2}} \right) (eQq_J)_D$$

for $I_D' = I_D = 1$:

$$(-1)^{2F_N+1+F}[(2F_N' + 1)(2F_N + 1)]^{1/2} \begin{Bmatrix} F_N' & F_N & 2 \\ 1 & 1 & F \end{Bmatrix} \begin{Bmatrix} 1 & F_N' & 1 \\ F_N & 1 & F \end{Bmatrix} \frac{27}{2} (eQq_J)_D$$

for $I_D' = 1, I_D = 3$:

$$(-1)^{2F_N+1+F}[(2F_N' + 1)(2F_N + 1)]^{1/2} \begin{Bmatrix} F_N' & F_N & 2 \\ 3 & 1 & F \end{Bmatrix} \begin{Bmatrix} 1 & F_N' & 1 \\ F_N & 1 & 2 \end{Bmatrix} (3\sqrt{21})(eQq_J)_D$$

[A.5] $\left\langle 011\, F_N' I_D FM \left| \sum_{i=1}^{3} I(D_i)\cdot C(D_i)\cdot J \right| 011\, F_N I_D FM \right\rangle = (-1)^{2F_N+I_D+F+1}$

$\times\ [(2F_N' + 1)(2F_N + 1)(2I_D + 1)(I_D + 1)I_D]^{1/2} \begin{Bmatrix} F_N' & F_N & 1 \\ I_D & I_D & F \end{Bmatrix} \begin{Bmatrix} 1 & F_N' & 1 \\ F_N & 1 & 1 \end{Bmatrix} (\sqrt{6})(C_J)_D$

[A.6] $\left\langle 011\, F_N' I_D FM \left| \sum_{i=1}^{3} I(N)\cdot D(ND_i)\cdot I(D_i) \right| 011\, F_N I_D FM \right\rangle = (-1)^{F_N+I_D'+F+1}$

$\times\ [3(2F_N' + 1)(2F_N + 1)(2I_D + 1)(I_D + 1)I_D]^{1/2} \begin{Bmatrix} F_N' & F_N & 1 \\ I_D & I_D & F \end{Bmatrix} \begin{Bmatrix} 1 & 1 & 2 \\ 1 & 1 & 1 \\ F_N' & F_N & 1 \end{Bmatrix}$

$\times\ 15\sqrt{2}\,\langle 11|D_{zz}(ND)|11\rangle$

$\langle 11|D_{zz}|11\rangle$ is the specialized form of $\langle J\,J|D_{zz}|J\,J \rangle$, the spin–spin interaction term, discussed by De Lucia and Cederberg (1971).

[A.7] $\left\langle 011\, F_N' I_D' FM \left| \frac{1}{2} \sum_{\substack{i,j=1 \\ i \neq j}} I(D_i)\cdot D(D_iD_j)\cdot I(D_j) \right| 011\, F_N I_D FM \right\rangle =$

for $I_D' = I_D = 3$:

$$(-1)^{2F_N+F+1}[(2F_N' + 1)(2F_N + 1)]^{1/2} \begin{Bmatrix} F_N' & F_N & 2 \\ 3 & 3 & F \end{Bmatrix} \begin{Bmatrix} 1 & F_N' & 1 \\ F_N & 1 & 2 \end{Bmatrix} (18\sqrt{14})\langle 11|D_{zz}(DD)|11\rangle$$

for $I_D' = I_D = 1$:

$$(-1)^{2F_N+F+1}[(2F_N' + 1)(2F_N + 1)]^{1/2} \begin{Bmatrix} F_N' & F_N & 2 \\ 1 & 1 & F \end{Bmatrix} \begin{Bmatrix} 1 & F_N' & 1 \\ F_N & 1 & 2 \end{Bmatrix} (-6)\langle 11|D_{zz}(DD)|11\rangle$$

for $I_D' = 1, I_D = 3$:

$$(-1)^{2F_N+F+1}[(2F_N' + 1)(2F_N + 1)]^{1/2} \begin{Bmatrix} F_N' & F_N & 2 \\ 3 & 1 & F \end{Bmatrix} \begin{Bmatrix} 1 & F_N' & 1 \\ F_N & 1 & 2 \end{Bmatrix} (-3\sqrt{21})\langle 11|D_{zz}(DD)|11\rangle$$

PRESSURE BROADENING OF HYDROGEN SULFIDE†

PAUL HELMINGER‡

Department of Physics, University of South Alabama, Mobile, AL 36688, U.S.A.

and

FRANK C. DE LUCIA

Department of Physics, Duke University, Durham, NC 27706, U.S.A.

Abstract—Microwave measurements of the self-broadening parameters of four pure rotational transitions of H_2S have been carried out in the millimeter and submillimeter wavelength region. The resulting parameters are (in MHz torr^{-1}): $1_{1,0} - 1_{0,1}$, 7.18 ± 0.5; $2_{2,0} - 2_{1,1}$, 6.78 ± 0.5; $2_{1,1} - 2_{0,2}$, 9.10 ± 0.5; $3_{3,0} - 3_{2,1}$, 7.76 ± 0.5. In addition, Anderson theory calculations have been carried out for these transitions and are found to be in good agreement.

INTRODUCTION

BECAUSE H_2S is a light asymmetric rotor without transitions in the conventional microwave region, we have used high resolution millimeter and submillimeter microwave techniques[1] to measure the self-broadening parameters of four pure-rotational transitions of H_2S in the region between 150 and 400 GHz. To the best of our knowledge, these results are the first experimental measurements of the pressure broadening parameters of H_2S. We have also carried out Anderson theory[2] calculations and find them to be in good agreement with our experimental values.

These results are of both theoretical and practical importance. H_2O is the only other light asymmetric species for which experimental line-broadening data have been reported and some of these data are in substantial conflict with theoretical predictions.[3] H_2S is both a minor constituent of the atmosphere and one of the principal molecular components of the interstellar medium.

EXPERIMENTAL TECHNIQUE AND RESULTS

We have discussed in previous publications the techniques for producing and detecting millimeter and submillimeter microwave energy.[1] Our pressure-broadening measurement technique follows closely the double modulation scheme of RUSK.[4] Figure 1 shows an outline of our apparatus. Millimeter wave energy in the 50–60 GHz region was produced by an OKI 55V11 klystron. A small amount of this energy was compared with an accurate local frequency standard and the rest coupled onto a crystal harmonic generator. The resultant harmonic energy in the 150–400 GHz region was transmitted by quasi-optical techniques through the sample cell and detected by a 1.6°K InSb photodetector. The pressure-broadened line acted as a discriminator for the small 10 kHz FM modulation that was applied to the tube. The resulting 10 kHz signal was amplified by the tuned amplifiers of a PAR HR-8 lock-in and displayed on an oscilloscope. A cathetometer and oil manometer were used to monitor pressure. Although H_2S is well behaved and reaches equilibrium pressure rapidly, measurements were made both in series of increasing and decreasing pressure and on different days to avoid possible systematic effects. Because rotational transitions of light asymmetric rotors are such strong absorbers in the millimeter and submillimeter spectral region, we used absorption cell lengths as short as 10 cm. Even so, it was necessary to include a correction for the large absorption by[5]

$$\Delta \nu = \sqrt{(3)}\delta\nu \left(1 - \frac{1}{4} a_0 l + \frac{5}{32} (a_0 l)^2 - \cdots \right). \tag{1}$$

PAUL HELMINGER and FRANK C. DE LUCIA

Table 1. Hydrogen sulfide line broadening parameters

Transition	Line Frequency (GHz)	Experimental[a] Broadening Data (MHz/Torr)	Corrected Self Broadening Parameter (MHz/Torr)	Anderson Theory Value (MHz/Torr)
$1_{1,0} - 1_{0,1}$	168	7.80	7.18 ± 0.5	6.58
$2_{0,2} - 2_{1,1}$	216	8.69	8.10 ± 0.5	7.21
$2_{2,0} - 2_{1,1}$	393	7.14	6.73 ± 0.5	6.92
$3_{3,0} - 3_{2,1}$	300	8.52	7.76 ± 0.5	7.14

[a] Line widths measured at $300°$ K.

DISCUSSIONS

Until this work, H_2O was the only light asymmetric rotor for which comparison could be made of experimental and theoretical pressure-broadening parameters. Unfortunately, only the microwave measurements of the $3_{1,3} - 2_{2,0}$[4] and $6_{1,6} - 5_{2,3}$[11] transitions are in good agreement with the theoretical predictions. Several i.r. measurements all gave results that are about 50% higher than the values of BENEDICT and KAPLAN.[3] The good agreement between our microwave results and theory, coupled with the fact that the apparent discrepancies in H_2O are all based on lower resolution i.r. measurements, would indicate that Anderson's theory is capable of giving good results for pure rotational transitions of light asymmetric species. Recent microwave work by NERF[12] on the somewhat heavier H_2CO leads to the same conclusion.

TEJWANI and YENUNG[13] have recently carried out Anderson's theory calculations on H_2S with and without the inclusion of higher order interactions. Their results are in general agreement with ours ($\sim 10\%$) although the differences are substantially greater than the differences between our H_2O calculations and those of Benedict and Kaplan.

REFERENCES

1. P. HELMINGER, F. C. DE LUCIA and W. GORDY, *Phys. Rev. Lett.* **25**, 1397 (1970).
2. P. W. ANDERSON, *Phys. Rev.* **76**, 647 (1949).
3. G. BIRNBAUM, *Advan. Chem. Phys.* **12**, 487 (1967).
4. J. R. RUSK, *J. Chem. Phys.* **42**, 493 (1965).
5. H. J. BABROV, Private communication.
6. P. A. HELMINGER and F. C. DE LUCIA, *Bull. Am. Phys. Soc.* **21**, 380 (1976).
7. W. S. BENEDICT and L. D. KAPLAN, *JQSRT* **4**, 453 (1964).
8. C. J. TSAO and B. CURNUTTE, *JQSRT* **2**, 41 (1962).
9. P. HELMINGER, R. L. COOK and F. C. DE LUCIA, *J. Chem. Phys.* **56**, 4581 (1972).
10. C. HUISZOON and A. DYMANUS, *Physica* **31**, 1049 (1965).
11. H. J. LIEBE, M. C. THOMPSON, JR. and T. A. DILLON, *JQSRT* **9**, 1 (1969).
12. R. B. NERF, *J. Molec. Spectrosc.* **58**, 451 (1975).
13. G. D. T. TEJWANI and E. S. YEUNG. *JQSRT* to be published.

"Forbidden" Rotational Spectra of Symmetric-Top Molecules: PH_3 and PD_3[1]

DAVID A. HELMS AND WALTER GORDY

Department of Physics, Duke University, Durham, North Carolina 27706

A millimeter-wave spectrometer having a sensitivity of 4×10^{-10} cm^{-1} in the 2-mm region has been constructed for observation of extremely weak millimeter-wave spectra of gases. It has been used to measure $J \rightarrow J$, $K = 0 \leftarrow 3$ transitions in PH_3 and $J \rightarrow J$, $K = 0 \leftarrow 3$ as well as $K = \pm 1 \leftarrow \pm 4$ transitions in PD_3. The B_0 and C_0 spectral constants (in MHz) are: for PH_3, $B_0 = 133\,480.15 \pm 0.12$ and $C_0 = 117\,488.85 \pm 0.16$; for PD_3, $B_0 = 69\,471.10 \pm 0.03$ and $C_0 = 58\,974.37 \pm 0.05$. The effective ground-state values obtained for the bond angle and bond length are: for PH_3, r_0 (Å) $= 1.420_9$ and $\alpha_0(°) = 93.34_5$; for PD_3, r_0 (Å) $= 1.417_6$ and $\alpha_0(°) = 93.35_9$. The corresponding zero-point-average values were calculated to be: for PH_3, r_z (Å) $= 1.4269_9 \pm 0.0002$ and $\alpha_z(°) = 93.228_7$; for PD_3, r_z (Å) $= 1.4226_5 \pm 0.0001$ and $\alpha_z(°) = 93.256_7 \pm 0.004$. For both species, the equilibrium values are r_e (Å) $= 1.4115_9 \pm 0.0006$ and $\alpha_e(°) = 93.32_8 \pm 0.02$.

1. INTRODUCTION

The pure rotational transitions normally observed for symmetric-top molecules conform to the selection rules $\Delta J = \pm 1$, $\Delta K = 0$. As a result of their axial symmetry, there is no off-axis component of the permanent dipole moment to couple a radiation field with the rotation about the symmetry axis. Hence, resonance radiation does not normally induce changes in the K quantum number which measures the angular momentum about this axis. Consequently, the moment of inertia for rotation about the symmetry axis, and the associated centrifugal distortion constants, cannot be obtained from the normal rotational spectra.

As a result of theoretical developments and notable advancements in the experimental techniques for spectral detection, it has become possible to detect rotational transitions in the ground vibrational state corresponding to changes in the energy of rotation about the symmetry axis of symmetric-top molecules, i.e., changes in the K quantum number. For molecules with C_{3v} symmetry, such as PH_3 and PD_3 which are reported here, the observable transitions—forbidden in the normal theory—correspond to K changes of ± 3.

The possibility of $\Delta K = \pm 3$ changes in molecules of C_{3v} symmetry was apparently first recognized in 1967 by Hanson (*1*). The basic theory for such transitions was later contributed by Watson (*2*). These transitions were first detected as pure rotational spectra in 1973 by Chu and Oka (*3*), who observed $\Delta J = 0$, $K = \pm 1 \leftarrow \mp 2$ transitions in PH_3 occurring in the 43.7 to 47.4 GHz region. In 1974 they reported (*4*) similar

measurements of $\Delta J = 0$, $K = \pm 1 \leftarrow \mp 2$ transitions for PD₃ in the 29.9 to 30.8 GHz region, and for AsH₃ in the 21.2 to 21.8 GHz region. Chu and Oka were helped in their measurements by the line frequency predictions based on the previous observation of $\Delta(K - l) = \pm 3$ vibration–rotation transitions of PH₃ and AsH₃ by Maki, Sams, and Olson (5). Likewise, our detection (6) of the higher-frequency $K = 0 \leftarrow 3$ forbidden transition of PH₃ and PD₃ was assisted by a preliminary prediction of their frequencies from the results of Maki *et al.* as well as those of Chu and Oka.

The need for observation of these higher K transitions described in this paper was indicated by Chu and Oka (4), who reported that their spectrometer was not sufficiently sensitive at the higher frequencies to detect them. Measurements of these transitions confirm the assignments of the frequencies measured by Chu and Oka and provide increased accuracy in the values of the spectral constants, particularly those influenced by the distortion caused by rotation about the symmetry axis. For observation of weak transitions such as these in the shorter millimeter-wave region, we designed the exceptionally sensitive millimeter-wave spectrometer described below.

The Q-branch $\Delta K = \pm 3$ transitions represent only one class of forbidden transitions in symmetric molecules included in the general theory of Watson *et al.* (2, 7) and others (8, 9). Oka (10) has recently written an excellent review of the experimental and theoretical developments of this relatively new type of spectra. It should be mentioned that forbidden transitions of symmetric-top molecules in vibrationally excited states were theoretically predicted many years earlier by Mizushima and Venkateswarlu (11), before sufficiently sensitive spectrometers were available for their detection. In the ground vibrational state the off-axis dipole moment which couples the radiation field to the rotation is induced by centrifugal distortion. The selection rules are determined by the molecular symmetry. In the molecules studied here, the rotation about the b axis of inertia induces a small dipole moment perpendicular to the symmetry axis which leads to a slight admixture of the K levels and a breakdown of the $\Delta K = 0$ selection rule. The threefold symmetry about the c axis limits this admixture to K levels differing by 3. It is of interest that centrifugal distortion due to rotation about the symmetry axis can likewise generate a small dipole component along the symmetry axis. This component is of no particular consequence in molecules such as PH₃, which already has a permanent dipole moment along the symmetry axis, but it can give rise to forbidden $\Delta J = \pm 1$ transitions in molecules such as CH₄, which has no permanent dipole moment. In fact, $\Delta J = 1$ rotational transitions of CH₄, SiH₄, and GeH₄ have been observed by Rosenberg *et al.* (12–15) in the far-infrared region. Forbidden transitions of CH₄ in the ground vibrational state have also been detected in the microwave region by Holt, Gerry, and Ozier (16). These and other forbidden spectra of symmetric-top molecules are treated in Oka's review (10). He also reports that he and his associates have recently detected $\Delta K = \pm 3$ transitions of NH₃ with an infrared laser (17).

2. EXPERIMENTAL DETAILS

The microwave spectrometer used in these measurements has: for the millimeter-wave source, a klystron-driven harmonic generator; for the absorption cell, a high-Q Fabry–Perot transmission cavity (semiconfocal arrangement); and for millimeter-wave

detection, an indium–antimonide detector operated at 1.6 K. The power from the harmonic generator is injected into the cavity by way of a small, rectangular aperture (0.075 × 0.034 in.) in the center of the flat, circular mirror. The power level in the cavity is monitored by radiation from another small, rectangular aperture in the same plate, the output from which is channeled to the indium–antimonide detector. The Q of the resonant cavity mode as indicated by the $\nu_0/\Delta\nu$, the resonant frequency divided by the half-width of the Lorentzian mode shape, is approximately 600 000 at 140 GHz.

In operation, the resonant cavity is filled with the absorbing sample of gas to a pressure of about 15 to 25 μm. The klystron is tuned so that the proper harmonic coincides with the predicted absorption frequency, and the cavity is adjusted to resonate at that frequency. The klystron harmonic is then locked to the peak of the cavity resonance, and the cavity is tuned through the molecular absorption line. The drop in the monitored power resulting from the change in the loaded Q of the cavity corresponds to the detected spectral line.

To achieve control of the klystron frequency by the cavity, a 2.6 kHz sine wave is superimposed on the klystron reflector to sweep the harmonic back and forth across the center of the cavity resonance. The signal produced at the detector (with the loop opened) changes phase by 180° as the klystron is tuned through the cavity resonance. This detector signal is processed by a phase-lock-in amplifier which generates a correction voltage with the proper phase-and-time response to lock the klystron harmonic to the peak of the cavity resonance. Thus, as the cavity is tuned by movement of the curved mirror in and out, the klystron harmonic and the cavity resonance track together. In practice, the amplitude of the 2.6 kHz stabilizing signal is reduced to about 40 mV, or less, to keep most of the harmonic power within the envelope of the cavity-response curve.
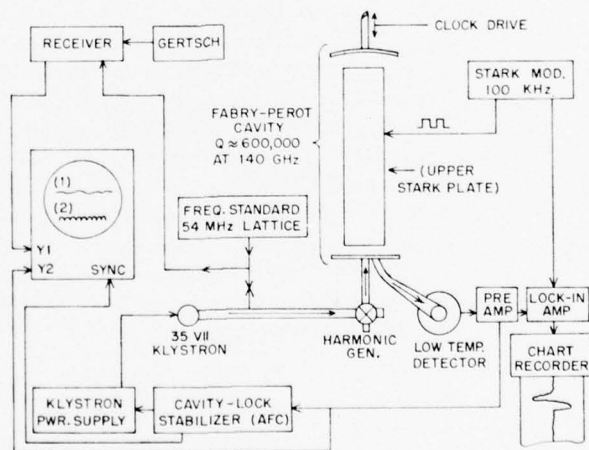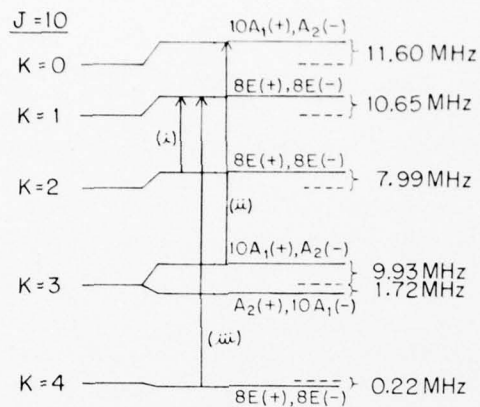

FIG. 1. Diagram of spectrometer.

ROTATIONAL ENERGY LEVELS OF PD_3

FIG. 2. Energy level diagram of the first five K states for $J = 10$ of PD₃ showing the energy shifts caused by the $\mathcal{H}'$ perturbation, the $K = 3$ splitting, the level symmetry (under particle exchange), and the nuclear spin degeneracy. The transition indicated by (i) is that measured by Chu and Oka (4). Those indicated by (ii) and (iii) were measured in this work.

The inside of the cavity is fitted with Stark-modulation plates which are positioned well out of the microwave field to avoid lowering the Q. A square-wave generator is used to produce Stark modulation of the absorption line at 100 kHz. As the clock-driven cavity tunes through the absorption, the detector signal is processed by a phase-lock-in amplifier referenced to the 100-kHz signal. The first-derivative line-shape signal from the amplifier is displayed on the chart recorder (see Fig. 1). After exploratory scans to establish the shape of the line, the peak of the cavity response is tuned to the center of the absorption-line contour, and the corresponding klystron frequency is measured with a frequency standard monitored by station WWVB. Repeated measurements are made for each direction of approach to the line center. The accuracy achieved for the line-frequency measurements is estimated to be 1 part in 10^8. The sensitivity of our spectrometer ($\approx 4 \times 10^{-10}$ cm^{-1} at 144 GHz for a time constant of 1 sec) enables us to measure the weak $\Delta K = \pm 3$ transitions with this high precision. The factors limiting the sensitivity appear to be the degree of klystron stability, the power available from the harmonic generator, and the extraneous vibrations of the cavity end plates.

3. THEORETICAL BACKGROUND

As a result of centrifugal distortion, the rotational wavefunction $\psi_{J,K}$ of a molecule having C_{3v} symmetry mixes slightly with the wavefunction $\psi_{J,K\pm 3}$ in the ground vibrational state. The term in the Hamiltonian responsible for the interaction may be ex-

pressed (18) as

$$\mathcal{H}' = (\hbar^4 \tau_{zzzz}/4)[(J_+^3 + J_-^3)J_z + J_z(J_+^3 + J_-^3)], \tag{1}$$

where τ_{zzzz} is a centrifugal distortion constant and J_z, J_+, and J_- are rotational operators.

In the absence of the perturbing $\mathcal{H}'$ term, the rotational levels are all doubly degenerate for each value of K ($K \neq 0$). Figure 2 illustrates the effect of the perturbation on the $J = 10$ energy levels in PD_3. The energy levels corresponding to $K \neq 3$ are raised or lowered, but they remain degenerate with symmetry E. The $K = 3$ level is, however, split into A_1 and A_2 components. The $+$ and $-$ signs indicate the parity of the total wavefunction. The symmetry assignments A_1, A_2, and E indicate the symmetry of the rovibrational wavefunction (excluding spin) for an interchange of two hydrogens. The integer preceding the symmetry assignment (A_1, A_2, or E) indicates the nuclear statistical weight of the state. The symmetry selection rules for Q-type $\Delta K = \pm 3$ transitions (19) are $\pm \leftrightarrow \pm$, along with $A_1 \leftrightarrow A_1$, $A_2 \leftrightarrow A_2$, or $E \leftrightarrow E$.

Each unperturbed energy level of a symmetric-top molecule is normally doubly degenerate for each nonzero value of K. It is necessary to form linear combinations of $\psi_{J,+K}$ and $\psi_{J,-K}$ in order to obtain wavefunctions which have the proper symmetry for an exchange of two of the hydrogens. The new wavefunctions for PH_3, $\psi^+_{J,K}$ and $\psi^-_{J,K}$, are defined in terms of the wavefunctions $\psi_{J,+K}$ and $\psi_{J,-K}$ and the nuclear wavefunctions $\alpha\beta\beta$, $\alpha\beta\alpha$, etc. (where α and β stand for spin up and spin down, respectively) as follows (20): for $K \neq 0$ or a multiple of 3,

$$\psi^\pm_{J,K} = (1/6^{\frac{1}{2}})[\psi_{J,+K}(\beta\alpha\alpha + \alpha\beta\alpha e^{2\pi iK/3} + \alpha\alpha\beta e^{4\pi iK/3})$$
$$\pm \psi_{J,-K}(\beta\alpha\alpha + \alpha\beta\alpha e^{-2\pi iK/3} + \alpha\alpha\beta e^{-4\pi iK/3})] \tag{2}$$

and

$$\psi^\pm_{J,K} = (1/6^{\frac{1}{2}})[\psi_{J,+K}(\alpha\beta\beta + \beta\alpha\beta e^{2\pi iK/3} + \beta\beta\alpha e^{4\pi iK/3})$$
$$\pm \psi_{J,-K}(\alpha\beta\beta + \beta\alpha\beta e^{-2\pi iK/3} + \beta\beta\alpha e^{-4\pi iK/3})]; \tag{3}$$

for $K = 0$,

$$\psi^+_{J,0} = (1/3^{\frac{1}{2}})\psi_{J,0} \begin{Bmatrix} \beta\alpha\alpha + \alpha\beta\alpha + \alpha\alpha\beta \\ \alpha\beta\beta + \beta\alpha\beta + \beta\beta\alpha \end{Bmatrix}, \tag{4a}$$

and for $K = 3$

$$\psi^\pm_{J,K} = (1/6^{\frac{1}{2}})(\psi_{J,+K} \pm \psi_{J,-K}) \begin{Bmatrix} \alpha\alpha\alpha \\ \beta\beta\beta \\ \beta\alpha\alpha + \alpha\beta\alpha + \alpha\alpha\beta \\ \alpha\beta\beta + \beta\alpha\beta + \beta\beta\alpha \end{Bmatrix}. \tag{4b}$$

The similar wavefunctions for PD_3 are more complicated because of the spin value $I = 1$ for D.

The formulas giving the energy levels may be expressed (21, 22) for $K \neq 3$ as:

$$\frac{E(J,K)}{h} = F(J,K)$$

$$+ \left(\frac{h^4\tau_{zzzz}}{4h}\right)^2 \left\{ \frac{(2K-3)^2[J(J+1)-K(K-1)][J(J+1)-(K-1)(K-2)][J(J+1)-(K-2)(K-3)]}{F(J,K)-F(J,K-3)} \right.$$

$$\left. + \frac{(2K+3)^2[J(J+1)-K(K+1)][J(J+1)-(K+1)(K+2)][J(J+1)-(K+2)(K+3)]}{F(J,K)-F(J,K+3)} \right\} ; \quad (5)$$

and for $K=3$ as

$$\frac{E^-(J,3)}{h} = F(J,3) + \left(\frac{h^4\tau_{zzzz}}{4h}\right)^2 \left\{ \frac{81[J(J+1)-12][J(J+1)-20][J(J+1)-30]}{F(J,3)-F(J,6)} \right\}$$

$$+ \left[h_0 - \frac{18(h^4\tau_{zzzz}/4h)^2}{F(J,0)-F(J,3)} \right] J(J+1)[J(J+1)-2][J(J+1)-6], \quad (6)$$

and

$$\frac{E^+(J,3)}{h} = F(J,3) + \left(\frac{h^4\tau_{zzzz}}{4h}\right)^2 \left\{ \frac{81[J(J+1)-12][J(J+1)-20][J(J+1)-30]}{F(J,3)-F(J,6)} \right\}$$

$$- h_0 J(J+1)[J(J+1)-2][J(J+1)-6], \quad (7)$$

where

$$F(J,K) = B[J(J+1)-K^2] + CK^2 - D_J J^2(J+1)^2 - D_{JK}J(J+1)K^2 - D_K K^4$$

$$+ H_{JJK}J^2(J+1)^2K^2 + H_{JKK}J(J+1)K^4 + L_{JJKK}J^2(J+1)^2K^4 + L_{JJJK}J^3(J+1)^3K^2. \quad (8)$$

These $K = 3$ levels contain the term $\pm h_0 J(J + 1)[J(J + 1) - 2][J(J + 1) - 6]$, first derived by Nielsen and Dennison (23) in their explanation of the anomalous effects in $K = 3$ lines observed by early microwave spectroscopists. The total splitting of the $K = 3$ levels is

$$\Delta \nu = [E^-(J, 3) - E^+(J, 3)]/h$$

$$= \left[2h_0 - \frac{18(h^4 \tau_{xxxz}/4h)^2}{F(J, 0) - F(J, 3)}\right] J(J + 1)[J(J + 1) - 2][J(J + 1) - 6]. \quad (9)$$

The part of Eq. (9) that is enclosed in brackets is not a constant because of the presence of the $F(J, 0) - F(J, 3)$ expression in the denominator. The denominator $F(J, 0) - F(J, 3)$ is a power series in $J(J + 1)$:

$$F(J, 0) - F(J, 3) = 9(B - C)\left[1 + \frac{9D_K}{B - C} + \frac{D_{JK} - 9H_{JKK}}{B - C} J(J + 1)\right.$$

$$\left. - \frac{H_{JJK} + 9L_{JJKK}}{B - C} J^2(J + 1)^2 - \frac{L_{JJJK}}{B - C} J^3(J + 1)^3\right]. \quad (10)$$

It is not sufficient to retain only the first term, $9(B - C)$. We found that a simultaneous, least-squares fit of the available data for normal transitions and forbidden transitions for the molecular constants did not converge properly unless the full expression was used.

The line strengths of the forbidden $\Delta K = \pm 3$ transitions (1, 2) are given by

$$S = \tfrac{1}{4}(\theta^{xx}_x)^2_{\text{eff}}(J \mp K)(J \mp K - 1)(J \mp K - 2)$$

$$\times (J \pm K + 1)(J \pm K + 2)(J \pm K + 3)(2J + 1)/J(J + 1) \quad (11)$$

where

$$(\theta^{xx}_x)_{\text{eff}} = \theta^{xx}_x + h^4 \tau_{xxxz}\mu_z/[2h(B - C)] \quad (12)$$

is the effective dipole moment inducing the transition. The term,

$$\theta^{xx}_x = 2(B)^2\left[\frac{a^{xx}_3}{\nu^2_3}\left(\frac{\partial \mu_x}{\partial Q_3}\right) + \frac{a^{xx}_4}{\nu^2_4}\left(\frac{\partial \mu_x}{\partial Q_4}\right)\right], \quad (13)$$

is an induced dipole component which results from admixture of the ground vibrational state with excited vibrational modes. This contribution, first recognized by Watson (2), is called vibrational intensity borrowing by Oka (10). The last term results from centrifugally induced mixing of rotational levels of the ground vibrational state. This contribution to the forbidden transitions, first derived by Hansen (1), is called rotational intensity borrowing by Oka (10). In this expression τ_{xxxz} is the centrifugal distortion constant in $\mathfrak{IC}'$ of Eq. (1), μ_z is the permanent dipole moment, and C and B are the spectral constants with reference to the symmetry axis and the perpendicular axis, respectively.

For the present molecules, the contribution of the vibrational intensity borrowing is small in comparison with that of the rotational intensity borrowing. For PH_3, Chu and Oka (4) calculated that $\theta^{xx}_x = 1.6 \times 10^{-5}$ D and that the centrifugally induced moment, the second term of Eq. (12), is 8.3×10^{-5} D. The relative contributions of these mo-

ments to the forbidden line strengths, Eq. (12), is $(1.6/8.3)^2 = 0.037$. Thus, for PH_3 in the ground vibrational state, the contribution of the vibrational mixing to the intensities of the $\Delta K = \pm 3$ transitions is negligible in comparison with that from rotational mixing. Chu and Oka also estimate that the centrifugal rotational intensity borrowing is the dominant term for PD_3.

4. RESULTS

Twelve $K = 0 \leftarrow 3$ transitions of PH_3 as well as ten $K = \pm 1 \leftarrow \pm 4$ and five $K = 0 \leftarrow 3$ transitions in PD_3 were measured. The observed frequencies are given in Tables I and II. Displacement in positions of lines of PH_3 caused by the Nielsen–Dennison splitting (23) of the $K = 3$ levels (105 MHz for $J = 10$ in PH_3) increased the difficulty of their detection. This splitting does not occur in the transitions observed by Chu and Oka (4), but it has been directly observed for PH_3 by Davis et al. (24) in a molecular beam resonance experiment. Location of the $K = 0 \leftarrow 3$ transitions would have been even more difficult were it not for our access to their molecular beam measurements.

The $\Delta K = \pm 3$ transitions exhibit a rapid change in the observed intensity with increasing value of J. Figure 3 illustrates the calculated intensity profile (see Eq. (14)). This variation is due partly to the increase in the rotationally induced coupling moment with J and partly to the variation in the population of J states. At the temperature of the observation, 300 K, the intensity reaches a maximum for $J = 10$. The solid vertical bars in Fig. 3 correspond to transitions that we have measured. The dashed vertical bars representing calculated lines have been included for better indication of the trend. Figure 4 shows actual recordings of two lines.

The peak absorption coefficients listed in Tables I and II were calculated from the formula,

$$\alpha(\text{cm}^{-1}) = \frac{1.147 \times 10^{-13}}{\Delta \nu T^{\frac{3}{2}}} \nu^2_0 \left(1 - \frac{h\nu_0}{2kT} \right)$$

$$\times \exp(-E_{J,K}/kT)[(B^2C)^{\frac{1}{2}} g_K g_I S[(J, K \pm 3) \leftarrow (J, K)]], \quad (14)$$

where the line-strength factor S is given by Eq. (11), $T = 300$ K, g_I is the reduced nuclear statistical weight factor (25), g_K is the statistical weight factor for each K level, and $\Delta \nu = 20$ MHz is the line breadth at a pressure of 1 Torr. This value for the $\Delta \nu$ is the same as that used by Chu and Oka (4) for PH_3. Other factors included in the numerical constant are described in Ref. (25).

We had little difficulty in detecting the $J = 3$, $\Delta J = 0$, $K = 0 \leftarrow 3$ transition which has a predicted intensity of only 7×10^{-10} cm^{-1}. From comparisons of the signal-to-noise ratios for the four weaker lines of PH_3 and PD_3 with the calculated line intensities given in Tables I and II, we estimate the sensitivity of our spectrometer to be approximately 4×10^{-10} cm^{-1}.

A combined computer analysis was made of the available frequencies for different types of transitions measured by us and by others as listed in Tables I and II. The analysis consisted of a least-squares fitting of 10 molecular constants to the observed frequencies of PH_3 and 9 to those of PD_3. The program calculates the difference in the energy levels by use of Eqs. (5)–(8) with assumed values of the molecular constants.

TABLE I

Observed Frequencies and Calculated Intensities for the FH_3 Transitions

Transition		Observed Frequency ν (MHz)	ν Obs − ν Calc	q_{max} (Calc) $(10^{-6} cm^{-1})$
Normal Rotational Transitions				
$J+1 \leftarrow J$ $K \leftarrow K$ (a)				
$J = 0$	$K = 0$	266 644.88	0.00	
1	0	533 794.32	0.00	
1	1	533 916.01	0.00	
Forbidden Rotational Transitions				
$J \leftarrow J$ $K = \pm 1 \leftarrow \mp 2$ (b)				
$J = 6$		47 961.18	0.41	2.2
7		47 178.68	−0.27	3.4
8		48 932.04	0.09	4.6
9		48 671.48	−0.14	5.3
10		48 377.80	−0.03	5.7
11		48 068.52	−0.06	5.5
12		48 714.84	−0.06	5.0
13		46 347.84	−0.07	4.2
14		44 658.68	−0.14	3.3
15		44 648.88	0.04	2.4
16		44 112.90	0.53	1.6
17		43 671.08	−0.32	1.1
$J \leftarrow J$ $K = 0 \leftarrow 3$ (c)				
$J = 3$		143 701.53	−0.09	0.7
4		143 331.01	−0.13	3.4

TABLE I (continued)

Transition	Observed Frequency ν (MHz)	ν Obs − ν Calc	q_{max} (Calc) $(10^{-6} cm^{-1})$
5	142 892.63	0.06	8.8
6	142 319.00	0.12	17.1
7	144 679.05	0.13	27.2
8	140 950.44	0.02	37.1
9	140 133.10	−0.14	44.8
10	139 226.51	0.07	48.5
11	138 228.01	−0.03	47.9
12	137 134.99	−0.02	43.5
13	135 941.42	0.00	36.6
14	134 741.42	0.02	28.6
Molecular Beam Resonance Transitions			
$K = 3$ Splittings (d)			
$J = 3$	0.052	0.000	
4	0.434	−0.002	
5	1.734	−0.007	
6	6.190	−0.010	
7	12.959	−0.027	
8	28.423	−0.025	
9	56.965	0.031	

(a) F. Helminger and W. Gordy, Phys. Rev. 188, 100 (1969).

(b) Chu and Oka, Ref. 4.

(c) Present work.

(d) Davies, et al., Ref. 24.

TABLE II (continued)

Transition	Observed Frequency ν (MHz)	ν Obs - ν Calc	q_{max} (MHz) $(10^{-8}\ cm^{-1})$
$J \rightarrow J$ $K = 0 \rightarrow -3$ (c)			
$J = 9$	93 905.96	-0.04	2.2
10	94 226.70	0.03	3.0
11	95 000.89	-0.06	3.7
12	94 724.43	-0.01	4.3
13	92 456.45	0.06	4.7
$J \rightarrow J$ $K = 1 \rightarrow +4$ (c)			
$J = 9$	165 467.87	-0.02	7.8
10	166 072.95	0.00	10.7
11	166 143.32	0.01	13.6
12	164 947.99	0.15	16.1
13	164 207.02	0.00	18.0
14	163 682.42	-0.08	19.0
15	163 104.72	-0.07	19.1
16	162 534.73	-0.08	18.4
17	161 913.22	-0.04	16.9
18	161 224.35	0.09	14.9

(a) F. Helminger and W. Gordy, Phys. Rev. 188, 100 (1969).

(b) Chu and Oka, Ref. 4.

(c) Present work.

TABLE II

Observed Frequencies and Calculated Intensities for the PH₃ Transitions

Transition	Observed Frequency ν (MHz)	ν Obs - ν Calc	q_{max} (MHz) $(10^{-? }\ cm^{-1})$
Normal Rotational Transitions			
$J+1 \leftarrow J$ $K \rightarrow K$ (a)			
$J = 0$ $K = 0$	133 928.17	0.06	
1 0	177 261.71	-0.01	
1 1	177 560.03	-0.04	
2 0	419 712.39	0.03	
2 1	419 724.18	-0.03	
2 2	419 747.81	0.01	
Forbidden Rotational Transitions			
$J \rightarrow J$ $K = 1 \rightarrow +2$ (b)			
$J = 13$	30 502.64	0.16	0.72
14	30 700.67	-0.04	0.80
15	30 587.40	0.06	0.82
16	30 471.60	-0.02	0.78
17	30 347.33	-0.11	0.71
18	30 017.40	0.16	0.62
19	30 061.32	0.15	0.53
20	29 694.20	0.22	0.43

PH$_3$ K = 0 ← 3 TRANSITIONS

FIG. 3. Calculated intensities for the $K = 0 \leftarrow 3$ lines observed in the present work (solid lines) and for some not observed (dotted lines).

Transition frequencies are calculated and compared to the measured transition frequencies to generate new estimates of the molecular constants. This iterative process is repeated many times by the computer until convergence is attained. The degree of fitting of the complete frequency set is shown by column 3 of Tables I and II. The molecular constants for PH$_3$ and PD$_3$ obtained from the combined analyses are listed in Table III. The constants h_0 and τ_{xxxz} for PD$_3$ are rather well determined since we were able to measure both the $K = \pm 1 \leftarrow \pm 4$ and $0 \leftarrow 3$ transitions. These same two constants for PH$_3$ are not nearly so well determined, because of their high statistical correlation and the lack of data from the $K = \pm 1 \leftarrow \pm 4$ transitions. The large uncertainties in the relative values of h_0 and the τ_{xxxz} do not appreciably limit the accuracy of the values of the other constants for PH$_3$.

There are only two independent structural parameters in PH$_3$ or PD$_3$, the bond angle and bond length. With the two measured moments, $I_b = h/8\pi^2 B_0$ and $I_c = h/8\pi^2 C_0$, an effective zero-point vibrational structure can be calculated for both species. The effective structural parameters thus derived are listed in Table IV. They are limited in

PH$_3$ K = 0 ← 3 TRANSITIONS
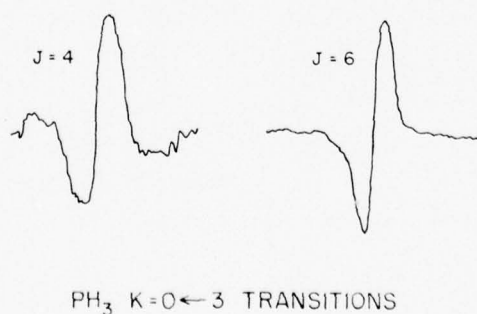
FIG. 4. Recordings of the $J = 4$ and $J = 6$, $K = 0 \leftarrow 3$, lines for PH$_3$ at 300 K.

TABLE III

Molecular Constants

Molecular Constant	PH_3	PD_3
B_0	$133\,480.15 \pm 0.12$ MHz	$69\,471.10 \pm 0.03$ MHz
C_0	$117\,483.85 \pm 0.16$ MHz	$58\,974.37 \pm 0.05$ MHz
D_J	3.947 ± 0.016 MHz	1.021 ± 0.002 MHz
D_{JK}	-5.182 ± 0.001 MHz	-1.312 ± 0.001 MHz
D_K	4.177 ± 0.011 MHz	1.023 ± 0.002 MHz
$\hbar^4 \tau_{xxxx}/4h$	0.62 ± 0.03 MHz	0.221 ± 0.005 MHz
H_{JJK}	-1.09 ± 0.04 kHz	-0.091 ± 0.004 kHz
h_0	67.6 ± 2.2 Hz	9.41 ± 0.22 Hz
L_{JJKK}	4.7 ± 0.7 Hz	
L_{JJJK}	0.32 ± 0.03 Hz	0.044 ± 0.005 Hz

accuracy by the uncorrected inertial defect. A second structure, the zero-point average structure (4) can also be calculated for each species from the observed B_0 and C_0 values. This structure was calculated by Chu and Oka for PH_3. We have recalculated the zero-point average values for the structural parameters with the B_0 and C_0 values derived from a computer analysis of the measured ground-state rotational transitions, as described above. The resulting parameters, listed in Table IV, are essentially the same as those obtained by Chu and Oka; the method used for calculation of the average

TABLE IV

Comparison of Different Structures for Phosphine

	Zero-point Effective[a]	Zero-point Average[b]	Equilibrium[b]
		PH_3	
r_{PH} (Å)	1.420_0	$1.4269_0 \pm 0.0002$	$1.4115_0 \pm 0.0006$
$\angle HPH$ (°)	93.34_5	$93.228_7 \pm 0.005$	$93.32_8 \pm 0.02$
		PD_3	
r_{PD} (Å)	1.417_6	$1.4226_5 \pm 0.0001$	$1.4115_0 \pm 0.0006$
$\angle DPD$ (°)	93.35_0	$93.256_7 \pm 0.004$	$93.32_8 \pm 0.02$

a. Uncorrected for inertial defects.

b. Calculated as described by Chu and Oka, Ref. 4.

structural values is the one they describe. Discussion of the significance or meaning of the various types of structures and methods for calculations of each type is given by Gordy and Cook (25).

REFERENCES

1. H. M. HANSON, *J. Mol. Spectrosc.* **23**, 287 (1967).
2. J. K. G. WATSON, *J. Mol. Spectrosc.* **40**, 536 (1971).
3. F. Y. CHU AND T. OKA, *J. Mol. Spectrosc.* **48**, 612 (1973).
4. F. Y. CHU AND T. OKA, *J. Chem. Phys.* **60**, 4612 (1974).
5. A. G. MAKI, R. L. SAMS, AND W. B. OLSON, *J. Chem. Phys.* **58**, 4502 (1973).
6. D. HELMS AND W. GORDY, *Bull. Am. Phys. Soc.* **21**, 380 (1976).
7. J. K. G. WATSON, *J. Mol. Spectrosc.* **55**, 498 (1975).
8. F. MICHELOT, J. MORET-BAILLY, AND K. FOX, *J. Chem. Phys.* **60**, 2606, 2610 (1974).
9. I. OZIER, *J. Mol. Spectrosc.* **56**, 124 (1975).
10. T. OKA, Forbidden rotational transitions, *in* "Molecular Spectroscopy: Modern Research" (K. Narahari Rao and C. W. Mathews, Eds.), Vol. II, p. 229, Academic Press, New York, 1976.
11. M. MIZUSHIMA AND P. VENKATESWARLU, *J. Chem. Phys.* **21**, 705 (1953).
12. A. ROSENBERG, I. OZIER, AND A. K. KUDIAN, *J. Chem. Phys.* **57**, 568 (1972).
13. A. ROSENBERG AND I. OZIER, *Chem. Phys. Lett.* **13**, 400 (1973).
14. A. ROSENBERG AND I. OZIER, *Can. J. Phys.* **52**, 575 (1974).
15. A. ROSENBERG AND I. OZIER, *J. Chem. Phys.* **58**, 5168 (1973).
16. C. W. HOLT, M. C. L. GERRY, AND I. OZIER, *Phys. Rev. Lett.* **31**, 1033 (1973).
17. D. LAUGHTON, S. M. FREUND, AND T. OKA, *J. Mol. Spectrosc.* **62**, 263 (1976).
18. T. OKA, *J. Chem. Phys.* **47**, 5410 (1967).
19. G. HERZBERG, "Infrared and Raman Spectra of Polyatomic Molecules," Van Nostrand–Reinhold, Princeton, N. J., 1945. See also JON T. HOUGEN, *J. Chem. Phys.* **37**, 1433 (1962).
20. T. M. SUGDEN AND C. N. KENNEY, "Microwave Spectroscopy of Gases," Van Nostrand, New York, 1965.
21. G. AMAT, H. H. NIELSEN, AND G. TARRAGO, "Rotation–Vibration of Polyatomic Molecules," Marcel Dekker, New York, 1971.
22. W. B. OLSON, private communication.
23. H. H. NIELSEN AND D. DENNISON, *Phys. Rev.* **72**, 1011 (1947).
24. P. DAVIES, R. NEUMANN, S. WOFSY, AND W. KLEMPERER, *J. Chem. Phys.* **55**, 3564 (1971).
25. W. GORDY AND R. COOK, "Microwave Molecular Spectra," Wiley–Interscience, New York, 1970.

The study of laser processes by millimeter and submillimeter microwave spectroscopy[a)]

Frank C. De Lucia

Department of Physics, Duke University, Durham, North Carolina 27706
(Received 5 July 1977; accepted for publication 31 August 1977)

Millimeter and submillimeter microwave spectroscopy is shown to be a powerful technique for the study of the fundamental processes of molecular lasers. The calculation of absolute chemical compositions, excitation parameters, and the observation of collisional deexcitation are demonstrated for the HCN FIR laser.

Although a number of techniques have been described for the study of the fundamental processes of molecular lasers,[1-5] much remains to be understood about their chemistry, excitation mechanisms, and decay pathways. This letter reports the results of experiments that demonstrate the unique capabilities of millimeter and submillimeter microwave spectroscopy in this field.

In this spectral region, molecular laser plasmas are transparent except at molecular resonances and emit insignificant noise. This latter property is directly related to the well-known difficulty of producing radiation in the submillimeter/far-infrared region of the spectrum. Equally important, the noise modulation of the probing signal due to plasma fluctuations decreases rapidly as the signal frequency is increased from the centimeter-wave region into the millimeter and sub-

millimeter region. Rotational line strengths also increase as approximately $1/\lambda^3$ and their transition moments are orders of magnitude stronger than those of the vibrational transitions studied in the infrared. Because of the widely tunable spectral coverage of our technique, studies of both nonradiative states and species as well as those that participate directly in the lasing process are possible. The sharpness of the resonances ($\Delta\nu \leq 1$ MHz) is such that the different states and species are well resolved and can be studied independently. Of equal importance is the direct relation between the experimental observables (frequencies, absorption coefficients, linewidths, and lifetimes) and the dynamics of the molecular laser systems.

Our experiment is shown in Fig. 1.[6] Microwave energy in the 30−60-GHz range is produced by a reflex klystron. A small portion of this signal is compared with a frequency standard and the rest matched onto a crystal harmonic generator. The harmonic output of this generator (typically 3rd → 12th harmonic) is trans-

FIG. 1. Spectrometer for the study of laser plasmas.

FIG. 3. Excitation of the 10^00 and 00^01 vibrational states of HCN.
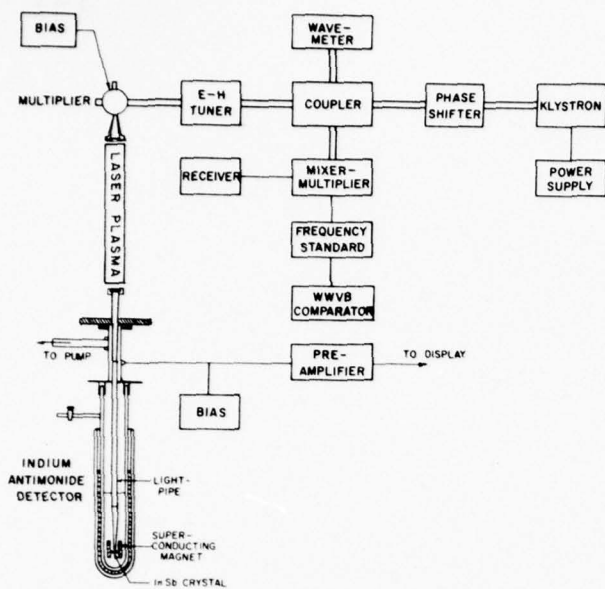
mitted through the laser tube by quasioptical techniques and detected by a 1.4 K InSb photodetector. The sensitivity of this technique is such that states whose populations are $\sim 10^9/cm^3$ can be seen in real time on an oscilloscope screen with large signal to noise.

It can be shown that to a good approximation the absorption coefficient α for a linear molecule can be written

$$\alpha \ (cm^{-1}) = (4.94 \times 10^{-3}) F_v \mu^2 \nu_0^3 / \Delta \nu T^2, \qquad (1)$$

where ν_0 (GHz) is the transition frequency, $\Delta \nu$ (MHz/Torr) is the linewidth, μ (D) is the dipole moment, T (K) is the temperature, and F_v is the fraction of molecules in the vibrational state.[7] This relation assumes that the rotational states and molecular velocities are in equilibrium and can be described by a temperature T. For pure rotational spectra μ and ν_0 are known to high accuracy and $\Delta \nu$ can be accurately measured from the high-resolution microwave data. The

relation

$$\Delta P/P = 1 - \exp(-\alpha l) \qquad (2)$$

relates the experimental data $\Delta P/P$ with α and ultimately with F_v.

Three studies of the HCN FIR molecular laser which illustrate the kinds of information that can be acquired are described below. CH_3CN was used as the fuel.

The total HCN concentration is an important, but unknown, parameter of the laser. Chantry[8] estimates it as 1 μm partial pressure for typical operating conditions, and Schötzan and Kneubühl[1] have measured with a mass spectrometer the *relative* concentration as a function of discharge current. Figure 2 shows results calculated from measurements on the $J = 0 \rightarrow 1$ transition of the 00^00 vibrational state. In our experiment, the HCN concentration is maximum at a remarkably low current (typically 0.01 A) and decreases substantially at higher currents.

The well-known HCN laser mechanism of Lide and Maki[3] depends upon the near degeneracy of $J = 10$ in the 11^10 and 04^00 vibrational states and a population inversion between them in the laser plasma. This inversion has often been attributed[8,9] to the metastable nature of the 10^00 state and the bending stack built upon it. Figure 3 shows the absolute populations of the 10^00 and 00^01 states as a function of the discharge current. It should be noted that these states are essentially equally populated and that the "metastable" nature of 10^00 is thus shown not to be a requirement for a population excess.
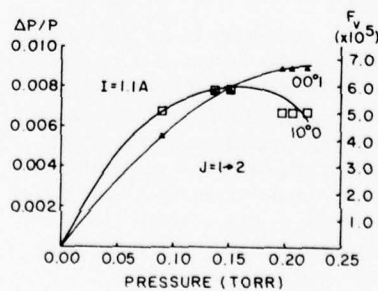

FIG. 2. Total HCN concentration derived from the $J = 0 \rightarrow 1$ rotational absorption in the ground vibrational state.

FIG. 4. Pressure dependence of the excitation of the 10^00 and 00^01 vibrational states of HCN.

Figure 4 shows the population of $10^0 0$ and $00^0 1$ as a function of pressure. These results are consistent with a model in which resonant deexcitation between the $(0, n, 0)$ and $(1, n-3, 0)$ bending stacks is an important limiting factor on the operating pressure of the HCN laser. On the other hand, the $(0, n, 1)$ stack is not in close resonance with another family of states and maintains its excitation at substantially higher pressures.

In conclusion, we have demonstrated the kinds of information that can be obtained in a very direct manner from our experiments. It is clear that they have applicability both to other states and species found in the HCN laser and to molecular lasers in general. These data provide both constraints and tests for models of the complex dynamics of these systems as well as suggestions for new models.

[1] H. J. Schötzau and F. Kneubühl, IEEE J. Quantum Electron. QE-11, 817 (1975).
[2] L. E. Sharp and A. T. Wetherell, Appl. Opt. 11, 1737 (1972).
[3] D. R. Lide and A. G. Maki, Appl. Phys. Lett. 11, 52 (1967).
[4] H. J. Schötzau and F. Kneubühl, Appl. Phys. 6, 25 (1975).
[5] M. Yamanaka, T. Yamauchi, and H. Yoshimaga, Jpn. J. Appl. Phys. 10, 1601 (1971).
[6] P. Helminger, F. C. De Lucia, and W. Gordy, Phys. Rev. Lett. 25, 1397 (1970).
[7] W. Gordy and R. L. Cook, *Microwave Molecular Spectra* (Wiley-Interscience, New York, 1970).
[8] G. W. Chantry, *Submillimetre Spectroscopy* (Academic, New York, 1971).
[9] J. P. Pichamuthu, J. Phys. D 7, 1096 (1974).

NOTES

Centrifugal Distortion in Water and Hydrogen Sulfide[1]

It is the intent of this note to present specific results pertaining to the changes in molecular geometry of water and hydrogen sulfide which are induced by centrifugal effects in rotational states of the molecules. Hydrogen, deuterium, and tritium substitutions are considered. A general expression for centrifugally induced geometry changes has been presented by Toyama et al. (1) but specific results included only the symmetric forms of water, H_2O and D_2O. A sign error is present in that work but appears to be only typographical, as the numerical results given are correct. The term $\mu \sin \alpha$ in Eq. (53) should be negative. Considerable simplification occurs in the symmetric cases and a calculation of centrifugal distortion in HDO, DTS, etc., must proceed from the most general approach.

TABLE I. Coefficients of Eq. (3) for Water and Hydrogen Sulfide[a]

	ρ	$\Delta r/r$	$\Delta\alpha$			$\Delta r/r$	$\Delta\alpha$
H_2O	a	1.016	-10.742		H_2S	0.300	-2.878
	b	0.293	3.041			0.212	2.238
	c	0.247	0.000			0.126	0.012
D_2O	a	0.565	-5.976		D_2S	0.159	-1.525
	b	0.147	1.521			0.106	1.120
	c	0.126	0.070			0.064	0.025
T_2O	a	0.415	-4.390		T_2S	0.112	-1.075
	b	0.098	1.016			0.071	0.748
	c	0.086	0.090			0.044	0.029

	ρ	$\Delta r_1/r_1$	$\Delta r_2/r_2$	$\Delta\alpha$		$\Delta r_1/r_1$	$\Delta r_2/r_2$	$\Delta\alpha$
HDO	a	0.969	0.673	-9.192	HDS	0.372	0.083	-2.639
	b	0.065	0.293	1.488		0.008	0.179	0.705
	c	0.111	0.204	0.030		0.046	0.088	0.013
HTO	a	0.955	0.606	-9.160	HTS	0.374	0.075	-2.855
	b	0.028	0.232	0.857		0.002	0.125	0.370
	c	0.066	0.170	0.034		0.026	0.074	0.012
DTO	a	0.541	0.449	-5.334	DTS	0.189	0.071	-1.359
	b	0.072	0.157	1.117		0.021	0.116	0.632
	c	0.084	0.117	0.076		0.037	0.054	0.022

[a] All coefficients have been multiplied by 10^4; angles are in radians; r_1 is associated with the lighter atom in the asymmetric species.

330

The general expression for the distortion effects are given in Ref. (*1*) in matrix form

$$\langle R \rangle_{cent} = F_R{}^{-1}G_R{}^{-1}B\Phi X,\tag{1}$$

where

$$\langle R \rangle_{cent} = \begin{pmatrix} \Delta r_1 \\ \Delta r_2 \\ (r_1 r_2)^{\frac{1}{2}}\Delta\alpha \end{pmatrix}\tag{2}$$

and **X** is, in the case of the bent triatomic molecule, a nine component vector describing the position of the three nuclei in a body fixed Cartesian coordinate system which is parallel to the molecular inertial axes. F_R, G_R, **B**, and Φ are defined in Ref. (*1*). As was shown by the authors of Ref. (*1*), it is convenient to rewrite Eq. (1) as

$$\langle R \rangle_{cent} = \rho_a \langle P_a{}^2 \rangle + \rho_b \langle P_b{}^2 \rangle + \rho_c \langle P_c{}^2 \rangle,\tag{3}$$

where a, b, and c designate the molecular inertial axes and $\langle P_a{}^2 \rangle$, etc., are the expectation values of the angular momentum component operators along the molecular equilibrium axes. These values may be easily calculated for any specific rotational level of a given molecule (*2*). The vector coefficients ρ_a, ρ_b, and ρ_c of Eq. (3), which are defined in Ref. (*1*), have been evaluated and are presented in Table I for water and hydrogen sulfide. Coefficients for H_2O and D_2O have been recalculated for completeness.

The force constants used are those of Cook, De Lucia, and Helminger (*3*, *4*). As noted by the authors of Refs. (*3*) and (*4*), model errors produce significant uncertainties in the values of the force constants. The constants used are those obtained from infrared data with equal weighting. These uncertainties are the primary limitation to the accuracy of the coefficients of this work and those of Ref. (*1*). Symmetric forms of water and hydrogen sulfide distort symmetrically and only one coefficient is necessary to describe the change in bond length. In the case of the asymmetric forms, changes in both bonds must be specified. In Table I, r_1 refers to the bond extending from the apex atom to the atom of least mass.

REFERENCES

1. M. TOYAMA, T. OKA, AND Y. MORINO, *J. Mol. Spectrosc.* **13**, 193 (1964).
2. W. GORDY AND R. L. COOK, "Microwave Molecular Spectra," Wiley-Interscience, New York, 1970.
3. R. L. COOK, F. C. DE LUCIA, AND P. HELMINGER, *J. Mol. Spectrosc.* **53**, 62 (1974).
4. R. L. COOK, F. C. DE LUCIA, AND P. HELMINGER, *J. Mol. Struct.* **28**, 237 (1975).

R. MICHAEL GARVEY[2]

Department of Physics
Duke University
Durham, North Carolina 27706

[2] Present address: National Bureau of Standards, Boulder, Colorado 80302.

Millimeter spectrum and molecular constants of silicon monoxide*

E. Lowry Manson, Jr., William W. Clark, Frank C. De Lucia, and Walter Gordy

Department of Physics, Duke University, Durham, North Carolina 27706

(Received 4 August 1976)

A new high-temperature millimeter-wave microwave spectrometer has been constructed and used to measure a wide range of vibrational and rotational states of silicon monoxide. This work results in accurate rest frequencies for all of the interstellar SiO maser transitions that have been observed as well as accurate measurements or predictions of all transitions that are likely to be of astrophysical interest. In addition, the Dunham spectral and potential constants are calculated for the three major isotopic species. For $^{28}Si^{16}O$: $Y_{01} = 21787.453(11)$ MHz, $Y_{11} = -151.026(11)$ MHz, $Y_{21} = 70.5(24)$ kHz, $Y_{02} = -29.38(13)$ kHz, $a_0 = 5.390(22) \times 10^5$ cm^{-1}, $a_1 = -2.9899(41)$, $a_2 = 5.7(7)$, $a_3 = -9.0(5)$. The calculated equilibrium parameters for $^{28}Si^{16}O$ are $B_e = 21787.5(10)$ MHz, $\omega_e = 1252.(3)$ cm^{-1}, $\omega_e x_e = 5.96(71)$ cm^{-1}, and $r_e = 1.50973(4)$ Å.

INTRODUCTION

In 1968, Törring[1] reported the laboratory measurement of the $J = 0 \rightarrow 1$ rotational transitions of $^{28}Si^{16}O$ in the 43-GHz region for four vibrational states, $v = 0, 1, 2, 3$. Meanwhile, a maser signal at 86243 MHz, observed by radioastronomers[2] in the nebular source Orion A, has been assigned to the $J = 2 \rightarrow 1$, $v = 1$ transition of $^{28}Si^{16}O$ by Lovas and Johnson[3] from a theoretical prediction of the frequency based on Törring's measurement of the $J = 0 \rightarrow 1$ transition. Since that time, SiO maser emission lines corresponding to the transitions $v = 1$, $J = 1 \rightarrow 0$; $v = 1$, $J = 2 \rightarrow 1$; $v = 1$, $J = 3 \rightarrow 2$; and $v = 2$, $J = 1 \rightarrow 0$ have been observed in 20 astronomical sources.[4]

With the present work, direct laboratory measurements have been made of the frequencies of all of the transitions which give rise to the important maser signals from outer space, and measurements of the rotational spectrum of $^{28}Si^{16}O$ are extended to 303926.96 GHz. These measurements, shown in Table I, include seven rotational transitions of $^{28}Si^{16}O$ in five vibrational states. They allow precise evaluation of the centrifugal distortion effects which influence all rotational and vibrational constants of the molecule and which cannot be evaluated from the $J = 0 \rightarrow 1$ transition alone. These constants make possible the accurate prediction of all transitions that are likely to be of astrophysical interest. Figure 1 shows the laboratory, real-time oscilloscope display of the most commonly observed astrophysical maser, the $J = 2 \rightarrow 1$, $v = 1$ transition.

EXPERIMENT

A sufficient concentration of silicon monoxide vapor for microwave absorption measurements was produced by the heating of a homogeneous mixture of silicon and silicon dioxide to 1350 °C in a high-temperature reaction chamber which also served as the microwave absorption cell. This combination of reaction chamber and absorption cell consisted of a Mullite MV30 ceramic tube (9×45 cm) concentrically positioned inside a cold-rolled steel pipe (25×105 cm) which was connected to a pumping line. For the purpose of mechanical support and thermal insulation, the volume between the ceramic tube and the outer steel jacket was filled with A.P. Green G-26 insulating firebricks. The heating element was constructed from ten graphite welding rods which were electrically connected in series and equally spaced around the inside of the Mullite tube.

A tapered horn combined with a Teflon lens focused the microwave radiation into the reaction chamber and through the vapor above the reactants. The radiation emerging from the reaction zone was then focused onto a sensitive InSb radiation detector operated at 1.6 °K. The detected absorption-line signals, after amplification, were displayed on an oscilloscope for the frequency measurements. Description of the millimeter-wave spectrometer and measuring techniques are given in an earlier publication.[5]

DATA AND ANALYSIS

The most accurate formulas for analysis of the rotational spectra of diatomic molecules are provided by Dunham theory.[6] Dunham solved the Schrödinger wave equation for the diatomic vibrating rotor with a potential function of the form

$$V(\xi) = cha_0\xi^2(1 + a_1\xi + a_2\xi^2 + \cdots), \qquad (1)$$

where $\xi = (r - r_e)/r_e$, $a_0 = \omega_e^2/4B_e$, and $a_1, a_2, \ldots$ are the potential constants. His solution for the rotation-vibration energies is expressed by the

TABLE I. Observed transitions of silicon monoxide.

$J \to J+1$	v	Measured frequencies (MHz)	Difference from calculated frequencies (MHz)
		$^{28}\text{Si}^{16}\text{O}$	
$0 \to 1$	0	43 423.76 [a]	−0.04
	1	43 122.03 [a]	0.00
	2	42 820.48 [a]	−0.06
	3	42 519.34 [a]	0.01
$1 \to 2$	0	86 846.96	0.07
	1	86 243.37	0.02
	2	85 640.46	0.09
$2 \to 3$	0	130 268.61	0.04
	1	129 363.24	−0.02
$3 \to 4$	0	173 688.31	0.16
	1	172 481.15	0.09
	2	171 275.28	0.18
	3	170 070.35	0.07
$4 \to 5$	0	217 104.98	0.09
	1	215 595.95	−0.09
	2	214 088.54	−0.06
	3	212 582.60	0.04
	4	211 077.87	−0.07
$5 \to 6$	0	260 518.02	−0.09
	1	258 707.45	−0.04
$6 \to 7$	0	303 926.96	−0.15
		$^{29}\text{Si}^{16}\text{O}$	
$0 \to 1$	0	42 879.82 [a]	0.00
		$^{30}\text{Si}^{16}\text{O}$	
$0 \to 1$	0	42 373.34 [a]	0.00

[a] Reference 1.

series

$$E_{v,J} = h \sum_{l,m} Y_{l,m}(v+\tfrac{1}{2})^l [J(J+1)]^m , \qquad (2)$$

in which the coefficients $Y_{l,m}$ are now known as

FIG. 1. Video display of the $J = 1 \to 2$, $v = 1$ transition of $^{28}\text{Si}^{16}\text{O}$.

Dunham's constants. Each $Y_{l,m}$ is a function of the molecular parameters $r_e, a_0, a_1, a_2, \ldots$ which appear in Eq. (1). In terms of the familiar spectroscopic constants,

$$Y_{10} \approx \omega_e , \quad Y_{01} \approx B_e , \quad Y_{11} \approx -\alpha_e , \quad Y_{21} \approx \gamma_e ,$$
$$Y_{20} \approx -\omega_e x_e , \quad Y_{02} \approx -D_e , \quad Y_{12} \approx -\beta_e , \quad Y_{03} \approx H_e . \qquad (3)$$

With the selection rules $J \to J+1$ and $v \to v$ for pure rotational transitions, Eq. (2) predicts the rotational frequencies to be

$$\nu_{v,\,J \to v,\,J+1} = 2\big[Y_{01} + Y_{11}(v+\tfrac{1}{2}) + Y_{21}(v+\tfrac{1}{2})^2 + \cdots \big](J+1)$$
$$+ 4Y_{02}(J+1)^3 + \cdots , \qquad (4)$$

where only terms which give a detectable contribution to the spectra reported in this paper are retained. For the less abundant isotopic species the Dunham isotope relation,

$$Y'_{l,m} = (\mu/\mu')^{(l+2m)/2} Y_{l,m} , \qquad (5)$$

is accurate to within experimental error for all $Y_{l,m}$ except $Y_{0,1}$. In Eq. (5) μ' denotes the reduced mass of the less abundant species, and the unprimed parameters, $Y_{l,m}$ and μ, refer to the parent species ($^{28}\text{Si}^{16}\text{O}$).

The silicon monoxide microwave spectrum was analyzed by substitution of each measured absorption frequency and the appropriate J and v quantum numbers into Eq. (4). In this manner a

TABLE II. Comparison of molecular constants measured in this work with previous values.

Constants	$^{28}\text{Si}^{16}\text{O}$		$^{29}\text{Si}^{16}\text{O}$		$^{30}\text{Si}^{16}\text{O}$	
	This work [a]	Others	This work	Others	This work	Others
Y_{01} (MHz)	21 787.453(11)	21 787.462(25) [b]	21 514.046(13)	21 514.074(25) [b]	21 259.494(13)	21 259.425(25) [b]
Y_{11} (MHz)	−151.026(11)	−151.05(4) [b]	−148.193(11)	−148.22(4) [b]	−145.570(11)	−145.59(4) [b]
Y_{21} (kHz)	70.5(24)	76.(1) [b]	68.7(24)	74.(1) [b]	67.1(24)	72.(1) [b]
Y_{02} (kHz)	−29.38(13)	−29.9(1) [b,c]	−28.64(13)	−29.2(1) [b,c]	−27.97(13)	−28.5(1) [b,c]
B_e (MHz)	21 787.5(10)		21 514.1(10)		21 259.5(10)	
ω_e (cm^{-1})	1 252.(3)	1 241.4(1)	1 244.(3)		1 237.(3)	
$\omega_e x_e$ (cm^{-1})	5.96(71)	5.9(1)	5.89(71)		5.82(71)	

[a] Numbers in parentheses represent one standard deviation.
[b] Reference 1.
[c] Reference 7.

TABLE III. Potential constants and equilibrium bond length for silicon monoxide.

	This work[a]	Ref. 1
a_0	$5.390(22) \times 10^5$ cm^{-1}	$5.298(1) \times 10^5$ cm^{-1}
a_1	$-2.9899(41)$	$-2.973(2)$
a_2	$5.7(7)$	$5.58(10)$
a_3	$-9.0(5)$	$-8.32(75)$
r_e	$1.509\,733(40)$ Å	$1.509\,732(40)$ Å

[a] Errors are in standard deviation.

set of N simultaneous equations in six unknowns was constructed, where N is the number of experimentally measured frequencies and where the six unknown constants are Y_{01}, Y_{11}, Y_{21}, and Y_{02} for $^{28}Si^{16}O$, plus the Y_{01} values for $^{29}Si^{16}O$ and $^{30}Si^{16}O$. By the method of least squares, this set

of equations was solved for these constants. The vibrational constants Y_{10} and Y_{20} were calculated for each isotopic species by use of the following relations:

$$Y_{10} = (4Y_{01}^3/- Y_{02})^{1/2} \qquad (6)$$

and

$$Y_{20} = \tfrac{3}{2} Y_{01}(a_2 - \tfrac{5}{4} a_1^2) , \qquad (7)$$

where a_1 and a_2 are the Dunham potential constants which appear in Eq. (1).

RESULTS AND COMMENTS

Table II summarizes the results of this analysis and gives a comparison of the rotational, vibrational, and potential constants derived from our measurements with those obtained by others.

TABLE IV. Predicted rotational spectrum of silicon monoxide.

		$^{28}Si^{16}O$		$^{29}Si^{16}O$		$^{30}Si^{16}O$	
Transition		Predicted		Predicted		Predicted	
v	$J \rightarrow J'$	frequency	Uncertainty	frequency	Uncertainty	frequency	Uncertainty
0	0 → 1	43 423.798	0.015	42 879.820	0.025	42 373.340	0.025
1	0 → 1	43 122.027	0.015	42 583.710	0.028	42 082.469	0.028
2	0 → 1	42 820.539	0.015	42 287.874	0.030	41 791.866	0.030
3	0 → 1	42 519.332	0.015	41 992.314	0.030	41 501.531	0.030
4	0 → 1	42 218.407	0.026	41 697.028	0.035	41 211.465	0.034
5	0 → 1	41 917.764	0.052	41 402.018	0.053	40 921.667	0.052
0	1 → 2	86 846.891	0.028	85 758.953	0.050	84 746.009	0.050
1	1 → 2	86 243.350	0.020	85 166.732	0.056	84 164.266	0.056
2	1 → 2	85 640.373	0.022	84 575.061	0.060	83 583.060	0.060
3	1 → 2	85 037.959	0.025	83 983.940	0.060	83 002.391	0.060
4	1 → 2	84 436.110	0.052	83 393.369	0.070	82 422.259	0.069
5	1 → 2	83 834.824	0.103	82 803.348	0.106	81 842.663	0.103
0	2 → 3	130 268.574	0.037	128 636.710	0.076	127 117.335	0.076
1	2 → 3	129 363.262	0.027	127 748.379	0.085	126 244.721	0.085
2	2 → 3	128 458.796	0.030	126 860.873	0.092	125 372.912	0.092
3	2 → 3	127 555.176	0.034	125 974.192	0.092	124 501.908	0.092
4	2 → 3	126 652.402	0.075	125 088.335	0.105	123 631.710	0.104
5	2 → 3	125 750.473	0.153	124 203.303	0.158	122 762.317	0.154
0	3 → 4	173 688.142	0.046	171 512.406	0.104	169 486.647	0.104
1	3 → 4	172 481.060	0.035	170 327.964	0.118	168 323.162	0.117
2	3 → 4	171 275.105	0.041	169 144.623	0.127	167 160.750	0.127
3	3 → 4	170 070.278	0.045	167 962.381	0.126	165 999.411	0.126
4	3 → 4	168 866.579	0.098	166 781.239	0.142	164 839.147	0.140
5	3 → 4	167 664.008	0.202	165 601.196	0.210	163 679.957	0.205
0	4 → 5	217 104.891	0.058	214 385.351	0.138	211 853.275	0.137
1	4 → 5	215 596.037	0.052	212 904.800	0.157	210 398.918	0.156
2	4 → 5	214 088.594	0.061	211 425.623	0.168	208 945.902	0.167
3	4 → 5	212 582.560	0.062	209 947.820	0.166	207 494.230	0.165
4	4 → 5	211 077.936	0.122	208 471.392	0.183	206 043.899	0.181
5	4 → 5	209 574.722	0.249	206 996.339	0.264	204 594.912	0.258
0	5 → 6	260 518.114	0.084	257 254.860	0.181	254 216.546	0.180
1	5 → 6	258 707.489	0.086	255 478.198	0.206	252 471.317	0.204
2	5 → 6	256 898.557	0.095	253 703.185	0.219	250 727.699	0.217
3	5 → 6	255 091.317	0.094	251 929.823	0.216	248 985.692	0.214
4	5 → 6	253 285.768	0.152	250 158.109	0.232	247 245.296	0.228
5	5 → 6	251 481.912	0.298	248 388.046	0.322	245 506.510	0.315

Törring[1] could not determine the effects of centrifugal distortion from his microwave measurements alone; but, by combining his accurate measurements of the $J = 0 \rightarrow 1$ transition with the earlier measurements of the vibrational spectra of SiO by Lagerqvist and Uhler,[7] he was able to make corrections for these effects in his derived constants. We believe that the vibrational constant ω_e, which we have derived entirely from microwave measurements (see Table II), is more accurate than the values obtained more directly from vibrational spectra. The inclusion of Törring's frequencies for the $J = 0 \rightarrow 1$ transitions with our results did not alter the constants derived from our results alone. We conclude that his measurements are at least as accurate as ours.

Table III gives the Dunham potential constants a_0, a_1, a_2, a_3 which were calculated from the $Y_{l,m}$'s of Table II. The Y_{12} constant, which is necessary for the computation of the constants a_2 and a_3 but not recorded in Table II, was found to be zero within the limits of experimental error. A contribution to the uncertainty in the a_i from a calculated upper limit for Y_{12} is included in our estimates of the uncertainty in the a_i. This contribution, as well as other contributions, was neglected in Törring's uncertainties. Although our listed uncertainties are somewhat larger than those quoted for previous work, our a_i values are, in fact, substantially more accurate. The values for B_e which appear in Table II were obtained from Y_{01} by application of the Dunham correction. The wobble-stretch correction is zero to within experimental error, but a calculated upper limit on it is included in the uncertainty.[5]

Table IV shows a set of predictions of all transitions that appear to be of possible astrophysical interest as well as the uncertainties in these predictions. For the higher v, J states, these predictions are comparable in accuracy with the experimental observations, but at low v, J they are substantially better.

---

[1]T. Törring, Z. Naturforsch. 23a, 777 (1968).

[2]L. E. Snyder and D. Buhl, Astrophys. J. 189, L31 (1974).

[3]F. J. Lovas and D. R. Johnson (unpublished).

[4]L. E. Snyder and D. Buhl, Astrophys. J. 197, 329 (1975).

[5]E. L. Manson, F. C. De Lucia, and W. Gordy, J. Chem. Phys. 62, 1040 (1975).

[6]J. L. Dunham, Phys. Rev. 41, 721 (1932).

[7]A. Lagerqvist and U. Uhler, Ark. Fys. 6, 95 (1953).

Millimeterwave spectroscopy of active laser plasmas; the excited vibrational states of HCN[a)]

Franck C. De Lucia

Department of Physics, Duke University, Durham, North Carolina 27706

Paul A. Helminger[b)]

Department of Physics, University of South Alabama, Mobile, Alabama 36688
(Received 30 June 1977)

Millimeter and submillimeter microwave techniques have been used for the spectroscopic study of an HCN laser plasma. Forty-seven rotational transitions in 12 excited vibrational states have been observed. Numerous rotational, vibrational, and perturbation parameters have been calculated from these data. A discussion of experimental techniques is included.

I. INTRODUCTION

The selective excitation of vibrational states in discharges or in the products of discharges is the basis for a number of important molecular lasers. Calculations based on oscillation threshold conditions show that these highly excited states are sufficiently populated in active laser plasmas for study by the techniques of quasioptical millimeter and submillimeter microwave spectroscopy. Most molecular lasers are active on small molecular species with large rotational constants and favorable partition functions. As a result, spectral coverage throughout the millimeter region and into the submillimeter region is required if for no other reason than to reach the transitions of interest. Microwave studies of these highly excited vibrational states are uncommon due to their vanishingly small populations at room temperature.

Many interesting and complex vibration–rotation interactions become important at microwave resolution and can be studied by these techniques. In addition, they are a powerful means for the study of the physics of the complex molecular laser systems. We have given a preliminary report on a study of the HCN laser[1] and a full discussion will be published elsewhere.

HCN has been extensively studied in the infrared and has been the prototype molecule for investigations of vibration–rotation interactions in linear molecules.[2–6] Rotational transitions in the ground vibrational state were among the first to be observed by millimeter microwave spectroscopy[7] and transitions in low lying, thermally populated vibrational states have also been investigated.[5,6,8] In this paper are reported spectroscopic studies in the millimeter and submillimeter microwave region of 12 excited vibrational states of HCN. Included are the 11^10 and 04^00 states which are the basis of the well known laser emission in the far infrared.

II. EXPERIMENTAL

The millimeter and submillimeter wave region of the spectrum is in many ways ideal for the study of the

molecular species contained in laser plasmas. A corollary of the well-known difficulty of producing radiation in this spectral region is that laser plasmas emit almost no interfering radiation. It can also be shown that the noise modulation of the microwave signal due to fluctuations in the index of refraction which result from plasma instabilities decreases systematically with increases in frequency. In addition, at lower microwave frequencies, the quasioptical techniques that allow the remote sampling of the plasma are difficult and rotational line strengths decrease as approximately ν^3. At infrared wavelengths the vibrational transitions are orders of magnitude weaker than the strong pure-rotational transitions studied in this work, and the emission of noise increases sharply. It is interesting to note that other spectroscopic techniques have been unable to establish the existence of HCN in *any* vibrational state in the laser plasma.[9]

Figure 1 shows the details of the system used for this study.[10] Energy in the millimeter and submillimeter region is produced by klystron driven crystal harmonic generation. The output of this generator is focused by quasioptical techniques through the laser plasma and detected by an InSb photodetector which operates at $1.4\,^\circ$K. Because only the stretching modes are preferentially excited in a laser discharge,[1] the lower energy bending modes were thermally populated in a cell at $600\,^\circ$K. The sensitivity of this technique is such that all studies reported in this paper are either the result of real time measurements on an oscilloscope screen or lock-in techniques with $\tau \leqslant 1$ sec.

III. THEORY

In principle, the energy levels and rotational transition frequencies of HCN can be calculated by construction and diagonalization of the vibration–rotation Hamiltonian. Although this procedure leads directly to the unperturbed spectral constants, it requires iterative nonlinear fitting and makes prediction of unobserved spectral lines cumbersome. As a result, the emphasis in this section will be placed upon the relation between effective constants defined by

$$E_r = B_{eff} J(J+1) - D_{eff} J^2 (J+1)^2 + H_{eff} J^3 (J+1)^3 , \quad (1)$$

and the unperturbed spectral constants of the several vibrational states, B_v, D_v, q_v, q_v', etc.
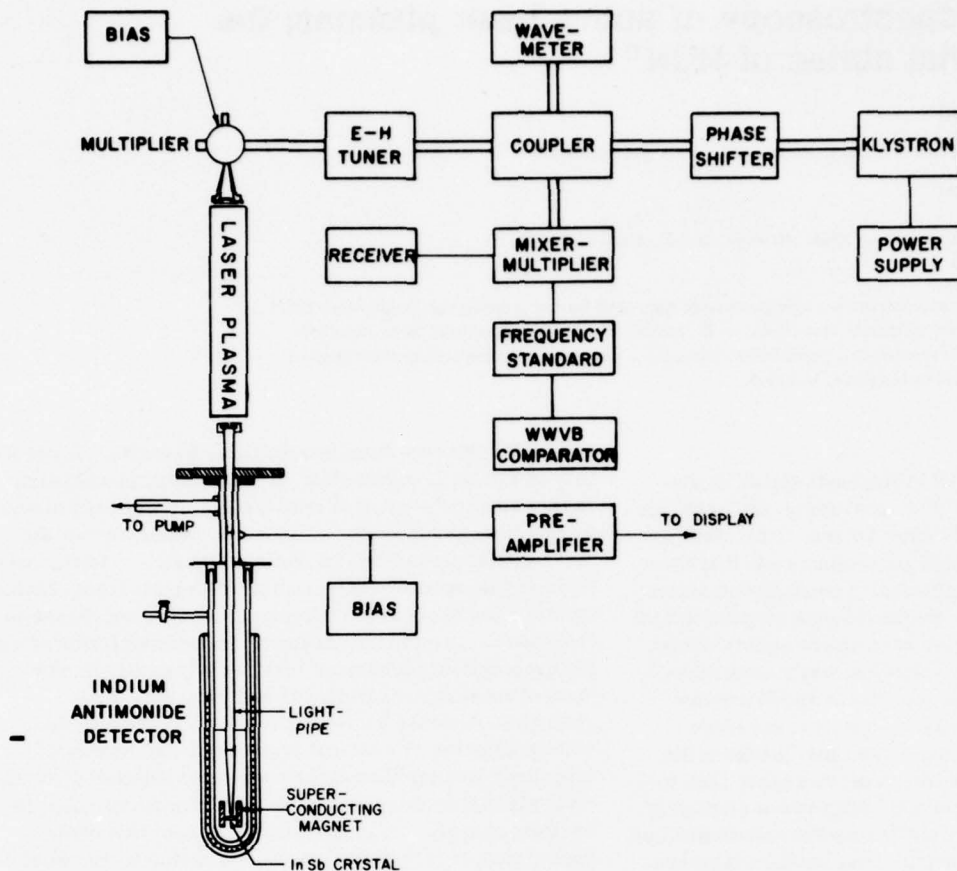
FIG. 1. Spectrometer for the study of laser plasmas.

A. Effects of l-type doubling

The basic theory of l-type doubling has been developed by Amat and Nielsen[11,12] and extended and applied by Maki and Lide.[5] The notation used here is consistent with that of Ref. 5.

For linear triatomic molecules vibrational states are specified as v_1, v_2^l, v_3, and states with $l = 0, 1, 2, 3 \ldots$ are referred to as Σ, π, Δ, Φ, $\ldots$. For all states with $v_2 \geq 1$, there exists a multiplet of vibrational states that is degenerate in the harmonic approximation. The contributions of l-type resonances to the lifting of these degeneracies can be calculated by the solution of a secular determinant of dimension $(v_2 + 1)$.

For $v_2 = 1$, the secular determinant is of the form

$$\begin{vmatrix} E_r^0 - \epsilon & \tfrac{1}{2}W_{11} \\ \tfrac{1}{2}W_{11} & E_r^0 - \epsilon \end{vmatrix} = 0 , \tag{2}$$

with $W_{11} = q_v J(J+1)$. E_r^0 is the unperturbed energy of the 01^10 state. The rotational contribution to this energy is

$$E_r = B_v[J(J+1) - l^2] - D_v[J(J+1) - l^2]^2 . \tag{3}$$

When centrifugal distortion in the l-type doubling constant is included, Eq. (2) gives for its solutions

$$E_r^\pm = B_v[J(J+1) - l^2] \pm \tfrac{1}{2}q_v J(J+1)$$

$$\mp \tfrac{1}{2}q_v' J^2(J+1)^2 - D_v[J(J+1) - l^2]^2 . \tag{4}$$

It should be recognized that this equation contains terms of the form $B_v l^2$ and $D_v l^4$ that are not functions of J and do not contribute to the rotational frequencies. In this paper these will be considered to be part of the vibrational energy, thereby making Eqs. (1) and (3) compatible. Equation (4) can be factored into coefficients of $J(J+1)$ and $J^2(J+1)^2$ to give

$$B_{eff}^\pm = B_v \pm \tfrac{1}{2}q_v + 2D_v \tag{5}$$

$$D_{eff}^\pm = D_v \pm \tfrac{1}{2}q_v' . \tag{6}$$

For $v_2 = 2$ the secular determinant is of the form[5]

$$\begin{vmatrix} E_\Delta^0 - \epsilon & W_{20} & 0 \\ W_{20} & E_\Sigma^0 - \epsilon & W_{20} \\ 0 & W_{20} & E_\Delta^0 - \epsilon \end{vmatrix} = 0 \tag{7}$$

with

$$W_{20} = (q_v/\sqrt{2})[J^2(J+1)^2 - 2J(J+1)]^{1/2} .$$

Solution of this equation gives

$$E_\Sigma = E_\Sigma^0 + \tfrac{1}{2}\delta - \tfrac{1}{2}\{\delta^2 + 4q_v^2[J^2(J+1)^2 - 2J(J+1)]\}^{1/2} \tag{8}$$

$$E_{\Delta d} = E_\Delta^0 \tag{9}$$

$$E_{\Delta_c} = E_\Delta^0 - \tfrac{1}{2}\delta + \tfrac{1}{2}\left\{\delta^2 + 4q_v^2\left[J^2(J+1)^2 - 2J(J+1)\right]\right\}^{1/2} , \tag{10}$$

where $\delta = E_\Delta^0 - E_\Sigma^0$. The rotational contribution to E_Σ^0 and E_Δ^0 is given by Eq. (3).

For transitions in the millimeter and submillimeter microwave region, these expressions can be expanded and compared with Eq. (1) to give

$$E_\Sigma = E_\Sigma^0 - (q_v^2/\delta)\left[J^2(J+1)^2 - 2J(J+1)\right] \tag{11}$$

$$B_v = B_{eff} - 2(q_v^2/\delta) \tag{12}$$

$$D_v = D_{eff} - (q_v^2/\delta) \tag{13}$$

$$E_{\Delta c} = E_\Delta^0 + (q_v^2/\delta)\left[J^2(J+1)^2 - 2J(J+1)\right] \tag{14}$$

$$B_v = B_{eff} + 2q_v^2/\delta - 8D_v \tag{15}$$

$$D_v = D_{eff} + (q_v^2/\delta) \tag{16}$$

$$E_{\Delta d} = E_\Delta^0 \tag{17}$$

$$B_v = B_{eff} - 8D_v \tag{18}$$

$$D_v = D_{eff} . \tag{19}$$

For $v_2 = 3$, the secular determinant is of the form

$$\begin{vmatrix} E_\Phi^0 - \epsilon & W_{31} & 0 & 0 \\ W_{31} & E_\pi^0 - \epsilon & W_{11} & 0 \\ 0 & W_{11} & E_\pi^0 - \epsilon & W_{31} \\ 0 & 0 & W_{31} & E_\Phi^0 - \epsilon \end{vmatrix} = 0 , \tag{20}$$

with $W_{31} = \left[\sqrt{3}\, q_v/2\right]\left[J^2(J+1)^2 - 8J(J+1) + 12\right]^{1/2}$. Solution of this equation gives

$$E_{\pi_d} = E_\pi^0 + \tfrac{1}{2}\delta + \tfrac{1}{2}W_{11} - \tfrac{1}{2}\left\{\left[\delta - W_{11}\right]^2 + 4W_{31}^2\right\}^{1/2} \tag{21}$$

$$E_{\Phi_d} = E_\Phi^0 - \tfrac{1}{2}\delta + \tfrac{1}{2}W_{11} + \tfrac{1}{2}\left\{\left[\delta - W_{11}\right]^2 + 4W_{31}^2\right\}^{1/2} \tag{22}$$

$$E_{\pi_c} = E_\pi^0 + \tfrac{1}{2}\delta - \tfrac{1}{2}W_{11} - \tfrac{1}{2}\left\{\left[\delta + W_{11}\right]^2 + 4W_{31}^2\right\}^{1/2} \tag{23}$$

$$E_{\Phi_c} = E_\Phi^0 - \tfrac{1}{2}\delta - \tfrac{1}{2}W_{11} + \tfrac{1}{2}\left\{\left[\delta + W_{11}\right]^2 + 4W_{31}^2\right\}^{1/2} , \tag{24}$$

where $\delta = E_\Phi^0 - E_\pi^0$. When centrifugal distortion is included, for π_d states

$$B_v = B_{eff} - q_v - 6q_v^2/\delta - 2D_v \tag{25}$$

$$D_v = D_{eff} - q_v' - \tfrac{3}{4}(q_v^2/\delta) \tag{26}$$

$$H_v = H_{eff} + q_v^3/\delta^2 \tag{27}$$

For π_c states:

$$B_v = B_{eff} + q_v - 6q_v^2/\delta - 2D_v \tag{28}$$

$$D_v = D_{eff} + q_v' - \tfrac{3}{4}(q_v^2/\delta) \tag{29}$$

$$H_v = H_{eff} - q_v^3/\delta^2 . \tag{30}$$

Only the $l = 0$ state of $v_2 = 4$ was studied and since there is no l degeneracy for this state, perturbation theory may be used to calculate the effects of l doubling.

$$E_\Sigma = E_\Sigma^0 + \frac{2\left[W_{02}\right]^2}{E_\Sigma - E_\Delta} = E_\Sigma^0 - \frac{3q_v^2}{\delta}\left[J^2(J+1)^2 - 2J(J+1)\right]$$
$$+ \frac{12\gamma_{11}q_v^2}{\delta^2}\left[J^3(J+1)^3 - 2J^2(J+1)^2\right] , \tag{31}$$

and

$$B_v = B_{eff} - 6q_v^2/\delta \tag{32}$$

$$D_v = D_{eff} - \frac{3q_v^2}{\delta} - \frac{24\gamma_{11}q_v^2}{\delta^2} \tag{33}$$

$$H_v = H_{eff} - 12\gamma_{11}q_v^2/\delta^2 . \tag{34}$$

The term which contains γ_{11} results from the expansion of $E_\Sigma - E_\Delta$ and accounts for the difference between the rotational constants of the 04^00 and 04^20 states.

B. Effects due to Coriolis coupling between 11^10 and 04^00

Because a near degeneracy exists between the rotational levels of the 11^10 and 04^00 vibrational states at $J = 10$, it is not possible to fit either the 11^10 or 04^00 data on the basis of the effective constants of Eq. (1). The perturbation between the states can be given by[4]

$$\Delta^2 = \delta^2 + 4J(J+1)W_{ni}^2 , \tag{35}$$

where δ is the separation of the unperturbed states, Δ the separation of the perturbed states, and W_{ni} the Coriolis constants. δ is a function of J and can be expressed as

$$\delta = \Delta E_0 - \Delta BJ(J+1) + \Delta DJ^2(J+1)^2 , \tag{36}$$

where ΔE_0 represents vibrational energy difference between the two states.

III. RESULTS

A. Observed frequencies and effective rotational constants

Table I displays the forty-seven rotational transitions in 12 different excited vibrational states that have been observed. With the exception of the rotational transitions in the 04^00 and 11^10 states, all may be represented by the effective rotational constants of Eq. (1). These effective constants are shown in Table II. Also included are precise ground-state constants which were calculated from the results of a beam maser experiment of De Lucia and Gordy.[13]

B. Unperturbed rotational constants

Since the rotational levels of the 10^00, 20^00, 00^01, 00^02, and 10^01 are essentially unperturbed, the effective constants of Table II are also the unperturbed spectral constants for these states.

Table III shows the unperturbed rotational constants for all states for which corrections between the effective and unperturbed constants are necessary. Equations (5) and (6) show that the constants for 01^10 can be obtained by the averaging of the effective constants for the two components and subtracting $2D_v$. A similar procedure was used for the 01^11 state. Equations (11)–(13) were used to calculate the constants of the 02^00 and the results of Eqs. (14)–(19) were used for the 02^20 state. Because the $J = 0 \to 1$ and $1 \to 2$ transitions do not exist for states with $l = 2$, there is no experimental redundancy within the 02^20 state and the listed standard deviations reflect estimated experimental uncertainty. Equations (25)–(30) were used to calculate the constants for the 03^10 state.

TABLE I. Observed transition frequencies in vibrationally excited HCN (MHz).[a]

State	$J=0\to1$ Observed	Obs.–calc.	$J=1\to2$ Observed	Obs.–calc.	$J=2\to3$ Observed	Obs.–calc.	$J=3\to4$ Observed	Obs.–calc.
$01^{1c}0$	⋯		177 238.73[b]	0.04	265 852.68	−0.02	354 460.33	0.01
$01^{1d}0$	⋯		178 136.50[b]	−0.02	267 199.37	0.01	356 255.71	0.00
02^00	89 087.69[b]	0.04	178 170.38	0.01	267 243.15	−0.07	356 301.33	0.04
$02^{2d}0$	⋯		⋯		267 109.37		356 135.46	
$02^{2c}0$	⋯		⋯		267 120.02		356 162.77	
$03^{1c}0$	⋯		177 698.78	0.02	266 540.00	−0.04	355 371.69	0.02
$03^{1d}0$	⋯		179 547.32	−0.10	269 312.89	0.16	359 067.86	−0.07
04^00			179 127.26[c]		268 663.29[c]			
10^00	88 027.28[d]	0.03	176 052.38	−0.01	264 073.30	−0.01	352 087.89	0.01
20^00	87 419.40[d]	0.06	174 836.53	−0.04	262 249.60	0.01	349 656.27	−0.00
00^01	88 006.69[d]	0.03	176 011.26	0.03	264 011.53	−0.08	352 005.76	0.04
00^02			174 725.29		262 082.87			
10^01	87 415.29	0.07			262 237.31	−0.07	349 640.22	0.04
$01^{1c}1$	⋯				264 005.10		351 996.75	
$01^{1d}1$	⋯		176 919.08		265 373.12			
$11^{1c}0$	⋯				264 019.77[c]	−0.09	352 016.88[c]	0.07
$11^{1d}0$	⋯		176 913.10		265 364.36			

[a]Corrected for quadrupole splittings.
[b]From Ref. 6.
[c]See footnote b, Table II.

[d]These lines have also been observed by R. C. Woods (private communication).

C. The $11^10/04^00$ system

The 11^10 and 04^00 states must be considered together because of the Coriolis coupling between them. This is an exceedingly important and interesting system. It is the basis of the well known far-infrared laser.[14] The absolute frequency measurement of the laser emissions[15] coupled with the pure rotational transition measured in this study make possible the calculation of a number of parameters to high accuracy, including the centrifugal distortion parameters for both states, the Coriolis interaction constant W_{nl}, and the energy difference between the two vibrational states ΔE_0. These constants are shown in Table IV and the transition frequencies calculated from them are compared with the observed frequencies shown in Table V. It is interesting to note that vibrational energy difference between the 04^00 and 11^10 states has been calculated to ±0.0001 cm⁻¹.

In addition to the Coriolis perturbation, both the 11^10 and 04^00 states are affected by l-type doubling. Equations (32) and (33) provide the corrections for the 04^00 state, but values of q_v and δ are required. The value of q_v can be extrapolated from the values for the 01^10, 02^20, and 03^10 states and Maki gives $E_\Delta^0 - E_\Sigma^0$ to be 15.225 cm⁻¹. The unperturbed values of both B_{04^00} and D_{04^00} are shown in Table III. D_{04^00} is a very sensitive test of q_v and δ. Its value is in good agreement with its expected value and this serves as a confirmation of the values of q_v and δ used in Eq. (33).

TABLE II. Effective rotational constants for excited vibrational states of HCN (MHz).

State	B_{eff} Constant	σ	D_{eff} Constant	σ
00^00	44 315.9757	0.0004	0.08724	0.00006
$01^{1c}0$	44 310.381	0.013	0.0888	0.0005
$01^{1d}0$	44 534.851	0.004	0.0902	0.0002
02^00	44 544.233	0.014	0.2054	0.0006
$02^{2d}0$	44 519.895		0.0926	
$02^{2c}0$	44 519.563		−0.0245	
$03^{1c}0$	44 425.766[a]	0.013	0.1350[a]	0.0005
$03^{1d}0$	44 887.974[a]	0.050	0.1397[a]	0.0021
04^00	44 785.584[b]	0.051	0.45297[b]	0.00034
10^00	44 013.803	0.006	0.0881	0.0003
20^00	43 709.846	0.014	0.0879	0.0006
00^01	44 003.505	0.015	0.08716	0.0006
00^02	43 681.998		0.0844	
10^01	43 707.783	0.036	0.0863	0.0014
$01^{1c}1$	44 002.465		0.0898	
$01^{1d}1$	44 230.503		0.0917	
$11^{1c}0$	44 004.714[b]	0.037	0.08873[b]	0.00016
$11^{1d}0$	44 229.006		0.0912	

[a]Interactions with 03^30 produce an H_{eff} that makes a significant contribution at low J. To reproduce the calculated frequencies of Table I; for $03^{1c}0$, $H_{eff} = -1.52\times10^{-5}$ MHz, and for $03^{1d}0$, $H_{eff} = +1.52\times10^{-5}$ MHz.
[b]Because of the Coriolis perturbation between the rotational levels of the 04^00 and $11^{1c}0$ states, these constants will not reproduce the rotational levels without the use of Eqs. (35) and (36) and the constants in Table IV.

TABLE III. Unperturbed rotational constants of the perturbed excited vibrational states of HCN (MHz).

State	B_v Constants	σ	D_v Constant	σ
01^10	44 422.438	0.007	0.0895	0.0003
02^00	44 544.004	0.014	0.0908	0.0006
02^20	44 519.112	0.050	0.0914	0.0015
03^10	44 656.332	0.026	0.0933	0.0010
04^00	44 784.866	0.05	0.0937	0.0005
01^11	44 116.303	0.05	0.0908	0.0010
11^10	44 116.680	0.05	0.0900	0.0010

TABLE IV. Spectral constants calculated from the $04^00/11^{1c}0$ system (MHz).

Constant	Value	σ
W_{ni}	112.27	0.06
ΔE_0	78663.1	4.0
$(B_{04}0_0)_{eff}$	44785.58	0.05
$(D_{04}0_0)_{eff}$	0.45297	0.00034
$(B_{11}1c_0)_{eff}$	44004.71	0.04
$(D_{11}1c_0)_{eff}$	0.08873	0.00016

D. Vibrational effects of moments of inertia

The relation between the effective and equilibrium constants can be expressed as

$$B_v = B_e - \sum_i \alpha_i(v_i + \tfrac{1}{2}d_i) + \sum_{ij} \gamma_{ij}(v_i + \tfrac{1}{2}d_i)(v_j + \tfrac{1}{2}d_j)$$
$$+ \sum_{ijk} \epsilon_{ijk}(v_i + \tfrac{1}{2}d_i)(v_j + \tfrac{1}{2}d_j)(v_k + \tfrac{1}{2}d_k) + \gamma_{11}l^2 . \quad (37)$$

Table VI shows a comparison between the constants calculated from extensive infrared data and the previously existing microwave data[6] and an analysis of our microwave data alone. It is necessary to include the ϵ_{222} term in our expansion because of the significantly larger amount of microwave data now available. Previously, microwave data for only two excited bending modes were available and they essentially determined a_2 and γ_{22}. It is interesting to note that ϵ_{222} makes a significant con-

TABLE V. Analysis of the $04^00/11^{1c}0$ system (MHz).

Transition $v'-v''$ $J'-J''$	Observed	Obs.-calc.	Coriolis Perturbation
04^00-04^00 2-1	179127.26	0.12	-0.69
04^00-04^00 3-2	268663.29	-0.08	-1.15
04^00-04^00 9-8	804750.9[a]	0.00	-61.35
04^00-04^00 10-9	894414.2[a]	0.28	524.42
11^10-04^00 10-9	890760.7[a]	-0.27	-327.87
11^10-04^00 11-10	964313.4[a]	0.28	-517.22
11^10-11^10 2-1	176016.82	0.08	0.69
11^10-11^10 3-2	264019.77	-0.09	1.15
11^10-11^10 4-3	352016.88	0.07	1.79
11^10-11^10 11-10	967965.8[a]	-0.28	335.07

[a]Measured frequencies of HCN laser emission lines from Ref. 14.

TABLE VI. Equilibrium rotational constant expansion (MHz).

Con-stant	This work Value	σ	Reference 6 Value	σ
B_e	44511.62	0.03	44512.36	0.23
α_1	300.028	0.03	299.043	0.57
α_2	-108.369	0.05	-106.774	0.075
α_3	312.983	0.03	313.163	0.270
γ_{11}	-0.893	0.009	-1.049	0.300
γ_{12}	-3.583	0.033	-4.116	0.075
γ_{13}	6.448	0.027	6.625	0.210
γ_{22}	0.762	0.027	1.532	0.015
γ_{23}	6.332	0.033	6.434	0.075
γ_{33}	-4.521	0.018	-4.527	0.008
ϵ_{222}	0.094	0.003	...	...
γ_{ll}	-6.224	0.006	-6.056	0.010

tribution to the B_v of the lower bending modes as evidenced by the differences between the B_e, a_2, and γ_{22} of the two analyses.

Although our constants result from a fit of 12 constants to only 13 microwave data points, the constants which result accurately predict, with the several exceptions, the infrared ΔB which were used in the previous analysis and the weighted addition of this infrared data to our analysis makes no significant change in our calculated constants.

The ΔB's which are not well predicted are interesting. The value of ΔB for $02^20 - 02^00$ is $-80.72 \pm 0.30 \times 10^{-5}$ cm^{-1}.[5] The microwave value for this ΔB is $-83.02 \pm 0.17 \times 10^{-5}$ cm^{-1}, an analysis of all microwave data predicts $-83.05 \pm 0.03 \times 10^{-5}$ cm^{-1}, and an analysis of all microwave data except B_{02^20} predicts -83.09×10^{-5} cm^{-1}. Since the calculation of the previous value requires a complicated and indirect calculation, assumptions about other spectroscopic constants, and since a more recent version of this calculation now gives $-82.23 \pm 0.24 \times 10^{-5}$ cm^{-1},[16] it would seem reasonable to conclude that this does not represent any real inconsistency with our analysis.

Our predictions of the ΔB for the 12^00-01^10 band differs by about three times the stated uncertainty of $\pm 0.7 \times 10^{-5}$ cm^{-1}. But the difference between this ΔB and the ΔB for the $12^20 - 01^10$ is $-80.80 \pm 1.1 \times 10^{-5}$ cm^{-1}. This value is in excellent agreement with the $02^20 - 02^00$ ΔB of Ref. 6, but differs from both the newer $\Delta B_{02^20-02^00}$ of Ref. 16 and our microwave data.

The value of ΔB for $05^10 - 01^10$ of 1590 ± 15 cm^{-1} differs from our predicted value by 20 cm^{-1}. It is interesting to note that the 12^00, 12^20 and 05^10 are involved in a Coriolis interaction and were analyzed together.

Recently, Maki[16] has made some highly precise measurements on hot bands of HCN and has results which question the completeness of Eq. (37). For example, he finds $\Delta B(12^00 - 02^00) = -999.26(31) \times 10^{-5}$ cm and $\Delta B(12^20 - 02^20) = -999.95(29) \times 10^{-5}$ cm. In the context of Eq. (37) these two values should be the same. At face value these results require terms to be added to Eq. (37) which mix v_i and l. However, it is also possible that since the analyses used to produce these re-

sults require the fixing of energy levels and spectroscopic constants derived from microwave and other infrared experiments and since the uncertainties quoted do not include systematic errors in the experiments, errors in the fixed energy levels and constants, or model errors, the actual uncertainties are somewhat larger and no inconsistency exists. It should be pointed out that the ΔB predicted from the microwave numbers and Eq. (37) generally fall within the range of values for the infrared multiplet. In addition to providing improved spectral parameters, this calculation is necessary for the assignment of the rotational transitions in several of the vibrational states studied. This is because of the near degeneracy caused by the similar values of B_{eff} for $11^{14}0$ and $01^{1d}1$ and for 001, $11^{1c}0$, and $01^{1c}1$.

IV. CONCLUSIONS

It has been demonstrated that millimeter and sub-millimeter microwave spectroscopy is an effective and sensitive probe of active laser plasmas. Since these plasmas contain large, nonequilibrium populations in excited vibrational states, these studies also yield substantial amounts of new, high precision microwave data. These results make possible the calculation of the rotational spectrum of HCN over a wide range of vibrational and rotational states. For most states these calculations are especially convenient because of the relations provided between the effective and unperturbed constants.

It should also be noted that this is a technique that can be used for the study of the otherwise inaccessible excited vibrational states of many molecules. Because the kinetic and rotational temperatures remain approximately ambient, this technique is substantially more sensitive than the hot cell method, especially for highly excited states.

[1]F. C. De Lucia, Ohio State Molecular Spectroscopy Symposium, RE2 (1976).
[2]D. H. Rank, G. Shorinko, D. P. Eastman, and T. A. Wiggins, J. Opt. Soc. Am. 50, 421 (1960).
[3]W. W. Brim, J. M. Hoffman, H. H. Nielsen, and K. Narahari Rao, J. Opt. Soc. Am. 50, 1208 (1960).
[4]A. G. Maki and L. R. Blaine, J. Mol. Spectrosc. 12, 45 (1964).
[5]A. G. Maki and D. R. Lide, Jr., J. Chem. Phys. 47, 3206 (1967).
[6]G. Winnewisser, A. G. Maki, and D. R. Johnson, J. Mol. Spectrosc. 31, 149 (1971).
[7]A. G. Smith, W. Gordy, J. W. Simmons, and W. V. Smith, Phys. Rev. 75, 260 (1949).
[8]T. Torring, Z. Physik 161, 179 (1961).
[9]G. W. Chantry, Submillimeter Spectroscopy, (Academic, London and New York, 1971).
[10]P. Helminger, F. C. De Lucia, and W. Gordy, Phys. Rev. Lett. 25, 1397 (1970).
[11]G. Amat and H. W. Nielsen, J. Mol. Spectrosc. 2, 152 (1958).
[12]G. Amat and H. H. Nielsen, J. Mol. Spectrosc. 2, 163 (1958).
[13]F. C. De Lucia and W. Gordy, Phys. Rev. 187, 58 (1969).
[14]D. R. Lide, Jr. and A. G. Maki, Appl Phys. Lett. 11, 62 (1967).
[15]L. O. Hocker and A. Javan, Phys. Lett. 25A, 489 (1967).
[16]A. G. Maki, J. Mol. Spectrosc. 58, 308 (1975).

"Forbidden" Millimeter-Wave Transitions in Arsine [1]

DAVID A. HELMS AND WALTER GORDY

Department of Physics, Duke University, Durham, North Carolina 27706

A millimeter-wave spectrometer having a sensitivity of 4×10^{-10} cm^{-1} in the 2-mm region has been used for observation of the "forbidden" transitions $J \to J$, $K = \pm 4 \to \pm 1$ and $J \to J$, $K = \pm 5 \to \pm 2$ in AsH$_3$. A comprehensive computer analysis was made of the frequencies measured in this work together with available microwave frequencies of other transitions. This analysis provides accurate values of the rotational constants, nuclear quadrupole couplings, and effective structural parameters of the molecule. The spectral constants B_0 and C_0 (in MHz) are 112 470.597 and 104 884.665, respectively.

I. INTRODUCTION

In a previous paper (*1*) we reported observations of forbidden $\Delta K = \pm 3$ microwave transitions in PH$_3$ and PD$_3$. Our measurements of $K = 3 \to 0$ transitions in PH$_3$ and $K = 3 \to 0$ and $K = \pm 4 \to \pm 1$ transitions in PD$_3$ confirmed the assignments of the lower-frequency $K = \pm 2 \to \mp 1$ transitions of PH$_3$ and of PD$_3$ reported by Chu and Oka (*2*), and improved significantly the molecular constants, especially C_0. A similar investigation is here described for arsine.

Transitions in AsH$_3$ obeying the $\Delta J = 0$, $\Delta K = \pm 3$ selection rules were first observed by Chu and Oka (*2*). They reported eight transitions obeying the selection rules $\Delta J = 0$, $K = \pm 2 \to \mp 1$, $\Delta F = 0$ in the frequency range of 21.16 to 21.84 GHz. The large As quadrupole coupling splits the $K = \pm 2 \to \mp 1$ line into two doublets, each component of which is an unresolved doublet. Chu and Oka combined their value of C_0 with the known value of B_0 (*3*) and with other information to obtain the zero-point effective, the zero-point average, and the equilibrium structures. Recently, Olson *et al.* (*4*) reported their observation of "perturbation-allowed" transitions of the type $\Delta |K - l| = \pm 3$ in the ν_1 and ν_3 infrared bands of AsH$_3$. They combined their $\Delta |K - l| = \pm 3$ infrared measurements with the $K = \pm 2 \to \mp 1$ microwave measurements of Chu and Oka and with the normally allowed $\Delta K = 0$ microwave measurements of Helminger *et al.* (*3*) to obtain both a set of ground state molecular constants and an associated zero-point-effective structure. Olson *et al.* then used the constants for the ν_2 and ν_4 bands given by Sarka, *et al.* (*5*) with their constants for the ν_1 and ν_3 bands to determine the equilibrium structure. Our detection of the $K = \pm 4 \to \pm 1$ and the $K = \pm 5 \to \pm 2$ forbidden transitions was assisted by a preliminary prediction of their frequencies from the results of Helminger *et al.*, of Olson *et al.*, and of Chu and Oka.

473

The need for observation of the higher $K = \pm 4 \to \pm 1$ and $K = \pm 5 \to \pm 2$ milli-meter-wave transitions described in this paper was indicated by Chu and Oka (2), who reported that their spectrometer was not sufficiently sensitive at the higher frequencies to detect them. Measurements of these transitions confirm the assignments of the frequencies measured by Chu and Oka and provide increased accuracy in the values of the spectral constants, particularly those influenced by the distortion caused by rotation about the symmetry axis. For observation of very weak transitions such as these in the shorter millimeter-wave region, we designed an exceptionally sensitive millimeter-wave spectrometer, which is described in the earlier paper (1).

The Q-branch $\Delta K = \pm 3$ transitions represent only one class of forbidden transitions in symmetric top molecules included in the general theory of Watson (6, 7) and others (8, 9). Oka (10) has recently written an excellent review of the experimental and theoretical developments of this relatively new type of spectra. In the ground vibrational state, the off-axis dipole moment which couples the radiation field to the rotation is induced by centrifugal distortion. The selection rules are determined by the molecular symmetry. In AsH$_3$, the rotation about the b-axis of inertia induces a small dipole moment ($\approx 3.938 \times 10^{-5}$ D) perpendicular to the symmetry axis which leads to a slight admixture of the K levels and a breakdown of the familiar $\Delta K = 0$ selection rule. The threefold symmetry about the c-axis limits this admixture to K levels differing by three units. It is of interest that centrifugal distortion due to rotation about the symmetry axis can likewise generate a small dipole component along the symmetry axis. This component is of no particular consequence in molecules such as PH$_3$, PD$_3$, and AsH$_3$ which already have permanent dipole moments along the symmetry axis, but it can give rise to forbidden $\Delta J = \pm 1$ transitions in molecules such as CH$_4$ which has no permanent dipole moment. In fact, $\Delta J = 1$ rotational transitions in CH$_4$, SiH$_4$, and GeH$_4$ have been observed by Rosenberg et al. (11–14) in the far-infrared region. Kreiner et al. (15) have used Laser–Stark spectroscopy to measure the distortion-induced dipole moment of GeH$_4$. Forbidden transitions of CH$_4$ in the ground vibrational state have also been detected in the microwave region by Holt et al. (16). At a recent symposium, Kagann et al. (17) reported their observations of over 140 Q-type $\Delta K = \pm 3$ microwave transitions in OPF$_3$.

II. EXPERIMENTAL DETAILS

The millimeter-wave spectrometer and the experimental procedure used in these measurements are described in the earlier paper (1). The high sensitivity of this spectrometer ($\approx 4 \times 10^{-10}$ cm^{-1} at 144 GHz for a time constant of 1 sec) made possible the measurement of these weak $\Delta K = \pm 3$ transitions with an estimated accuracy of three parts in 10^7.

III. THEORETICAL BACKGROUND

As a result of centrifugal distortion, the rotational wavefunction $\psi_{J,K}$ of a molecule having C_{3v} symmetry mixes slightly with the wavefunction $\psi_{J,K\pm3}$ in the ground vibrational state. The term in the Hamiltonian responsible for the interaction may be ex-

pressed (*18*) as

$$H' = \frac{h^4 \tau_{xxxz}}{4} \left[(J_+{}^3 + J_-{}^3)J_z + J_z(J_+{}^3 + J_-{}^3) \right], \quad (1)$$

where τ_{xxxz} is a centrifugal distortion constant and J_z, J_+, and J_- are rotational operators.

In the absence of the perturbing H' term, the rotational levels are all doubly degenerate for each value of K, ($K \neq 0$). The energy levels corresponding to $K \neq 3$ are raised or lowered, but they remain degenerate with symmetry E. The $K = 3$ level, however, is split into A_1 and A_2 components. The designations A_1, A_2, and E indicate the symmetry of the rovibrational wavefunction (excluding spin). In the case of AsH$_3$, each of the energy levels is split further into $(2I + 1)$ components by the quadrupole interaction of the $As(I = \frac{3}{2})$ nucleus. The symmetry selection rules for Q-type $\Delta K = \pm 3$ transitions (*19*) are $+ \leftrightarrow -$, along with $A_1 \leftrightarrow A_2$, or $E \leftrightarrow E$.

The formulas giving the energy levels may be expressed (*20, 21*) for $K \neq 3$ as:

$$\frac{E(F, J, K)}{h} = G(J, K) + \tfrac{1}{2}[C_N + (C_K - C_N)K^2/J(J+1)]$$

$$\times [F(F+1) - I(I+1) - J(J+1)] - eQq \left[3\frac{K^2}{J(J+1)} - 1 \right] Y(J, \tfrac{3}{2}, F) + \left[\frac{h^4 \tau_{xxxz}}{4h} \right]^2$$

$$\times \left\{ \frac{(2K-3)^2[J(J+1) - K(K-1)][J(J+1) - (K-1)(K-2)][J(J+1) - (K-2)(K-3)]}{G(J, K) - G(J, K-3)} \right.$$

$$\left. + \frac{(2K+3)^2[J(J+1) - K(K+1)][J(J+1) - (K+1)(K+2)][J(J+1) - (K+2)(K+3)]}{G(J, K) - G(J, K+3)} \right\} ; \quad (2)$$

and for $K = 3$ as

$$\frac{E^-(F, J, 3)}{h} = G(J, 3) + \tfrac{1}{2}[C_N + (C_K - C_N)K^2/J(J + 1)]$$

$$\times [F(F + 1) - I(I + 1) - J(J + 1)] - eQq \left(3\frac{K^2}{J(J + 1)} - 1 \right) Y(J, \tfrac{3}{2}, F)$$

$$+ \left(\frac{h^4 \tau_{xxxz}}{4h} \right)^2 \frac{81[J(J + 1) - 12][J(J + 1) - 20][J(J + 1) - 30]}{G(J, 3) - G(J, 6)}$$

$$+ \left\{ h_0 - 18 \left(\frac{h^4 \tau_{xxxz}}{4h} \right)^2 \middle/ [G(J, 0) - G(J, 3)] \right\}$$

$$\times J(J + 1)[J(J + 1) - 2][J(J + 1) - 6], \quad (3)$$

HELMS AND GORDY

TABLE I

Observed Frequencies and Calculated Intensities for the AsH$_3$ Transitions

Transition			Observed Frequency ν (MHz)	ν Obs-ν Calc	a_{max} (calc) (10^{-10} cm^{-1})
Normal Rotational Transitions					
$J \to J+1$	$K \to K$	$F \to F'$ (a)			
$J = 0$	$K = 0$	$F = 3/2 \to 5/2$	224 937.78	-0.01	
0	0	$3/2 \to 3/2$	224 896.85	-0.02	
0	0	$3/2 \to 1/2$	224 969.88	0.02	
1	0	$5/2 \to 7/2$	449 792.43	0.02	
1	0	$5/2 \to 5/2$	449 751.38	0.00	
1	0	$3/2 \to 3/2$	449 821.08	0.02	
1	0	$1/2 \to 3/2$	449 748.06	-0.01	
1	1	$5/2 \to 7/2$	449 813.69	0.03	
1	1	$3/2 \to 5/2$	449 772.90	-0.01	
1	1	$1/2 \to 3/2$	449 823.85	-0.05	
Forbidden Rotational Transitions					
$J \to J$	$K = \pm 2 \to \mp 1$	$F \to F$ (b)			
$J = 9$		$F = 15/2$	21 835.96	0.01	1.7
10		17/2	21 627.60	-0.10	1.9
10		19/2	21 624.66	0.29	
11		19/2	21 402.76	0.08	2.0
11		21/2	21 399.84	-0.07	
12		21/2	21 161.96	-0.14	1.9
12		23/2	21 159.68	-0.07	
$J \to J$	$K = \pm 4 \to \mp 1$	$F \to F$ (c)			
$J = 8$		$F = 15/2$	110 694.86	0.03	13.7
9		19/2	109 737.88	-0.11	17.9
9		21/2	109 758.26	-0.04	17.9
9		15/2	109 761.53	-0.03	17.9
10		21/2	108 694.21	0.00	20.8
10		19/2	108 696.65	0.04	20.8
10		23/2	108 710.90	0.06	20.8
10		17/2	108 713.34	0.09	20.8

(*continued*)

and

$$\frac{E^{+}(F, J, 3)}{h} = G(J, 3) + \tfrac{1}{2}\left[C_N + (C_K - C_N)K^2/J(J+1)\right]$$

$$\times \left[F(F+1) - I(I+1) - J(J+1)\right] - eQq\left(3\frac{K^2}{J(J+1)} - 1\right)Y\left(J, \tfrac{3}{2}, F\right)$$

$$+ \left(\frac{h^4\tau_{xxxi}}{4h}\right)^2 \frac{81[J(J+1) - 12][J(J+1) - 20][J(J+1) - 30]}{G(J,3) - G(J,6)}$$

$$- h_0(J(J+1)[J(J+1) - 2][J(J+1) - 6], \quad (4)$$

where

$$G(J, K) = B[J(J+1) - K^2] + CK^2 - D_J J^2(J+1)^2 - D_{JK}J(J+1)K^2$$

$$- D_K K^4 + H_{JJK}J^2(J+1)^2K^2 + H_{JKK}J(J+1)K^4$$

$$+ L_{JJKK}J^2(J+1)^2K^4 + H_K K^6 + L_{JJJK}J^3(J+1)^3K^2. \quad (5)$$

TABLE I—*Continued*

Transition		Observed Frequency ν (MHz)	ν Obs-ν Calc	a_{max} (calc) $(10^{-10}$ cm$^{-1})$
$J \to J$ $K = \pm 4 \to \pm 1$ $F \to F$ (c) (continued)				
11	23/2	107 564.50	0.02	22.1
11	21/2	107 566.25	-0.05	22.1
11	25/2	107 578.28	-0.05	22.1
11	19/2	107 580.14	-0.02	22.1
12	25/2	106 354.89	-0.02	21.5
12	23/2	106 356.38	0.04	21.5
12	27/2	106 366.72	0.09	21.5
12	21/2	106 368.17	0.11	21.5
13	27/2	105 072.41	-0.06	19.4
13	25/2	105 073.65	0.06	19.4
13	29/2	105 082.50	-0.02	19.4
13	23.2	105 083.61	-0.03	19.4
14	29/2	103 725.04	-0.06	16.3
14	27/2	103 725.85	-0.16	16.3
14	31/2	103 733.80	0.00	16.3
14	25/2	103 734.66	-0.06	16.3
15	31/2	102 322.08	0.00	12.9
15	29/2	102 322.95	0.13	12.9
15	33/2	102 329.74	0.05	12.9
$J \to J$ $K = \pm 5 \to \pm 2$ $F \to F$ (c)				
$J = 8$	$F = 17/2$	155 785.04	0.07	20.3
8	15/2	155 791.36	0.02	20.3
8	19/2	155 820.52	-0.02	20.3
8	13/2	155 826.92	0.01	20.3
9	19/2	154 443.53	0.10	28.4
9	17/2	154 448.00	0.02	28.4
9	21/2	154 471.86	-0.03	28.4
9	15/2	154 476.40	-0.04	28.4
10	21/2	152 972.59	-0.07	34.7
10	19/2	152 976.92	-0.10	34.7
10	23/2	152 995.93	0.01	34.7
10	17/2	152 999.27	-0.03	34.7

(*continued*)

The $Y(J, I, F)$ which appears in the contribution from the quadrupole interaction may be expressed as:

$$Y(J, I, F) = \frac{\frac{3}{4}C(C + 1) - I(I + 1)J(J + 1)}{2I(2I - 1)(2J - 1)(2J + 3)}, \qquad (6)$$

where

$$C = F(F + 1) - I(I + 1) - J(J + 1), \qquad \text{and where } \mathbf{F} = \mathbf{J} + \mathbf{I}. \qquad (7)$$

($I = \frac{3}{2}$ in the case of AsH$_3$ considered here.) The $K = 3$ levels contain the term $\pm h_0 J(J + 1)[J(J + 1) - 2][J(J + 1) - 6]$, first derived by Nielsen and Dennison (22) in their explanation of the anomalous effects in $K = 3$ lines observed by early microwave spectroscopists. Unfortunately, we were unable to evaluate the splitting constant h_0 for AsH$_3$ because the frequencies of the Q-type $K = 3 \to 0$ series occur below the operating range of our spectrometer.

The line strengths of the forbidden $\Delta K = \pm 3$ transitions (6, 23) are given by

$$S = \frac{1}{4}(\theta_z^{xx})_{\text{eff}}^2(J \mp K)(J \mp K - 1)(J \mp K - 2)(J \pm K + 1)(J \pm K + 2)$$
$$\times (J \pm K + 3)(2J + 1)/J(J + 1), \qquad (8)$$

HELMS AND GORDY

TABLE I—*Continued*

Transition				Observed Frequency ν (MHz)	ν Obs-ν Calc	α_{max} (calc) $(10^{-10}\,cm^{-1})$

$J \to J$	$K = \pm b \to \pm 2$	$F \to F$	(c) (continued)			
11		23/2		151 380.19	-0.02	38.0
11		21/2		151 382.73	-0.03	38.0
11		25/2		151 399.62	0.02	38.0
11		19/2		151 402.07	-0.10	38.0
12		25/2		149 674.47	-0.02	37.9
12		23/2		149 676.46	-0.02	37.9
12		27/2		149 690.90	-0.01	37.9
12		21/2		149 692.95	0.06	37.9
13		27/2		147 865.05	0.06	34.8
13		25/2		147 866.70	0.14	34.8
13		29/2		147 879.07	0.02	34.8
13		23/2		147 880.72	0.09	34.8
14		29/2		145 962.56	0.07	29.7
14		27/2		145 963.82	0.06	29.7
14		31/2		145 974.66	-0.02	29.7
14		25/2		145 975.96	-0.01	29.7
15		31/2		143 979.43	-0.10	23.7
15		29/2		143 980.44	-0.14	23.7
15		33/2		143 990.14	-0.07	23.7
15		27/2		143 991.25	-0.00	23.7
16		33/2		141 930.83	0.02	17.8
16		31/2		141 931.74	0.07	17.8
16		35/2		141 940.26	0.04	17.8
16		29/2		141 941.05	-0.03	17.8

(a) P. Helminger, E. Beeson, Jr., and W. Gordy, Ref. 3.

(b) Chu and Oka, Ref. 2. One frequency from this reference was omitted.

(c) Present work.

where

$$(\theta_x{}^{xx})_{\text{eff}} = \theta_x{}^{xx} + h^4 \tau_{xxxx} \mu_z / [2h(B - C)] \tag{9}$$

is the effective dipole moment inducing the transition. The term,

$$\theta_x{}^{xx} = 2(B)^2 \left[\frac{a_3{}^{xx}}{\nu_3{}^2} \left(\frac{\partial \mu_x}{\partial Q_3}\right) + \frac{a_4{}^{xx}}{\nu_4{}^2} \left(\frac{\partial \mu_x}{\partial Q_4}\right) \right], \tag{10}$$

is an induced dipole component which results from admixture of the ground vibrational state with excited vibrational modes. The last term of Eq. (9) results from centrifugally induced mixing of rotational levels of the ground vibrational state. In this expression, τ_{xxxx} is the centrifugal distortion constant in H' of Eq. (1), μ_z is the permanent dipole moment, and C and B are the spectral constants with respect to the symmetry axis and the perpendicular axis, respectively.

The contribution of the "vibrational intensity borrowing" [first term in Eq. (9)] is small in comparison with that of the "rotational intensity borrowing" [second term in Eq. (9)] (2). For PH$_3$, the relative contribution of these two terms to the forbidden line strengths, Eq. (8), is $(1.6/8.3)^2 = 0.037$, and it is estimated that the relative contribution is even smaller in AsH$_3$. Thus, for AsH$_3$ in the ground vibrational state the contribution of the vibrational mixing to the intensities of the $\Delta K = \pm 3$ transitions
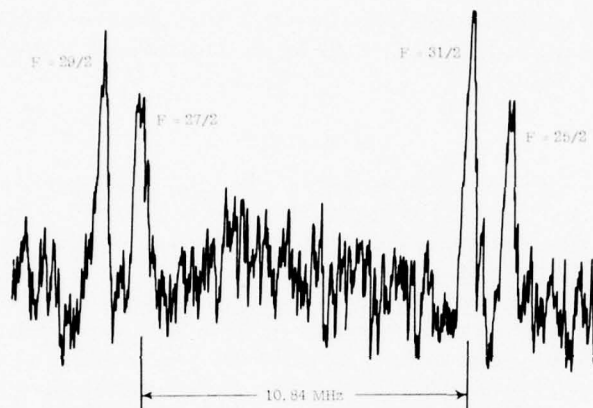
Fig. 1. Single scan of Q-type $K = \pm 5 \rightarrow \pm 2$ multiplet for $J = 14$.

is negligible in comparison with that from rotational mixing. We used the value of τ_{xxzz} from the analysis of the transition data to calculate the value of $(\theta_x{}^{xx})_{\text{eff}}$ used in the calculation of the intensities. The peak absorption coefficients, $\alpha_{\max}$, listed in Table I were calculated from the formula,

$$\alpha_{\max}(\text{cm}^{-1}) = \frac{1.147 \times 10^{-13}}{\Delta\nu T^{\frac{3}{2}}} \nu_0^2 \left(1 - \frac{h\nu_0}{2kT}\right)$$

$$\times \exp[-E(F, J, K)/kT](B^2C)^{\frac{1}{2}} g_K g_n S[(F, J, K \pm 3) \leftarrow (F, J, K)], \quad (11)$$

where S is given by Eq. (8), $T = 300$ K, g_n is the reduced nuclear statistical weight

TABLE II

Molecular Constants

Molecular Constant	Value	Standard Deviation $_{,}$*	
B_0	112 470.597	0.030	MHz
C_0	104 884.665	0.043	MHz
D_0^J	2.9297	0.0039	MHz
D^{JK}	-3.7164	0.0004	MHz
D_K	3.4126	0.0021	MHz
$(\tau^{(4)}\tau_{xxzz}/4h)$	0.679	0.003	MHz
H_{JJK}	-0.239	0.009	kHz
H_K	1.990	0.047	kHz
L_{JJJK}	0.701	0.011	Hz
L_{JJKK}	-1.729	0.067	Hz
C_N	0.111	0.016	MHz
C_K	0.113	0.017	MHz
(eQq)	-162.56	0.11	MHz
$[\tau^{(4)}\tau_{xxzz}\mu_z/2h(B-C)]$	3.938	0.017	10^{-6}D
r_0	1.5201381	0.0000002	Å
a_0	91.975798	0.000006	(°)

* One standard deviation.

factor, g_K is the statistical weight factor for each K level, and $\Delta\nu = 20$ MHz is the line breadth at a pressure of 1 Torr. This value for the $\Delta\nu$ is the same as that used by Chu and Oka (2) for AsH_3.

IV. RESULTS

Twenty-seven $K = \pm 4 \rightarrow \pm 1$ and thirty-six $K = \pm 5 \rightarrow \pm 2$ transitions were measured in this work. The observed frequencies are given in Table I. Figure 1 shows a chart recording of a single scan of the Q-type $K = \pm 5 \rightarrow \pm 2$ multiplet for $J = 14$. The quadrupole doublet is well resolved.

A combined computer analysis was made of the available frequencies for different types of transitions measured by us and by others as listed in Table I. The analysis consisted of a least-squares fitting of thirteen molecular constants to the observed frequencies of AsH_3. The program calculates the difference in the energy levels by use of Eqs. (2)–(7) with assumed values of the molecular constants. Transition frequencies are calculated and compared to the measured transition frequencies to generate new estimates of the molecular constants. This iterative procedure is repeated by the computer until convergence is attained. The degree of fitting of the complete frequency set is shown by column 3 of Table I. The molecular constants for AsH_3 obtained from the combined analysis are listed in Table II.

The two independent zero-point-effective structural parameters for AsH_3, r_0 and α_0, were calculated from the B_0 and C_0; the resulting values are listed at the bottom of Table II. The standard deviations recorded for these values reflect only those uncertainties in the measurement of B_0 and C_0 and do not indicate the possible errors in the absolute values which depend on Planck's constant.

RECEIVED: August 19, 1977

REFERENCES

1. D. HELMS AND W. GORDY, *J. Mol. Spectrosc.* **66**, 206 (1977).
2. F. Y. CHU AND T. OKA, *J. Chem. Phys.* **60**, 4612 (1974).
3. P. HELMINGER, E. L. BEESON, JR., AND W. GORDY, *Phys. Rev. A* **3**, 122 (1971).
4. W. B. OLSON, A. G. MAKI, AND R. L. SAMS, *J. Mol. Spectrosc.* **55**, 252 (1975).
5. K. SARKA, D. PAPOUSEK, AND K. NARAHARI RAO, *J. Mol. Spectrosc.* **37**, 1 (1971).
6. J. K. G. WATSON, *J. Mol. Spectrosc.* **40**, 536 (1971).
7. J. K. G. WATSON, *J. Mol. Spectrosc.* **55**, 498 (1975).
8. F. MICHELOT, J. MORET-BAILLY, AND K. FOX, *J. Chem. Phys.* **60**, 2606, 2610 (1974).
9. I. OZIER, *J. Mol. Spectrosc.* **56**, 124 (1975).
10. T. OKA, *in* "Molecular Spectroscopy: Modern Research," (K. N. Rao and C. W. Matthews, Eds.), Vol. II, p. 229, Academic Press, New York (1976).
11. A. ROSENBERG, I. OZIER, AND A. K. KUDIAN, *J. Chem. Phys.* **57**, 568 (1972).
12. A. ROSENBERG AND I. OZIER, *Chem. Phys. Lett.* **13**, 400 (1933).
13. A. ROSENBERG AND I. OZIER, *Canad. J. Phys.* **52**, 575 (1974).
14. A. ROSENBERG AND I. OZIER, *J. Chem. Phys.* **58**, 5168 (1973).
15. W. A. KREINER, U. ANDRESEN, AND T. OKA, *J. Chem. Phys.* **66**, 4662 (1977).
16. C. W. HOLT, M. C. L. GERRY, AND I. OZIER, *Phys. Rev. Lett.* **31**, 1033 (1973).
17. R. H. KAGANN, I. OZIER, AND M. C. L. GERRY, TG12, "Thirty-Second Symposium on Molecular Spectroscopy, Ohio State University, 13–17 June 1977."
18. T. OKA, *J. Chem. Phys.* **47**, 5410 (1967).

19. G. HERZBERG, "Infrared and Raman Spectra of Polyatomic Molecules," Van Nostrand–Reinhold, Princeton, N. J., 1945; see also J. T. HOUGEN, *J. Chem. Phys.* **37**, 1433 (1962).
20. G. AMAT, H. H. NIELSEN, AND G. TARRAGO, "Rotation-Vibration of Polyatomic Molecules," Dekker, New York, 1971.
21. W. B. OLSON, private communication.
22. H. H. NIELSEN AND D. DENNISON, *Phys. Rev.* **72**, 1011 (1947).
23. H. M. HANSON, *J. Mol. Spectrosc.* **23**, 287 (1967).

Centrifugal Distortion Analysis of the Ground Vibrational States of $H_2{}^{17}O$ and $H_2{}^{18}O$ [1]

PAUL HELMINGER[2]

Department of Physics, University of South Alabama, Mobile, Alabama 36688

AND

FRANK C. DE LUCIA

Department of Physics, Duke University, Durham, North Carolina 27706

Centrifugal distortion analyses of combined infrared-microwave data sets for $H_2{}^{17}O$ and $H_2{}^{18}O$ have been performed. These analyses make possible critical evaluation of data points and results in substantially improved energy levels. The Fraley-Rao interpolation rule for the prediction of $H_2{}^{17}O$ energy levels is examined and extended.

INTRODUCTION

Several years ago we published centrifugal distortion analyses for a number of isotopic species of water. Except for the $H_2{}^{16}O$ (*1*), $H_2{}^{17}O$ (*2*), and $H_2{}^{18}O$ (*3*) species these were based entirely upon microwave data. Because for these species it was not possible to measure enough microwave lines, it was necessary to include infrared data in our calculations. Although at the time of our analyses extensive $H_2{}^{16}O$ infrared data was available, only a modest amount of $H_2{}^{18}O$ data (*4, 5*) and virtually no $H_2{}^{17}O$ data had been published. In this paper we report new analyses of $H_2{}^{17}O$ and $H_2{}^{18}O$ that include substantial amounts of new infrared data in addition to our earlier microwave data.

Because a centrifugal distortion analysis has substantially fewer degrees of freedom than a purely algebraic combination difference analysis and because the former are more sensitive to "bad" data points which can be eliminated,[3] more accurate and reliable energy levels can be obtained. In addition, the independent analyses of the three isotopic species make possible a critical evaluation and refinement of the Fraley-Rao interpolation rule for the prediction of $H_2{}^{17}O$ energy levels.

---

[1] This work is supported by the U.S. Army Research Office, Grant DAAG29-77-G-0007.

[2] Travel to Duke University supported by Southern Regional Educational Board.

[3] For an enlightening discussion of a mathematician's view on the rejection of data, see F. J. Anscombe and J. W. Tukey, Technometrics **5**, 141 (1963).

$H_2^{17}O$ ANALYSIS

We have combined 46 of the far-infrared lines reported by Winther (6), 31 combination differences calculated from the data of Toth et al. (8), 20 combination differences calculated from the data of Camy-Peyret et al. (9), and our seven microwave lines (2) in a weighted Watson analysis.[4] The assigned weights were inversely proportional to the square of the expected uncertainty and ranged from 10^7 for the microwave lines to one for Winther's weakest lines. In order to carefully screen the data, each of the 104 data points was removed (in groups) from the analysis and predicted on the basis of the remaining data. With the exception of a few lines at high J_τ, the uncertainty in each of the predictions was $< \pm 0.01$ cm^{-1} and most were much better. For all the lines contained in the data set, the agreement between the calculated uncertainty in the prediction and the expected experimental uncertainty was satisfactory except for the data points listed in Table I. While only one of these data points is dramatically bad (the rest are off by about 0.05 cm^{-1}), they are all substantially worse than the data retained in the analysis. The spectral constants which result from our analysis are shown in Table II and the energy levels calculated from them in Table III. Four places are retained in the energy levels because it has been found that the analyses successfully predict unanalyzed microwave lines to this accuracy.

$H_2^{16}O$ AND $H_2^{18}O$ ANALYSES

The $H_2^{18}O$ energy levels shown in Table III result from an analysis very similar to the $H_2^{17}O$ analysis discussed above except that each of the data subsets is larger and a total of 240 data points were analyzed. At the highest J_τ, it was not possible to establish with certainty the reliability of the infrared data points because of the scattered nature of the data. However, at lower J_τ, the deviations of several points from the fit were inconsistent with their assigned weights and they were eliminated from the fit. These are shown in Table IV.

The $H_2^{16}O$ energy levels listed in Table III are those which result from the original analysis (1) of 15 microwave lines and the infrared data available to us at that time.

TABLE I

Data Points Removed from $H_2^{17}O$ Analysis

Levels	Obs-Calc (cm^{-1})	Ref.
$5_{32} - 5_{23}$	0.054	6
$4_{23} - 4_{14}$	0.049	6
$5_{41} - 6_{43}$	-0.567	9 [a]

[a] The reassignment by Winther (Ref. 6) of one of the transitions of Ref. 9 which leads to the $6_{16} - 8_{18}$ combination difference seems to be correct and is included in our analysis.

[4] For a detailed discussion of our analysis technique, see Ref. (1)

TABLE II

Rotation and Distortion Constants of the Ground Vibrational State of Water (MHz)

Constant	$H_2{}^{16}O$ Value[a]	σ	$H_2{}^{17}O$ Value[a]	σ	$H_2{}^{18}O$ Value[a]	σ
a	835 840.288	0.50	830 282.791	1.6	825 366.844	1.0
$\mathcal{B}$	435 351.717	0.45	435 357.289	2.6	435 356.685	0.8
c	278 138.700	0.45	277 505.735	2.6	276 948.998	0.8
Δ_J	37.59422	0.02	37.59414	0.09	37.54579	0.017
Δ_{JK}	-172.9128	0.17	-171.8532	0.3	-171.1683	0.13
Δ_K	973.29052	0.10	960.46634	0.5	949.88229	0.2
δ_J	15.21040	0.010	15.34663	0.04	15.23181	0.011
δ_K	41.0502	0.15	41.4538	1.2	38.8850	0.2
$H_J \cdot (10^2)$	1.56556	0.020	1.82110	0.12	1.53906	0.019
$H_{JK} \cdot (10^2)$	-4.2081	0.6			-3.1738	0.4
$H_{KJ} \cdot (10^1)$	-5.09508	0.10	-6.42468	2.6	-5.21898	0.12
$H_K \cdot (10^0)$	3.733028	0.008	3.745123	0.06	3.624767	0.017
$h_J \cdot (10^3)$	7.79579	0.09	10.18803	0.6	8.04641	0.14
$h_{JK} \cdot (10^2)$	-2.5165	0.11	3.7859	2.4	-2.4187	0.25
$h_K \cdot (10^0)$	1.0971	0.03	1.1495	0.13	1.0488	0.04
$L_{JK} \cdot (10^3)$	-3.0647	0.46			-4.6449	0.6
$L_{KKJ} \cdot (10^2)$	1.02952	0.12			1.46700	0.16
$L_K \cdot (10^2)$	-2.340138	0.08	-1.517327	0.17	-2.617359	0.11
$l_J \cdot (10^6)$					-2.59	0.8
$l_{JK} \cdot (10^4)$			-4.257	2.6		
$l_K \cdot (10^2)$	-1.3546	0.10	-0.328	0.2	-1.32008	0.13
$P_K \cdot (10^5)$	5.19841	0.07	4.71660	1.5	5.72244	0.4
$P_K \cdot (10^5)$	3.7603	1.0				

[a] The large number of digits retained in the higher order constants is required in order to reproduce the energy levels to experimental uncertainty.

More recent energy levels (*10*), based upon the high resolution experimental data of Guelachvili (and apparently upon our microwave data, too), result in essentially the same energy levels over the J_τ range of the original analysis.

FRALEY-RAO INTERPOLATION RULE

The Fraley-Rao (*4*) interpolation rule can be stated as

$$\frac{\nu_{17} - \nu_{16}}{\nu_{18} - \nu_{16}} = k \tag{1}$$

Table V shows the result of the application of this rule to the observed microwave transitions of $H_2{}^{17}O$. It is obvious that large deviations exist. A similar effect has been observed for microwave transitions of D_2O (*11*). However, critical inspection of the

HELMINGER AND De LUCIA

TABLE III

Energy Levels of the Ground Vibrational States of Water (cm^{-1})

	$H_2{}^{16}O$	$H_2{}^{17}O$	$H_2{}^{18}O$
1_{01}	23.7945	23.7735	23.7550
1_{11}	37.1372	36.9311	36.7487
1_{10}	42.3718	42.1870	42.0235
2_{02}	70.0911	70.0047	69.9276
2_{12}	79.4965	79.2273	78.9987
2_{11}	95.1762	94.9706	94.7888
2_{21}	134.9019	134.1453	133.4759
2_{20}	136.1642	135.4312	134.7833
3_{03}	136.7622	136.5378	136.3369
3_{13}	142.2788	141.9024	141.5682
3_{12}	173.3665	173.1102	172.8832
3_{22}	206.3019	205.4820	204.7561
3_{21}	212.1568	211.4389	210.7995
3_{31}	285.2199	283.5615	282.0950
3_{30}	285.4191	283.7677	282.3075
4_{04}	222.0536	221.6212	221.2344
4_{14}	224.8388	224.3043	223.8288
4_{13}	275.4981	275.1305	274.8037
4_{23}	300.3628	299.4389	298.6206
4_{22}	315.7801	315.0786	314.4592
4_{32}	382.5177	380.8068	379.2924
4_{31}	383.8433	382.1772	380.7033
4_{41}	488.1083	485.2089	482.6445
4_{40}	488.1348	485.2361	482.6736
5_{05}	325.3489	324.6613	324.0472
5_{15}	326.6261	325.8803	325.2161
5_{14}	399.4591	398.8787	398.3612
5_{24}	416.2094	415.1969	414.1680
5_{23}	446.5114	445.7931	445.1591
5_{33}	503.9687	502.1802	500.5973
5_{32}	508.8127	507.1764	505.7298
5_{42}	610.1160	607.1629	604.5461
5_{41}	610.3428	607.4014	604.7948
5_{51}	742.0744	737.6190	733.6817
5_{50}	742.0777	737.6225	733.6854
6_{06}	446.6976	445.7193	444.8467
6_{16}	447.2531	446.2446	445.3467
6_{15}	542.9078	541.9046	541.1810
6_{25}	552.9121	551.6058	550.4519
6_{24}	602.7743	601.9598	601.2382
6_{34}	648.9786	647.0694	645.3637
6_{33}	661.5480	659.9804	658.6111
6_{43}	756.7262	753.7094	751.0354
6_{42}	757.7816	754.8182	752.1890
6_{52}	888.6029	884.0865	880.0806
6_{51}	888.6368	884.1228	880.1159
6_{61}	1045.0623	1038.7644	1033.1986
6_{60}	1045.0627	1038.7648	1033.1991
7_{07}	586.2446	584.9403	583.7782
7_{17}	586.4800	585.1610	583.9869
7_{16}	704.2166	702.8811	701.6952
7_{26}	709.6092	708.0092	706.5992
7_{25}	782.4110	781.3750	780.4630
7_{35}	816.6931	814.6007	812.7628
7_{34}	842.3560	840.8691	839.5505
7_{44}	927.7438	924.6402	921.8983
7_{43}	931.2371	928.3024	925.7023
7_{53}	1059.6510	1055.0641	1050.9958
7_{52}	1059.8398	1055.2667	1051.2086
7_{62}	1216.1996	1209.82..	1204.1766
7_{61}	1216.2043	1209.82..	1204.1821
7_{71}	1394.8190	1386.41..	1378.9899
7_{70}	1394.8191	1386.41..	1378.9899

TABLE III—*Continued*

	$H_2{}^{16}O$	$H_2{}^{17}O$	$H_2{}^{18}O$
8_{08}	744.0648	742.3976	740.9125
8_{18}	744.1636	742.4895	740.9989
8_{17}	882.8934	881.0929	879.4956
8_{27}	885.6017	883.6428	881.9156
8_{26}	982.9139	981.4921	980.2218
8_{36}	1006.1139	1003.7614	1001.7065
8_{35}	1050.1580	1048.6671	1047.3304
8_{45}	1122.7063	1119.4733	1116.6389
8_{44}	1131.7742	1128.9485	1126.4425
8_{54}	1255.1689	1250.4961	1246.3755
8_{53}	1255.9137	1251.2943	1247.2128
8_{63}	1411.6216	1405.1541	1399.4402
8_{62}	1411.6520	1405.1877	1399.4754
8_{72}	1590.7053	1582.1979	1574.6833
8_{71}	1590.7059	1582.1986	1574.6840
8_{81}	1789.0395	1776.2960	1768.8142
8_{80}	1789.0395	1776.2960	1768.8142

energy levels of Table III show that they obey the rule

$$\frac{E_{17} - E_{16}}{E_{18} - E_{16}} = k \tag{2}$$

where $k = 0.5307 \rightarrow 0.5275$. This results directly from

$$\frac{A_{17} - A_{16}}{A_{18} - A_{16}} = 0.5307 \quad \text{and} \quad \frac{C_{17} - C_{16}}{C_{18} - C_{16}} = 0.5275$$

with the change in rotational energy due to isotopic substitution given by

$$\Delta E = \frac{\partial E}{\partial A} \Delta A + \frac{\partial E}{\partial B} \Delta B + \frac{\partial E}{\partial C} \Delta C \tag{3}$$

and $\Delta B \approx 0$ for an on axis isotopic substitution. As a result at high K_{-1} where

TABLE IV

Data Points Removed from $H_2{}^{18}O$ Analysis

Levels	Obs-Calc (cm^{-1})	Ref.
$2_{20} - 1_{11}$	0.029	6
$5_{24} - 4_{13}$	0.040	6
$6_{33} - 5_{24}$	-0.049	6
$7_{44} - 7_{35}$	0.040	6
$8_{54} - 7_{25}$	-0.041	6
$8_{27} - 8_{18}$	0.042	6
$7_{25} - 6_{25}$	0.047	8
$6_{52} - 5_{50}$	-0.021	9
$7_{25} - 6_{25}$	-0.884	9
$8_{27} - 7_{25}$	0.883	9

TABLE V

Values of the Fraley Rao Constant for Observed Microwave Transitions

Transition	k
$1_{10} - 1_{01}$	0.530807
$2_{11} - 2_{02}$	0.532543
$3_{13} - 2_{20}$	0.532021
$4_{14} - 3_{21}$	0.536887
$4_{23} - 3_{30}$	0.531228
$5_{15} - 4_{22}$	0.493528
$6_{16} - 5_{23}$	0.523757

$\partial E/\partial A = \langle P_a^2 \rangle$ is large and $\partial E/\partial C \approx \langle P_c^2 \rangle$ is small, $k \approx 0.5307$. Conversely at low K_{-1}, $k \approx 0.5275$.

Equation (2) can be rewritten for transitions as

$$\frac{\nu_{17} - \nu_{16}}{\nu_{18} - \nu_{16}} = k^l + (k^u - k^l)\frac{E_{18}{}^u - E_{16}{}^u}{\nu_{18} - \nu_{16}} \tag{4}$$

where the superscripts refer to the upper and lower energy levels of the transition. The correction term is large in regions where the dominant terms of Eq. (3) are changing, especially for transitions whose frequency changes little upon isotopic substitution. The lines of Table V which show the greatest deviations from Eq. (1) are the same lines that Eq. (4) predicts to have these variations.

COMPARISON WITH OTHER ENERGY LEVELS AND CONCLUSIONS

Our original $H_2^{17}O$ analysis was based upon our measured microwave data and distortion constants calculated from the $H_2^{16}O$ and $H_2^{18}O$ analyses. A comparison between the energy levels which resulted from this and those of Table III show exceedingly close agreement (typically 0.002 cm^{-1}) up to the 5_{41} level. At higher J_τ the agreement is still good (typically 0.002 cm^{-1} at low K_{-1} up to 0.02 cm^{-1} at high K_{-1}) except for the 6_{61} and 6_{60} levels. These are lower by 0.17 cm^{-1} in our latest analysis. This is because our earlier analysis of $H_2^{18}O$ was perturbed by infrared energy levels for 6_{60} and 6_{61} which were high by 0.30 cm^{-1} compared to the $H_2^{18}O$

TABLE VI

Comparison of Observed Energy Levels with those Calculated from Eq. (2) (cm^{-1})

State	Observed	Calculated	Difference
1_{10}	42.1870	42.1870	0.0000
2_{20}	135.4312	135.4313	-0.0001
3_{30}	283.7677	283.7678	-0.0001
4_{40}	485.2361	485.2365	-0.0004
5_{50}	737.6225	737.6239	-0.0014
6_{60}	1038.7648	1038.7667	-0.0019
7_{70}	1386.4179	1386.4186	-0.0007
8_{80}	1778.2960	1778.3059	-0.0099

energy levels shown in Table III. For medium values of J, the energy levels of Refs. (6) and (8) differ from the levels of Table III by substantially more (typically 0.01 cm^{-1}) than do our earlier energy levels. The energy levels of Ref. (6), which extend to higher J, than those of Ref. (8), deteriorate somewhat relative to the values of Table III, but all agree to within 0.05 cm^{-1} or better.

It is to be expected that our latest analysis is better than previous analyses because it contains the earlier data sets as subsets and because our analysis technique makes possible rather sensitive tests for bad data points and substantially reduces the degrees of freedom. It is perhaps somewhat surprising that our earlier analysis was so good.

Since all of the energy levels of the three isotopes were calculated independently, one check of their accuracy and also of the accuracy of Eq. (2) can be accomplished by the use of the $H_2^{16}O$ and $H_2^{18}O$ energy levels in this equation to calculate the energy levels of $H_2^{17}O$. Since it is most difficult to get good energy levels at high K_{-1} and since the isotopic splittings of the energy levels are also greatest there, the most stringent test would be the J_{J0} levels. The close argument shown in Table VI between the energy levels calculated directly from the $H_2^{17}O$ data and the levels calculated via Eq. (2) confirms both the accuracy of this relation and the quality of the energy levels for all three species.

RECEIVED: November 18, 1977

REFERENCES

1. F. C. DE LUCIA, P. HELMINGER, R. L. COOK, AND W. GORDY, *Phys. Rev.* A**5**, 487 (1972).
2. F. C. DE LUCIA AND P. HELMINGER, *J. Mol. Spectrosc.* **56**, 138 (1975).
3. F. C. DE LUCIA, P. HELMINGER, R. L. COOK, AND W. GORDY, *Phys. Rev.* A**6**, 1324 (1972).
4. P. E. FRALEY, K. NARAHARI RAO, AND L. H. JONES, *J. Mol. Spectrosc.* **29**, 312 (1969).
5. J. G. WILLIAMSON, K. NARAHARI RAO, AND L. H. JONES, *J. Mol. Spectrosc.* **40**, 372 (1971).
6. F. WINTHER, *J. Mol. Spectrosc.* **65**, 405 (1977).
7. F. J. ANSCOMBE AND W. TUKEY, *Technometrics* **5**, 141 (1963).
8. R. A. TOTH, J. M. FLAUD, AND C. CAMY-PEYRET, *J. Mol. Spectrosc.* **67**, 185 (1977).
9. C. CAMY-PEYRET, J. M. FLAUD, G. GUELACHVILI, AND C. AMIOT, *Mol. Physics* **26**, 825 (1973).
10. J. M. FLAUD, C. CAMY-PEYRET, AND J. P. MAILLARD, *Mol. Physics* **32**, 499 (1976).
11. J. BELLET, W. J. LAFFERTY, AND G. STEENBECKELIERS, *J. Mol. Spectrosc.* **47**, 388 (1973).

Millimeter-Wave Spectrum, Centrifugal Distortion Analysis, and Energy Levels of HNO₃[1]

GABRIELE CAZZOLI[2,3] AND FRANK C. DE LUCIA

Department of Physics, Duke University, Durham, North Carolina 27706

One hundred and eleven new rotational transitions of HNO_3 have been measured in the millimeter-microwave region. This data set is the basis for a centrifugal distortion analysis and for the calculation of a complete set of energy levels through $J = 50$. The constants which result from this analysis are (in megahertz): $A = 13\,011.0287 \pm 0.0057$, $B = 12\,099.8611 \pm 0.0057$, $C = 6260.6391 \pm 0.0006$, $\Delta_J = (14.038 \pm 0.026) \times 10^{-3}$, $\Delta_{JK} = (-20.1780 \pm 0.0037) \times 10^{-3}$, $\Delta_K = (7.4153 \pm 0.0108) \times 10^{-3}$, $\delta_J = (1.1828 \pm 0.00039) \times 10^{-3}$, $\delta_K = (-20.5648 \pm 0.0046) \times 10^{-3}$, $H_J = (-9.84 \pm 3.82) \times 10^{-8}$, $H_{JK} = (-9.933 \pm 0.367) \times 10^{-8}$, $H_{KJ} = (1.03 \pm 0.12) \times 10^{-7}$, $h_J = (-9.241 \pm 0.127) \times 10^{-9}$, $h_{JK} = (-1.398 \pm 0.032) \times 10^{-7}$, and $h_K = (1.135 \pm 0.027) \times 10^{-6}$.

INTRODUCTION

Nitric acid is a near-oblate asymmetric rotor with rotational constants of the order of 10 GHz and moderate centrifugal distortion. The presence of this species in the atmosphere and its basic role in chemistry have stimulated numerous spectroscopic studies. The rotational spectrum of HNO_3 has been studied in the centimeter-wave region (*1–3*), and Kaushik and Venkateswarlu (*4*) have performed a centrifugal distortion analysis of these data. They noted that the relatively large standard deviations of the resulting coefficients and the indeterminacy of τ_{cccc} must be ascribed to the data set available. Conventional infrared spectroscopy reveals only broad vibrational bands because of the dense rotational fine structure of HNO_3 (*5–8*). Recently, however, Brockman *et al.* (*9*) have published an unassigned diode laser spectrum of HNO_3 in the 11-μm region that clearly resolves the rotational fine structure. Several other diode laser studies of HNO_3 are also in progress (*10*).

In this paper we report the measurement of 111 rotational transitions in the region between 80 and 300 GHz. This spectral coverage results in a well-conditioned data set which makes possible an accurate centrifugal distortion analysis and calculation of energy levels through $J = 50$. These ground-vibrational-state energy levels can serve as a basis for the analysis of the complex rotation–vibration spectra which are now being recorded as well as for the study of

131

TABLE I

Observed Microwave Transitions of HNO$_3$ (MHz)

Transition	Observed frequency		Transition	Observed frequency		Transition	Observed frequency

a. See Refs. 1 and 2.

HNO$_3$ by direct microwave techniques. A preliminary report of this work has been given recently (*11*).

II. EXPERIMENTAL DETAILS

We have previously detailed our general experimental technique (*12, 13*). A brief description of the specific configuration for this work follows. Millimeter-wave energy was produced by King and Gordy (*14*) crystal harmonic generators driven by OKI klystrons in the 35-GHz range. This energy was focused by quasi-optical techniques through a 4-m-long absorption cell made of 10-cm-diameter KIMAX glass pipe and detected by a 1.6-K InSb photoconduction detector. The HNO$_3$ vapor was taken directly from a standard laboratory mixture of concentrated nitric acid.

Although most of the lines reported here are strong video oscilloscope lines, source modulation and lock-in techniques were used to record the weaker high-J lines. For this work the 35-GHz klystron was phase locked, via a phased-locked X-13 Varian klystron and transfer oscillator, to a crystal oscillator whose phase was continuously monitored against WWVB.

III. RESULTS AND DISCUSSION

We have used Watson's reduced centrifugal distortion Hamiltonian (*15*) and the computational and statistical techniques that we have previously discussed (*16, 17*) for the analysis of the rotational spectrum of HNO$_3$. A "bootstrap" assignment–analysis procedure was used. At each step lines that would provide a balance between a maximum of new, independent information for the analysis and a minimum risk of assignment error were selected for measurement. In practice this amounted to the selection of lines whose prediction uncertainties were several megahertz. This procedure was iterated until all of the approximately 5000 lines of significant strength below $J = 50$ were predicted with an uncertainty of 1 MHz or less.

Table I shows the 131 rotational transitions included in our analysis and Table II shows the spectral constants which result. In our analysis H_K was found to be only marginally determined and was subsequently eliminated from the constant set. The rms deviation of the analysis was 0.124 MHz with or without

TABLE II

Spectroscopic Constants of HNO$_3$ (MHz)

$a = 13\,011.0287 \pm 0.0057$ $B = 12\,099.8611 \pm 0.0057$ $C = 6\,260.6391 \pm 0.0006$

$\Delta_J = (14.038 \pm 0.026) \cdot 10^{-3}$ $\Delta_{JK} = (-20.1780 \pm 0.0037) \cdot 10^{-3}$ $\Delta_K = (7.4153 \pm 0.0108) \cdot 10^{-3}$

$\delta_J = (1.1828 \pm 0.00039) \cdot 10^{-3}$ $\delta_K = (-20.5648 \pm 0.0046) \cdot 10^{-3}$

$H_J = (-9.84 \pm 3.82) \cdot 10^{-8}$ $H_{JK} = (-9.933 \pm 0.367) \cdot 10^{-8}$ $H_{KJ} = (1.03 \pm 0.12) \cdot 10^{-7}$

$h_J = (-9.241 \pm 0.127) \cdot 10^{-9}$ $h_{JK} = (-1.398 \pm 0.032) \cdot 10^{-7}$ $h_K = (1.135 \pm 0.027) \cdot 10^{-6}$

TABLE III

Energy Levels of HNO_3 (cm^{-1})

J=							
0	0.837507						
1	2.515397		1.472932		3.612441		
2		2.747258		3.133938			
3			4.169544	3.133938	3.133716		
4			7.64422	7.49166	6.478392	6.476797	5.013942	5.013929
5		11.657031	11.63034	11.730746	11.657031	10.650342	9.19574	9.194961	7.311673
6			16.582343	15.669493	15.651503	14.208918	14.208358	12.328885
7			22.350913	21.517220	21.473954	20.055866	20.053836	18.180032
8			26.490215	26.230280 / 16.850272	28.110501 / 16.710689	26.734396	26.728415	24.864079
9			35.949798	35.353928 / 24.237338	35.556339 / 24.237338	34.243766 / 20.678945	34.228630 / 20.678945	32.379887
10			44.462768 / 35.733507	44.092283 / 32.598234	43.328760 / 32.598234	42.583721 / 29.041987	42.549760 / 29.041987	40.726232 / 25.064812
11			54.018645 / 47.627742	52.697983 / 44.923139	51.287121 / 41.792724	52.939603 / 41.792724	51.754681 / 38.239273	51.685821 / 38.239273	49.901946 / 34.264210

J= 12	J= 13	J= 14	J= 15	J= 16	J= 17	J= 18	J= 19	J= 20
59.05989	70.737642	82.396683	96.883554	108.199481	122.346505	137.327429	153.145683	169.805113
44.29781	55.165094	66.885428	53.259893	92.762640	106.958065	121.983647	137.838523	128.583918
				66.638513	80.852901	95.905597	111.781109	91.889094
61.40233	72.377420	83.924868	96.274415	109.432042	123.406764	139.209597	153.852863	172.349394
48.270210	59.134147	70.830377	83.58128	96.716570	110.904802	125.921856	141.766683	158.438152
		46.784158	59.328611	72.706954	86.918714	101.963393	117.860456	138.543942
						83.327919	83.327919	100.052749

TABLE III—Continued

333.788089	358.158882	383.393371	409.491512	436.653112	466.277879	492.965459
317.676263	317.261981	366.663597	392.379268	418.908025	449.269089	475.002179
292.086871	276.882408	344.202492	367.087528	392.736177	421.207472	442.309425
255.671760	232.905500	304.921765	323.861972	357.484027	385.005680	366.518157
208.669940		200.454276	286.370826	255.117994	280.699254	309.102066

333.806705	358.169907	383.359813	409.495232	436.455237	466.279081	492.966133
321.381937	345.209945	370.235767	395.853608	422.259880	449.437588	475.381878
298.087437	322.251804	344.249452	378.905543	395.691255	393.105114	442.343394
263.804386	288.209426	268.203805	294.053185	322.450176	393.105114	321.430992
218.914404	243.140036	212.801535	238.713138	265.453329	291.028774	255.560892

TABLE III—*Continued*

TABLE III—*Continued*

H_K as a variable. The spectral constants have been used to generate the energy levels shown in Table III. Because of the large number of rotational lines, the calculated spectrum is not reproduced here. It is available either from the Editorial Office of this Journal or from the second author.

An important point should be made about the use of these data in conjunction with other data sets, especially infrared rotation–vibration data sets. Although accurate ground-state energy levels are a convenient starting point for spectra assignments, from a statistical point of view it is preferable to use the observed microwave data directly in the final spectral analysis. The appropriate weightings for data are then reasonably straightforward. On the other hand, if energy levels or spectral constants are used, the appropriate statistical treatment requires the consideration of both the uncertainties in the spectral constants and in the correlation matrix (*18*). This is especially important in large centrifugal distortion analyses because of the significant correlations among the constants.

RECEIVED: August 14, 1978

REFERENCES

1. D. J. MILLEN AND J. R. MORTON, *Chem. Ind. (N. Y.)*, 954–954 (1956).
2. D. J. MILLEN AND J. R. MORTON, *J. Chem. Soc.*, 1523–1528 (1960).
3. A. P. COX AND J. M. RIVEROS, *J. Chem. Phys.* **42**, 3106–3112 (1965).
4. V. K. KAUSHIK AND P. VENKATESWARLU, *Chem. Phys. Lett.* **48**, 115–118 (1977).
5. G. E. McGRAW, D. L. BERNITT, AND I. C. HISATSUNE, *J. Chem. Phys.* **42**, 237–244 (1965).
6. A. GOLDMAN, F. S. BONOMO, W. J. WILLIAMS, AND D. G. MURCRAY, *J. Opt. Soc. Amer.* **65**, 10–12 (1975).
7. D. G. MURCRAY, T. G. KYLE, F. H. MURCRAY, AND W. J. WILLIAMS, *J. Opt. Soc. Amer.* **59**, 1131–1134 (1969).
8. H. COHN, C. K. INGOLD, AND H. G. POOLE, *J. Chem. Soc.* 4272–4282 (1952).
9. P. BROCKMAN, C. H. BAIR, AND F. ALLARIO, *Appl. Opt.* **17**, 91–100 (1978).
10. A. MAIK, private communication.
11. G. CAZZOLI AND F. C. DE LUCIA, Thirty-Third Symposium on Molecular Spectroscopy, 1978, Abstract WH 3.
12. P. HELMINGER, F. C. DE LUCIA, AND W. GORDY, *Phys. Rev. Lett.* **25**, 1397–1399 (1970).
13. F. C. DE LUCIA, *J. Mol. Spectrosc.* **55**, 271–277 (1975).
14. W. C. KING AND W. GORDY, *Phys. Rev.* **90**, 319–320 (1953).
15. J. K. G. WATSON, *J. Chem. Phys.* **45**, 1360–1361 (1966).
16. P. HELMINGER, R. L. COOK, AND F. C. DE LUCIA, *J. Mol. Spectrosc.* **40**, 125–136 (1971).
17. R. L. COOK, F. C. DE LUCIA, AND P. HELMINGER, *J. Mol. Spectrosc.* **41**, 123–136 (1972).
18. D. L. ALBRITTON, A. L. SCHMELTEKOPF, AND R. N. ZARE, *in* "Molecular Spectroscopy, Modern Research" (K. Narahari Rao, Ed.), Academic Press, New York, 1972.

Millimeter wave measurements of the rotational spectra of ClF, BrF, BrCl, ICl, and IBr

Robert E. Willis, Jr.[a] and William W. Clark, III[b]

Department of Physics, Duke University, Durham, North Carolina 27706
(Received 7 December 1979; accepted 18 January 1980)

The rotational spectra of all twelve stable isotopic species of ClF, BrF, BrCl, ICl, and IBr were observed and measured in the millimeter wave region by means of a sensitive microwave spectrometer. Transitions were detected over a wide range of frequencies for molecules in both the ground vibrational state and several excited states. The rotational spectrum of each molecule was split by the nuclear quadrupole interaction. Altogether, 250 new lines were measured. These correspond to 136 pure rotational transitions. Values of the Dunham coefficients Y_{01}, Y_{11}, Y_{21}, Y_{31}, Y_{02}, Y_{12}, and Y_{03} were obtained from a computer analysis of the measured frequencies. From these coefficients a number of equilibrium constants were derived to significantly greater accuracy than in previous work. In particular, the equilibrium distance, r_e, was found to two or three more significant figures.

INTRODUCTION

The mixed halide diatomic molecules described in this report have all been studied previously through techniques of microwave spectroscopy by various workers[1-8] whose results are presented in the N.B.S. tables of diatomic molecules.[9] However, most of their work was confined to the centimeter wave region and was concerned with nuclear quadrupole splittings of a few, low, rotational levels. Consequently, only a small number of rotational constants have been reported. The present work in the millimeter wave region has generated measurements of 136 new rotational transitions for molecules in a number of excited vibrational states. This has increased both the quantity and the accuracy of the rotational/vibrational constants which, in turn, has permitted the derivation of the equilibrium constants B_e, ω_e, $\omega_e x_e$, and r_e as well as the Dunham potential constants a_0, a_1, a_2, and a_3. In addition, this work has yielded rotational constants which are significantly different from previously reported values for six out of the 12 isotopic species studied.

THE SPECTROMETER

The spectrometer used for this study was similar in many respects to the ones used in other investigations of this laboratory.[10,11] Briefly, it consisted of a klystron-driven crystal harmonic generator, a quasi-free-space absorption cell, and a helium-cooled InSb photodetector. Most of the transitions were measured in real time on an oscilloscope screen, although a few were observed on a chart recorder with a lock-in amplifier and a phase-locked, slow-sweep klystron.[12]

For these experiments the absorption cell was a continuously evacuated 2 in. × 4 ft. nickel pipe with Teflon end plates to permit entry of the microwave radiation. The cell was encased by two 1400 W Linberg 2724-KSP semicircular heating elements. This arrangement allowed the temperature of the cell to be raised so that excited vibrational states could be populated. The

flanges and end plates were sealed with neoprene O rings. Because of reactions with the halogens, these rings had to be regreased or replaced frequently. A nitrogen cold trap was used to protect the forepump from the gases; nevertheless, the oil had to be changed occasionally, especially during the use of iodine compounds.

CHEMICAL PREPARATIONS

ClF and BrF

Chlorine trifluoride ClF_3 was used in the preparation of ClF and BrF. This is an extremely reactive gas[13] even at the pressures used in the experiment ($\sim 5 \times 10^{-2}$ Torr); therefore, a few special precautions were taken for the fluorine compounds: (1) The neoprene O rings were wrapped with Teflon tape and (2) copper tubing and brass fittings were used for connectors in place of rubber or glass tubing.

Chlorine monofluoride ClF was observed as a decay product of ClF_3 as the latter was was simply allowed to flow through the cell. This method was chosen over the use of ClF gas directly because ClF_3 is less expensive, easier to handle, and somewhat safer than ClF gas. However, the reaction $ClF_3 \rightarrow ClF + F_2$ proceeds very slowly at the low pressures of the absorption cell. As a result, the ClF lines were relatively weak. Adding chlorine gas to the stream caused the line strength to go down rather than up. Warming the cell to about 100 °C increased the reaction rate, but above 100 °C, the line strength decayed, dropping to 1/4 of the maximum strength at only 200 °C. The rapid signal decay at elevated temperatures made it difficult to observe higher vibrational states. This problem was common to all the molecules in this study but was most severe for ClF because of its small molecular weight.

Bromine monofluoride BrF has been found only in the gaseous state in equilibrium with Br_2 and BrF_3. For this reason BrF was made by simultaneously pumping room-temperature quantities of Br_2 and ClF_3 through a cell that varied in temperature from 25 to 450 °C. Optimum line strength occurred with the cell at 200 °C, and the lines disappeared at 500 °C. Temperatures as high as 450 °C were used to populate excited vibrational states. Often strong lines were observed when the bro-

mine flow was off. This agrees with the fact that in an equilibrium mixture of Br_2, BrF_3, and BrF, the relative fraction of BrF drops off sharply at Br_2 is added.

BrCl, ICl, and BrI

The compounds not involving fluorine were all easier to make and handle than the above two. Bromine monochloride, $BrCl$, was made when one-third mole each of bromine and chlorine were combined in a 22 l Pyrex flask. At room temperature such a mixture will be 57% $BrCl$. The $BrCl$, which boils at 20 °C, was then allowed to flow through the cell. The ground-state lines were strongest at room temperature and 200 °C was the highest temperature used to populate excited vibrational states.

Since the vapor pressure of iodine is too high for it to be placed directly in the cell, the iodine compounds were also made in the 22 l flask. Addition of one-third mole of chlorine to excess iodine resulted in a rapid exothermic reaction producing ICl, a red liquid or gas (melting point 27 °C), as well as ICl_3, a dark yellow solid. The ICl was then allowed to flow through the cell. All measurements were made at room temperature because ICl decomposes at 97 °C.

Iodine monobromide IBr was made in a similar manner from a mixture of iodine and bromine in the 22 l flask. This produced IBr, dark grey crystals that melt at 41 °C and sublime at 50 °C, as well as IBr_3, a brown liquid. The flask was heated slightly with an infrared lamp to produce flow rate sufficient for measurement. The IBR lines did not appear until the IBR_3 was pumped out of the flask. Since IBR decomposes at 116 °C, the cell was not heated. This did not prevent observation of higher vibrational states, since in molecules as heavy as IBr, excited vibrational states are well populated at room temperature.

ANALYSIS OF ROTATIONAL SPECTRA

The most accurate formulas for analysis of the rotational spectra of diatomic molecules are provided by Dunham theory.[14] Dunham solved the Schrödinger wave equation for the diatomic vibrating rotor with a potential function of the form

$$V(\xi) = cha_0\xi^2(1 + a_1\xi + a_2\xi^2 + \cdots) , \tag{1}$$

where $\xi = (r - r_e)/r_e$, and a_0, a_1, a_2, ... are the potential constants. His solution for the rotation–vibration energies is expressed by the series

$$E_{v,J} = h \sum_{l,m} Y_{l,m} (v + \tfrac{1}{2})^l [J(J+1)]^m , \tag{2}$$

in which the coefficients $Y_{l,m}$ are known as the Dunham coefficients. Each $Y_{l,m}$ is a function of the molecular parameters r_e, a_0, a_1, a_2, ... which appear in Eq. (1). In terms of the familiar spectroscopic constants,

$$Y_{10} \cong \omega_e, Y_{01} \cong B_e, Y_{11} \cong -\alpha_e, Y_{21} \cong \gamma_e ,$$
$$Y_{20} \cong -\omega_e x_e, Y_{02} \cong -D_e, Y_{12} \cong -\beta_e, Y_{03} \cong H_e . \tag{3}$$

For pure rotational transitions the transition frequencies are given by

$$\nu_{v,J} - \nu_{v,J+1} = 2\left[Y_{01} + Y_{11}(v+\tfrac{1}{2}) + Y_{21}(v+\tfrac{1}{2})^2 + Y_{31}(v+\tfrac{1}{2})^3 + \cdots\right]$$
$$\times (J+1) + 4\left[Y_{02} + Y_{12}(v+\tfrac{1}{2}) + \cdots\right](J+1)^3$$
$$+ Y_{03}(J+1)^3\left[(J+2)^3 - J^3\right] + \cdots , \tag{4}$$

where only terms which give a detectable contribution to the spectra of this report are retained.

The spectrum of each species was analyzed by substitution of each reduced experimental rotational frequency (see quadrupole analysis) and the appropriate J and v quantum numbers into Eq. (4). This produced a set of simultaneous equations which were solved by the method of least squares for the $Y_{l,m}$'s. Although it is possible to analyze each individual isotopic species independently, use of the Dunham isotope relationship

$$Y'_{l,m} = (\mu/\mu')^{(l+2m/2)} Y_{l,m} \tag{5}$$

allows all the isotopic data for each molecular species to be analyzed together. This results in significantly better values for the $Y_{l,m}$, especially in the case of less abundant species for which few transitions are observed. Equation (5) is accurate to within experimental error for all $Y_{l,m}$ except Y_{01}.

The Y_{03} was calculated from the Dunham relation

$$Y_{03} = \frac{Y_{11}}{3}\left(\frac{-Y_{02}}{Y_{01}}\right)^{3/2} + \frac{2Y_{02}^2}{Y_{01}} \tag{6}$$

and its contribution to the measured frequencies removed before the least-squares analysis. Although its value can be calculated directly from the spectra, the procedure used here results in a more accurate Y_{03} as well as improved values for the other constants.

After determination of the Dunham coefficients the first four potential constants of Eq. (1) can be found by the relations

$$a_0 \equiv \frac{\omega_e^2}{4B_e} = \frac{B_e^2}{D_e} \cong \frac{-Y_{01}^2}{Y_{02}} , \tag{7}$$

$$a_1 = \frac{Y_{11}Y_{10}}{6Y_{01}^2} - 1 = \frac{Y_{11}}{3(-Y_{02}Y_{01})^{1/2}} - 1 , \tag{8}$$

$$a_2 = \frac{Y_{12}}{6}\left(\frac{Y_{01}}{-Y_{02}^3}\right)^{1/2} + \frac{9}{8}a_1(2+a_1) + \frac{19}{8} , \tag{9}$$

$$a_3 = -\frac{2}{5}\frac{Y_{21}}{Y_{02}} + \frac{a_2}{5}(3+13a_1) - \frac{a_1}{2}\left[4+3a_1(1+a_1)\right] - 1. \tag{10}$$

The relations given in Eq. (3) and subsequently used in Eqs. (7)–(10) are not exact. The exact relations are power series in $(B_e/\omega_e)^2$. Since for the mixed halides this ratio is of the order 10^{-6}, these relations may be considered accurate to the experimental uncertainty except for Y_{01}, which can be calculated to a higher accuracy from precision spectral data. The precise relationship between Y_{01} and B_e is

$$Y_{01} = B_e\left[1 + C_3(B_e/\omega_e)^2\right] = B_e + \delta_3 . \tag{11}$$

This difference between B_e and Y_{01} is known as the Dunham correction (δ_3).

Two other small corrections to Y_{01} result from electronic effects which are not included in the Dunham theory. These arise from the nonspherical distribution

of the atomic electrons around their respective nuclei (δ_1) and the wobble–stretch effect (δ_2).[15,16] The first of these may be calculated from knowledge of the molecular g factor by

$$\delta_1 = -(m_e/m_p)g_J B_e . \tag{12}$$

Although δ_2 cannot be calculated directly from known molecular parameters, its reduced mass dependence of $(1/\mu)^2$ allows its calculation if two or more isotopic species are observable. Since δ_1 and δ_3 also have a $(1/\mu)^2$ dependence, the net effect of all three corrections may be calculated from the system of equations.

$$(B_e - Y_{01})_i - C/\mu_i^2 = 0 , \tag{13}$$

where $C = \delta_1 + \delta_2 + \delta_3$ and i is an isotopic species label.

The values of B_e thus calculated provide a very accurate determination of the equilibrium distance r_e by means of the definition of B_e:

$$B_e \equiv h/8\pi^2 \mu r_e^2 . \tag{14}$$

The zero-point vibration frequency ω_e can next be calculated from the relation

$$\omega_e = (4B_e^3/D_e)^{1/2} \cong [4B_e^3/(-Y_{02})]^{1/2} \tag{15}$$

and $\omega_e x_e$ is obtained from

$$\omega_e x_e = -3Y_{01}(a_2 - \tfrac{5}{4}a_1^2)/2 . $$

NUCLEAR QUADRUPOLE INTERACTIONS

Hyperfine structure which occurs in the diatomic halides causes the observed frequencies to deviate slightly from those given in Eq. (4). These deviations are caused by nuclear electric quadrupole interactions with the electric field gradient at the nucleus. This splits the rotational energy levels into $2I + 1$ sublevels, where I is the nuclear spin. The actual energy levels are found from perturbation theory and to first order are given by[17]

$$E_{J,v,F} = E_{J,v} - eQq Y(J, I, F) , \tag{16}$$

where $E_{J,v}$ is the rotational energy given by Eq. (2), eqQ is the quadrupole coupling constant, and $Y(J, I, F)$ is Casimer's[18] function. The F in Eq. (16) is the total
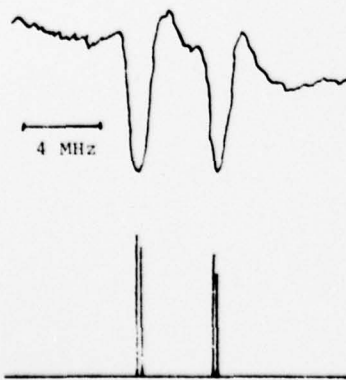

FIG. 1. Comparison of the theoretical and experimental quadrupole structure of ^{79}BrF, $J = 9 \to 10$, $v = 2$, at 209 379.84 MHz.

TABLE I. Dunham coefficients and equilibrium constants of chlorine monofluoride.

	$^{35}Cl^{19}F$	$^{37}Cl^{19}F$
Y_{01} (MHz)	15 483.2702(36)[a]	15 188.8247(30)
Y_{11} (MHz)	−129.6497(50)	−125.9687(49)
Y_{21} (kHz)	−520.3(1.7)	−500.7(1.6)
Y_{02} (kHz)	−26.91(2)	−25.90(2)
Y_{12} (kHz)	−0.14(2)	−0.13(2)
Y_{03} (Hz)	−5.47(3)×10⁻³	−5.16(3)×10⁻³
B_e (MHz)	15 484.4304(70)	15 189.9412(70)
r_e (Å)	1.628341(4)[b]	1.628341(4)[b]
ω_e (cm⁻¹)	783.553(30)	776.067(30)
$\omega_e x_e$ (cm⁻¹)	5.045(87)	5.026(84)

[a]Uncertainties represent one standard deviation.
[b]The uncertainty accrues from Planck's constant.

angular momentum quantum number which can assume the values $(J+1)$, $(J+I-1), \ldots, |J-I|$. Each rotational transition is thus split into a number of hyperfine lines, some of which are doubly degenerate or nearly degenerate. Figure 1 shows a typical rotational transition which is split by the quadrupole interaction.

For $J \to J+1$ rotational transitions, the selection rules for quadrupole structure are $\Delta F = 0, \pm 1$. For the high J values observed in this report, the $\Delta F = +1$ transitions dominate in strength. Therefore, the deviation in line frequency from Eq. (4) is given by

$$\Delta \nu = -eqQ[Y(J+1, I, F+1) - Y(J, I, F)] . \tag{17}$$

Since the frequency shift given in Eq. (17) decreases as $1/J^2$, the quadrupole structure was unresolved at high values of J. Nevertheless, quadrupole structure was observed in lower J transitions for all of the molecules in this report and had to be considered before the rotational analysis was attempted.

The frequencies of the unsplit rotational lines were determined in two ways. First, through measurement of the hyperfine splitting in this work, a reduced frequency could be determined from Eq. (17). The second method was to use the eqQ's obtained by the earlier lower frequency work, which yielded values one to two orders of magnitude more accurate than the eqQ's calculated from this work. This latter method gave a slightly different center frequency for each hyperfine component; the average of these frequencies was then averaged with the frequency resulting from the first method to yield a final value for the reduced rotational frequency.

For the species in which both nuclei have a quadrupole moment, the weaker quadrupole moment produced no observable splittings or shifts but did cause considerable broadening in some cases. The effect was strongest for low-frequency transitions in IBr and BrCl. Severely broadened transitions which could not be resolved were avoided in most instances because of difficulty in determination of the center frequency.

SPECTRAL CONSTANTS

The actual transition frequencies are not listed here but are recorded in the Ph.D. thesis of R. E. Willis.[19]

TABLE II. Dunham coefficients and equilibrium constants of bromine monofluoride.

	$^{79}Br^{19}F$	$^{81}Br^{19}F$
Y_{01} (MHz)	10 667.4502(35)[a]	10 616.3476(36)
Y_{11} (MHz)	−77.8629(79)	−77.3040(78)
Y_{21} (kHz)	−201.6(45)	−199.7(45)
Y_{31} (kHz)	−6.2(8)	−6.1(8)
Y_{02} (kHz)	−12.049(10)	−11.934(10)
Y_{12} (Hz)	−66(1)	−66(11)
Y_{03} (Hz)	$−3.937(7) \times 10^{-3}$	$−3.881(7) \times 10^{-3}$
B_e (MHz)	10 668.0970(69)	10 616.9882(69)
r_e (Å)	1.758987(4)[b]	1.758987(4)[b]
ω_e (cm^{-1})	669.679(28)	668.67(28)
$\omega_e x_e$ (cm^{-1})	3.863(76)	3.844(78)

[a]Uncertainties listed are one standard deviation.
[b]The uncertainty accrues from Planck's constant.

TABLE IV. Dunham coefficients and equilibrium constants of iodine monochloride.

	$^{127}I^{35}Cl$	$^{127}I^{37}Cl$
Y_{01} (MHz)	3422.3638(20)[a]	3277.4173(19)
Y_{11} (MHz)	−15.9751(43)	−14.9710(40)
Y_{21} (MHz)	−35.2(26)	−32.3(24)
Y_{31} (kHz)	−0.6(4)	−0.5(3)
Y_{02} (kHz)	−1.2081(6)	−1.108(6)
Y_{12} (Hz)	−5.9(6)	−5.5(6)
Y_{03} (Hz)	$−2.639(3) \times 10^{-4}$	$−2.318(3) \times 10^{-4}$
B_e (MHz)	3422.4275(38)	3277.4758(36)
r_e (Å)	2.320962(6)[b]	2.320962(6)[b]
ω_e (cm^{-1})	384.290(96)	376.064(94)
$\omega_e x_e$ (cm^{-1})	1.501(26)	1.437(25)

[a]Uncertainties listed are one standard deviation.
[b]The uncertainty accrues from Planck's constant.

The molecular constants are given; they can be used for calculation of the frequencies to high accuracy ($\lesssim 0.1$ MHz).

ClF

Previous microwave measurements of ClF have been made by White[1] and Gilbert.[2] They measured a number of quadrupole lines of the $J = 0 \to 1$ rotational transition in the 0, 1 vibrational states. The current work has produced measurements of 42 new transitions: 32 of ^{35}ClF and 10 of the lesser abundant ^{37}ClF. These measurements yielded 22 reduced rotational frequencies covering the rotational states from $J = 2$ up to $J = 11$ in the 0, 1, 2 vibrational states. The frequencies ranged from 92 GHz at $J = 2 \to 3$ to 339 GHz at $J = 10 \to 11$.

The Dunham coefficients obtained from these measurements are shown in Table I along with the equilibrium constants. Comparison of calculated frequencies with the measured frequencies yields a root mean square deviation of 35 kHz for both isotopes combined.

From the previous measurements and an infrared measurement of ω_e,[20] three Dunham coefficients (Y_{01}, Y_{11}, Y_{02}) were obtained (calculated by Ref. 9). These values are in rough agreement with our values, except for Y_{01} of ^{37}ClF which differs by 5 MHz.

BrF

Previous microwave measurements of BrF have been made by Smith et al.[3] As in the case of ClF, only the lowest rotational transition in the 0, 1 vibrational states was measured. In the current work 56 new transitions have been measured: 20 of ^{79}BrF and 26 of ^{81}BrF. These measurements produced 28 reduced rotational frequencies covering the rotational states from $J = 3$ to $J = 13$ and the vibrational states 0, 1, 2, 3. The measured frequencies ranged from 85 to 276 GHz and the rms deviation of the fitting was 37 kHz.

Table II shows the Dunham coefficients and equilibrium constants obtained from this work. The earlier measurements gave values for Y_{01} and Y_{11} (calculated by Ref. 9). While our values of Y_{11} are in agreement, our values of Y_{01} differ by about 50 MHz for both isotopes.

BrCl

For BrCl, 63 new transitions were measured: 28 of $^{79}Br^{35}Cl$, 17 of $^{81}Br^{35}Cl$, 10 of $^{79}Br^{37}Cl$, and eight of $^{81}Br^{37}Cl$. The number of reduced rotational frequencies obtained was 33, covering rotational states from $J = 13$ to $J = 34$ and vibrational states $v = 0$ to $v = 3$. The frequencies of the measurements ranged from 122 to 309

TABLE III. Dunham coefficients and equilibrium constants of bromine monochloride.

	$^{79}Br^{35}Cl$	$^{81}Br^{35}Cl$	$^{79}Br^{37}Cl$	$^{81}Br^{37}Cl$
Y_{01} (MHz)	4570.9687(13)[a]	4536.3140(13)	4399.8516(13)	4365.1979(12)
Y_{11} (MHz)	−23.1426(29)	−22.8800(29)	−21.8553(27)	−21.5976(27)
Y_{21} (kHz)	−61.9(18)	−61.0(18)	−57.4(17)	−56.5(16)
Y_{31} (kHz)	−0.9(3)	−0.9(3)	−0.8(3)	−0.8(3)
Y_{02} (kHz)	−2.1527(7)	−2.1202(7)	−1.9945(7)	−1.9632(7)
Y_{12} (Hz)	−10.7(8)	−10.5(8)	−9.7(8)	−9.5(8)
Y_{03} (Hz)	$−4.656(3) \times 10^{-4}$	$−4.551(3) \times 10^{-4}$	$−4.152(3) \times 10^{-4}$	$−4.055(3) \times 10^{-4}$
B_e (MHz)	4571.0295(26)	4536.3793(25)	4399.9082(25)	4365.2527(25)
r_e (Å)	2.136124(5)[b]	2.136124(5)[b]	2.136124(5)[b]	2.136124(5)[b]
ω_e (cm^{-1})	444.322(62)	442.634(62)	435.926(61)	434.206(61)
$\omega_e x_e$ (cm^{-1})	1.856(20)	1.849(20)	1.787(19)	1.771(2)

[a]Uncertainties listed are one standard deviation.
[b]The uncertainty accrues from Planck's constant.

TABLE V. Dunham coefficients and equilibrium constants of iodine monobromide.

	$^{127}\mathrm{I}^{79}\mathrm{Br}$	$^{127}\mathrm{I}^{81}\mathrm{Br}$
Y_{01} (MHz)	1703.79826(30)[a]	1677.85957(30)
Y_{11} (MHz)	$-5.90413(41)$	$-5.76982(40)$
Y_{21} (kHz)	$-13.66(15)$	$-13.25(15)$
Y_{31} (kHz)	$-0.14(2)$	$-0.13(2)$
Y_{02} (Hz)	$-304.91(2)$	$-295.70(2)$
Y_{12} (Hz)	$-1.50(2)$	$-1.44(2)$
Y_{03} (Hz)	$-3.9868(11) \times 10^{-5}$	$-3.8075(11) \times 10^{-5}$
B_e (MHz)	1703.8172(6)	1677.8780(6)
r_e (Å)	2.479078(6)[b]	2.469078(6)[b]
ω_e (cm^{-1})	268.69(9)	266.64(9)
$\omega_e x_e$ (cm^{-1})	0.826(6)	0.814(6)

[a]Uncertainties listed are one standard deviation.
[b]The uncertainty accrues from Planck's constant.

GHz, and the rms deviation of the fitting was 36 kHz. The Dunham coefficients and equilibrium constants of BrCl are shown in Table III.

Smith et al.[4] did earlier work on BrCl as well as BrF. As for the previous molecule, they measured a number of quadrupole lines of the $J = 0 \rightarrow 1$ rotational transition in two vibrational states $(0, 1)$. This yielded two Dunham coefficients for each species Y_{01} and Y_{11} (calculated by Ref. 9). Except for one instance, their numbers are in good agreement with our more accurate values. Their value of Y_{01} for $^{79}\mathrm{Br}^{37}\mathrm{Cl}$ differs by 100 MHz from ours. This may be a misprint because it clearly violates the isotopic relationship of Eq. (5) although it does appear in both the original article and in the review work of Ref. 9.

ICl

Weidner,[5] Townes et al.,[6] and Herbst and Steinmetz[7] have all studied ICl. These earlier studies produced measurements of over 150 quadrupole lines in three rotational and two vibrational states. These measurements, in turn, have given very accurate values of Y_{01} and Y_{11}.[7,9] The current work on ICl has yielded five additional Dunham coefficients, as shown in Table IV. These were obtained from 50 new quadrupole lines (42 of $\mathrm{I}^{35}\mathrm{Cl}$ and eight of $\mathrm{I}^{37}\mathrm{Cl}$) of 23 new rotational frequencies. The current work covered the rotational states from $J = 12$ to $J = 44$ and vibrational states $v = 0$ to $v = 3$. The frequencies involved ranged from 85 to 300 GHz. The rms deviation of the fitting was higher for ICl (50 kHz) than for any other molecule in this study because of difficulty in resolution of the quadrupole structure.

IBr

Like ICl, IBr is a heavy diatomic with a complicated quadrupole structure at low J. Jaseta[8] has measured over 150 quadrupole lines of two rotational transitions $(J = 4 \rightarrow 5$ and $J = 5 \rightarrow 6)$ in three vibrational states $(v = 0, 1, 2)$. In this study we have measured 40 new quadrupole lines (19 of $\mathrm{I}^{79}\mathrm{Br}$ and 21 of $\mathrm{I}^{81}\mathrm{Br}$) in 30 rotational states and five vibrational states $(0, 1, 2, 3, 4)$. The rotational states covered the range from $J = 43$ to $J = 96$ and the frequencies, from 150 to 325 GHz. The transitions above $J = 53 \rightarrow 54$ revealed no quadrupole structure.

TABLE VI. Dunham potential constants of the diatomic mixed halides.

	a_0 (cm^{-1})	a_1	a_2	a_3
ClF	$2.9712(25)^{a} \times 10^5$	$-3.1171(9)$	$5.63(11)$	$-8.8(8)$
BrF	$3.1503(26) \times 10^5$	$-3.2893(10)$	$6.29(15)$	$-9.5(11)$
BrCl	$3.2369(9) \times 10^5$	$-3.4590(5)$	$6.85(8)$	$-11.2(7)$
ICl	$3.2338(16) \times 10^5$	$-3.6188(5)$	$7.60(15)$	$-13.2(1.3)$
IBr	$3.17558(26) \times 10^5$	$-3.7305(2)$	$7.70(3)$	$-12.6(3)$

[a]Uncertainties represent one standard deviation.

In Table V are listed the Dunham coefficients obtained from this work. Jaseta[8] was able to obtain values for Y_{01} and Y_{11}, but our numbers are not in agreement with his.

POTENTIAL CONSTANTS

Shown in Table VI are the Dunham potential constants as calculated from Eqs. (7) through (10). To within experimental uncertainty, these constants are isotopically invariant, a result which confirms an initial assumption of Dunham theory. It is of interest to note that the values are similar for all the molecules, generally increasing slightly with increasing mass.

ACKNOWLEDGMENTS

[1]R. L. White, Rev. Mod. Phys. 27, 276 (1955).
[2]D. A. Gilbert, A. Roberts, and P. A. Griswald, Phys. Rev. 76, 1723 (1949).
[3]D. F. Smith, M. Tidwell, and D. V. P. Williams, Phys. Rev. 77, 420 (1950).
[4]D. F. Smith, M. Tidwell, and D. V. P. Williams, Phys. Rev. 79, 1007 (1950).
[5]R. T. Weidner, Phys. Rev. 72, 1268 (1947).
[6]C. H. Townes, B. D. Wright, and F. R. Merritt, Phys. Rev. 73, 1249A (1948).
[7]E. Herbst and W. Steinmetz, J. Chem. Phys. 56, 5342 (1972).
[8]T. S. Jaseta, J. Mol. Spectrosc. 5, 445 (1960).
[9]F. J. Lovas and E. Tiemann, J. Phys. Chem. Ref. Data 3 (1974).
[10]W. C. King and W. Gordy, Phys. Rev. 90, 319 (1953); 93, 407 (1954).
[11]E. Pearson and W. Gordy, Phys. Rev. 152, 42 (1966).
[12]F. C. De Lucia, J. Mol. Spectrosc. 55, 271 (1975).
[13]The Merck Index of Chemicals and Drugs (Merck, Rahway, 1960).
[14]J. L. Dunham, Phys. Rev. 41, 721 (1932).
[15]J. H. Van Vleck, J. Chem. Phys. 4, 327 (1936).
[16]B. Rosenblum, A. H. Nethercrot, and C. H. Townes, Phys. Rev. 109, 400 (1958).
[17]A general treatment of quadrupole interactions can be found in W. Gordy and R. Cook, Microwave Molecular Spectra (Wiley, New York, 1970).
[18]H. B. G. Casimer, "On the Interaction Between Atomic Nuclei and Electrons," Texler's Tweede Genootschap, E. F. Bohn, Haarlem, 1936.
[19]R. E. Willis, Jr., "Millimeter and Submillimeter Wave Spectra of the Mixed Diatomic Halides," unpublished Ph.D. dissertation, Duke University, 1979.
[20]A. L. Wahrhaftig, J. Chem. Phys. 10, 248 (1942).

Nuclear coupling of ^{33}S and the nature of free radicals in irradiated crystals of *N*-acetyl-L-cysteine

(electron spin resonance/^{33}S hyperfine structure)

JOSEPH H. HADLEY, JR.* AND WALTER GORDY[†‡]

* Department of Physics, Georgia State University, Atlanta, Ga. 30303; and [†] Department of Physics, Duke University, Durham, North Carolina 27706

ABSTRACT   Hyperfine structure due to ^{33}S in its natural abundance of 0.76% has been measured in the electron spin resonance of free radicals produced by x-irradiation of single crystals of *N*-acetyl-L-cysteine at 77 K. These measurements proved that the radicals produced at 77 K with principal *g* values of 1.990, 2.006, and 2.214 are monosulfide radicals with the $3p$ unpaired electron density of 0.70 on the S. They are believed to be negatively charged molecules RCH_2S^-H or neutral RCH_2SH_2 radicals in which 90% of the spin density of the captured electron is concentrated in a *d-p* hybrid orbital on the S. As the temperature is raised to 300 K, these, as well as the carbon-centered radicals produced at the lower temperature, are mostly converted to neutral disulfide radicals RCH_2SS like those observed in irradiated cystine.

Free radicals with electron spin density concentrated on sulfur (sulfur-centered radicals) have now been detected with electron spin resonance (ESR) in many irradiated organic and biochemical compounds containing sulfur. Their principal *g* values are usually in the range of 2.003–2.065. However, a sulfur-centered radical with an exceptional *g* tensor having principal values ranging from 1.99 to 2.29 was observed by Akasaka (1) in single crystals of L-cysteine·HCL irradiated with 1.5 MeV at 77 K (one MeV equals 1.6×10^{-13} joule). The *g* tensor was found to have approximately axial symmetry about the larger value.   In 1965, the structure of the crystal was unknown, and it was therefore impossible to relate the observed *g* tensor to the molecular structure. In the following year, Box *et al.* (2) observed radicals with principal *g* values of $g_u = 1.985$, $g_v = 2.004$, and $g_w = 2.251$ in single crystals of cysteine·HCl irradiated with UV at 77 K. The similarity in *g* tensors supported the conclusion that these radicals were probably of the same form as those observed by Akasaka. In the meantime, the structure of the cysteine·HCl crystals was obtained from x-ray diffraction by Ayyar and Srinivasan (3). This made it possible for Box *et al.* (2) to deduce that the largest *g* value had the direction of the CS bonds of the undamaged molecule. Later, this radical was also observed by Kayushin *et al.* (4). Recently Saxebøl and Herskedal (5) have observed sulfur radicals with principal *g* values of 1.990, 2.006, and 2.214 (denoted as "R_1" radicals) in single crystals of *N*-acetyl-L-cysteine irradiated at 77 K with 4.0 MeV electrons.

To distinguish between the different types of sulfur radicals and to gain more quantitative information about them, we initiated a program for measurement of the ^{33}S hyperfine structure in irradiated single crystals of sulfur compounds (6–8). Unlike the *g* tensor, the ^{33}S coupling gives a reliable distinction between disulfide and monosulfide radicals and provides quantitative values for the spin densities on particular S atoms. Because of the difficulty of obtaining sufficient quantities of compounds with enriched ^{33}S to grow the required single

crystals, we decided to concentrate our efforts on improvement of our spectrometer sensitivity so that reliable measurement could be made on crystals with ^{33}S in its natural abundance of 0.76%. To our gratification, we found that we were able to detect the ^{33}S lines for the hyperfine components, with ample sensitivity (signal response about 25 times greater than background noise level) to make reliable measurements of the ^{33}S coupling for certain irradiated crystals. In some instances where the ^{33}S splitting is small or the spin-lattice relaxation time is unfavorable, the ^{33}S components are masked by wings of the much stronger absorption lines of the normal isotopic species. Other factors of importance to detectability of the ^{33}S lines are the degree of *g* anisotropy of the various species of radicals in the irradiated sample and the number of magnetically distinguishable orientations for each species. We have now succeeded in measuring the ^{33}S hyperfine structure of the radicals with the unusual *g* tensors in crystals of both cysteine·HCl (H_2O) and *N*-acetyl-L-cysteine. The measurements prove that both are monosulfide radicals with similar electronic structures. A description of the results for *N*-acetyl-L-cysteine is given below.

EXPERIMENTAL DETAILS

The *N*-acetyl-L-cysteine crystals were grown by slow evaporation from saturated H_2O solutions as was done by Saxebøl and Herskedal (5). They were given 200 Mrad dosages of 50 keV x-rays at 77 K and were observed with an X-band (9.3 GHz) spectrometer like that employed in our earlier work (6). One Mrad equals 10^4 J/Kg.

Samples were annealed at 300 K to destroy a carbon-centered radical (5). Because the linewidth was too great to permit observation of the R_1 sulfur-centered radical at room temperature, the ESR spectra were obtained at 77 K.

Although the detailed structure of acetyl cysteine is unknown, our preliminary x-ray diffraction shows that the crystal is triclinic with one molecule in unit cell. An orthogonal *uvw* coordinate system coinciding with the principal directions of the *g* tensor was chosen for the hyperfine measurements. Our *u* axis corresponds to the *Z* axis employed by Saxebøl and Herskedal and our *u* and *w* axes are about 28° from their *Y* and *X* axes, respectively.

THE MONOSULFIDE RADICAL

This is the sulfur radical (R_1) with the exceptional *g* tensor described above. It is produced by the irradiation at 77 K and is relatively stable to temperatures well above 77 K, having a room-temperature half-life of the order of 1 day. However, the radical decays rapidly at temperatures of 400 K and above. Our measurements confirm the unusual *g* tensor observed by Saxebøl and Herskedal. We did not improve their rather accurate values: $g_u = 1.990$, $g_v = 2.006$, and $g_w = 2.214$.

Biophysics: Hadley and Gordy

Proc. Natl. Acad. Sci. USA 74 (1977) 217

The ESR spectrum of this radical has an essentially isotropic proton hyperfine structure consisting of four lines arising from two protons with couplings of 22 G and 29 G. (One gauss equals 1×10^{-4} tesla.) This structure is superimposed on each ^{33}S hyperfine component and provides a ready identification for them. Fig. 1 shows a typical pattern observed. In the central region is the characteristic pattern for the abundant ^{32}S species, with the receiver gain reduced by a factor of $1/500$. Beyond the breaks in the curve, on either side, where the gain is 500 times greater, are components of the ^{33}S species as indicated.

The ^{33}S hyperfine splitting was found to be maximum along the axis of g_u, the minimum principal g value, and to be very nearly axially symmetric about this axis. Fig. 2 shows plots of the observed displacements of the ^{33}S components as a function of angular deviation from the axis of g_u, as far as the components could be followed.

There is a small (3 MHz) low-field shift of the center of the ^{33}S patterns from the ^{32}S spectra due to a second-order Breit-Rabi type of interaction. However, this interaction did not measurably influence the component spacings which were fitted to the first-order formula expressed in the principal axes system as

$$A = (1/g)(g_u^2 A_u^2 l_u^2 + g_v^2 A_v^2 l_v^2 + g_w^2 A_w^2 l_w^2)^{1/2} \quad [1]$$

where

$$g = (g_u^2 l_u^2 + g_v^2 l_v^2 + g_w^2 l_w^2)^{1/2} \quad [2]$$

Here the l's are the cosines of the angles the external field makes with the orthogonal uvw coordinate system. A least-squares fitting of Eq. 1 to the observed hyperfine splittings with H in the uv and uw planes yielded (see Table 1) principal values of 199 ± 1, 38 ± 3, and 32 ± 6 MHz for the ^{33}S coupling. Note that the coupling is of approximately axial symmetry about the largest element. We therefore set

$$A_{\parallel} = A_u = 199 \text{ MHz}, \quad [3]$$

$$A_{\perp} \cong (A_v + A_w)/2 = 35 \text{ MHz}. \quad [4]$$

Substitution of these values in the axially symmetric coupling formulas,

$$A_{\parallel} = A_f + 2B \quad \text{and} \quad A_{\perp} = A_f - B. \quad [5]$$

yields

$$A_f = 90 \text{ MHz} \quad \text{and} \quad B = 54.7 \text{ MHz}$$

where A_f is the isotropic component and B is the anisotropic component of the ^{33}S coupling. These results are summarized in Table 1.

We can safely assume that the anisotropic component B arises primarily from $3p$ orbital spin density on the S. Although the g tensor gives evidence for some contribution from the $3d$ orbital, the $3d$ spin density is probably not greater than 0.20, and the coupling by a $3d$ electron is an order of magnitude less than that of a $3p$ electron. With the known atomic $3p$ orbital coupling of 78 MHz, the $3p$ orbital spin density is thus found from the anisotropic coupling to be $\rho_{3p} = 54.7/78 = 0.70$. Similarly, the isotropic component with the known $3s$ orbital coupling indicates that $\rho_{3s} = 90/2700 = 0.03$ on the S. This $3s$ spin density is of the order of that expected from a $\sigma-\pi$ configuration interaction.

Although the ^{33}S coupling proves that the spin density is concentrated mostly on a single sulfur, the g tensor of the monosulfide radical observed in acetyl cysteine indicates that this radical is not of the same type as the neutral radical RCH$_2$S observed at sub-room-temperatures in irradiated cystine (6). Akasaka (1) has proposed that the approximately axial sym-
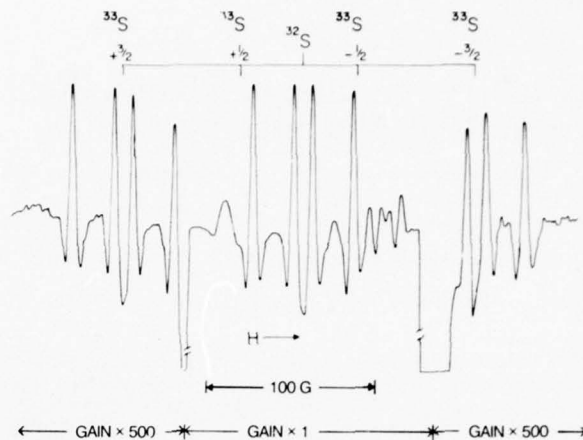

FIG 1. Second-derivative ESR spectrum for the monosulfide radical R$_1$ observed with magnetic field in the uw plane 20° from the u axis (direction of minimum g). The four-line proton pattern for the unpaired spin localized in a ^{32}S atom is shown in the center of the spectrum at reduced gain. The $-\frac{3}{2}$ and $+\frac{3}{2}$ ^{33}S components can be seen to the right and left at high gain. The $\pm\frac{1}{2}$ components are completely obscured by the stronger ^{32}S pattern and radicals stable at room temperature.

metry in g and the anomalously large $g_w = 2.29$ which he observed for irradiated cysteine·HCl(H$_2$O) at 77 K might be attributed to a radical of the type RCH$_2$S in which there is a near degeneracy of the p_x and p_y orbitals. However, this model does not account for the fact that the minimum g is less than the free spin value nor for the large deviations of the other principal g values from those of the RCH$_2$S radical in cystine·HCl. We propose that the two observed monosulfide radicals are basically distinct, that the one observed in acetyl cysteine utilizes five valence orbitals of the S whereas the one found in irradiated cystine utilizes only four. The five-orbital S radical may be a negatively charged molecule (RCH$_2$SX)$^-$ or a neutral radical RCH$_2$SX$_2$ in which the X is H in the radicals discussed here.

Probably the radical observed in L-cysteine·HCl(H$_2$O) at 77 K is the negatively charged molecule (RCH$_2$SH)$^-$ with the odd electron concentrated on the S. In N-acetyl-L-cysteine the sulfur radical is somewhat more stable than it is in cysteine and has a lower g_w (2.214 as compared with 2.29). Hydrogen bonding involving the S, as indicated in structure (I) may help to stabilize the negative charge on the S, or perhaps an internal shift of an H produces a more stable form (II),
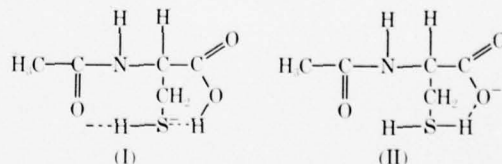
in which the negative charge is on an oxygen. The dotted lines indicate hydrogen bonds. A possible alternative is transfer of a proton from the COOH of an adjacent molecule in the crystal to the negatively charged SH group of (I) to form the neutral radical (III)
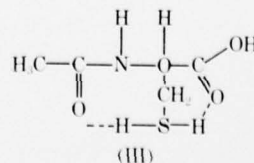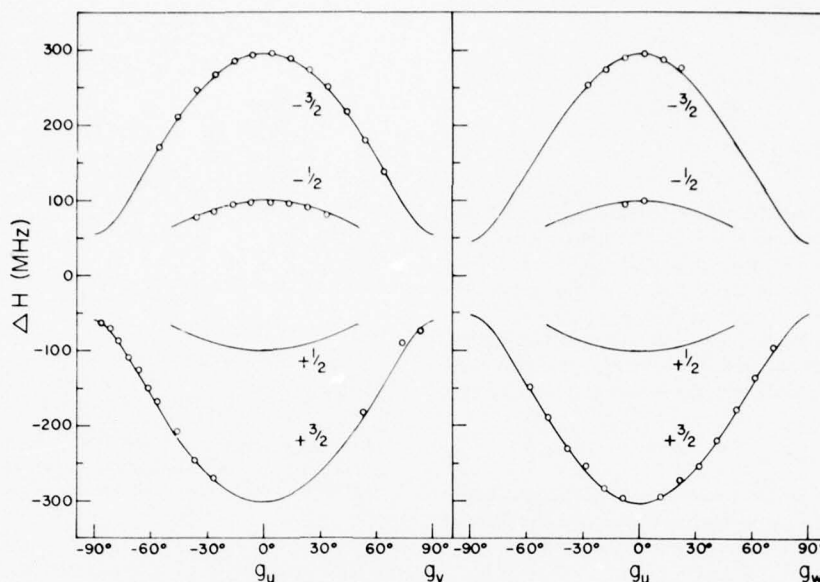
FIG. 2.   Plots of the ^{33}S hyperfine splitting for the monosulfide radical with **H** imposed in the *uv* (left) and *uw* (right) planes. The splittings, plotted in MHz because of the large g variation in the *uw* plane, are measured from the center of the ^{32}S resonance. The circles are data points; the solid lines are computer fits to the splitting between the $-\frac{3}{2}$ and $+\frac{3}{2}$ components. The ^{33}S pattern is shifted about 3 MHz (downfield) from the center of the ^{32}S pattern by second-order effects.

Without specific knowledge of the locations of the atoms in the crystal one cannot predict which form is the more probable.

Although a radical of type (I), (II), or (III) would have anisotropic SH proton hyperfine interactions, approximate calculations indicate that these would not cause resolvable splitting and that the resulting spread would fall within the observed line widths. Furthermore, Saxebøl and Herskedal proved with deuterated crystals that the observed four-line spectrum was associated with the CH$_2$ protons rather than exchangeable hydrogens.

The important characteristic of the forms (I), (II), or (III) is the utilization of five orbitals of the S. It appears that an electron captured by RSH goes into a *p-d* hybridized orbital of the S, whereas one captured by RSSR goes into an antibonding σ^* orbital formed by a linear combination of p orbitals of the two sulfurs (7). Evidently a similar configuration utilizing an antibonding orbital of the CS or SH bond of cysteine has higher energy than one utilizing a fifth atomic orbital on the S formed by a hybridization of $3d$ and $3p$ orbitals. Thus, the "three-electron bond" does not appear to be involved in the formation of three bonds to the sulfur, but rather the $3d$ shell is employed to expand the number of bonding orbitals of the S to accommodate the additional bond.

The many unknown parameters prevent determination of the specific amounts or kinds of d-orbital hybridization that

Table 1. ^{33}S couplings and S spin densities of the monosulfide radical R1

Radical R1	^{33}S coupling (MHz)		S spin density*
RCH$_2$S$^-$H	$A_u = 199 \pm 3$		
		$A_f = 90$	$\rho_{3s} = 0.03$
or	$A_v = 38 \pm 3$		
		$B = 55$	$\rho_{3p} = 0.70$
RCH$_2$SH$_2$	$A_w = 32 \pm 6$		

* A $3d$ spin density of 0.20 is also predicted (see *text*).

occur in the (RCH$_2$SH$^-$) or RCH$_2$SH$_2$ radical, but normalization of the unpaired electron density with the $3p$ spin density of 70% and the 10% positive spin density on CH$_2$ revealed by the proton coupling indicates that the $3d$ character of the unpaired electron orbital is approximately 20%. This amount is adequate to account for the observed reduction of g_u below the free-spin value and for the other unexplained features of the g tensor. The $3s$ spin density of 3% on the S is omitted from the normalization because it is likely due to spin polarization of the σ bonds and is hence counterbalanced by an equal and opposite spin density of these bonds.

The principal g values may be predicted from the second-order formula

$$g_j = g_f - 2\lambda \sum_n \frac{|(\phi_n | L_j | \phi_0)|^2}{E_n - E_0}. \qquad [6]$$

where ϕ_n includes all orbitals which are not orthogonal to $\phi_0' = L_j | \phi_0)$, i.e., for which $(\phi_n | \phi_0') \neq 0$. Thus, in this problem ϕ_n must include the $3d$ orbitals on the S.

The ground molecular orbital of the unpaired electron may be expressed as

$$\phi_0 = \rho_S^{1/2}(\psi_S^0 + \sum_n a_i \psi_i), \qquad [7]$$

where ρ_S is the unpaired electron density on the S and $\Sigma a_i{}^2 = 1 - \rho_S$ is that on the other atoms. Because the interactions on the other atoms i do not contribute significantly to the anisotropy in g, they can be neglected in the evaluation of the last term of Eq. **6**. As an approximation based on the observed spin density and S model described above, we express

$$\psi_S^0 = (4/5)^{1/2}(3p_x) + (1/5)^{1/2}(3d_{xy}). \qquad [8]$$

Contributions of the $3p$ and $3d$ components of the hybrid can be calculated separately. Because $L_x | 3p_x) = 0$ and $L_x | 3d_{xy}) = i(3d_{xz})$, with ψ_i neglected, we can set

$$L_x | \phi_0) = \rho_S^{1/2}(L_x | \psi_S^0) = i\rho_S^{1/2}(1/5)^{1/2}(3d_{xz}). \qquad [9]$$

and from Eq. **6** can obtain

$$g_u = g_x = g_f - \frac{2\lambda_d \rho_S}{5} \sum_n \frac{|(\phi_n|3d_{xz})|^2}{E_n - E_1}$$

$$= g_f - \frac{2\lambda_d \rho_S}{5} \left(\frac{1}{E_d - E_0}\right). \qquad [10]$$

The last form follows from the normalization $(d_{xz}|d_{xz}) = 1$ and from the orthogonality of all other combinations. Because the d shell is less than half-filled, the d spin-orbit coupling λ_d is here positive in sign. Thus, the contribution of the d character reduces g_u below the free-spin value of 2.0023, in agreement with observation. We do not know the specific value of the spin-orbit coupling constant for the $3d$ orbital of S nor $E_d - E_0$. However, with Eq. **10** we can evaluate experimentally the ratio $\lambda_d/(E_d - E_0)$ from

$$g_u - g_f = -2\lambda_d \rho_S/[5(E_d - E_0)] = -0.0123 \qquad [11]$$

Although the bonding orbitals may have some s hybridization and perhaps also some d character, we suggest as a simplifying approximation that the other occupied orbitals of the S are:

$$\phi_1 = (1/2)^{1/2}[(1/2)^{1/2}(3p_x) + (1/10)^{1/2}(3p_y)$$
$$+ (2/5)^{1/2} (3d_{xz}) + \psi_{H_1}]. \qquad [12]$$

$$\phi_2 = (1/2)^{1/2}[-(1/2)^{1/2}(3p_x) - (1/10)^{1/2}(3p_y)$$
$$+ (2/5)^{1/2} (3d_{xz}) + \psi_{H_1}]. \qquad [13]$$

$$\phi_3 = (1/2)^{1/2}[(3p_z) + \psi_C]. \qquad [14]$$

$$\phi_4 = (3s). \qquad [15]$$

All these orbitals are assumed to have electron pairs. Orbitals ϕ_1 and ϕ_2 would bond the two H atoms of structure (II) or (III) while ϕ_3 would form the σ bond to the C and ϕ_4 would have an unshared pair.

Eq. **6** with the orbitals of Eqs. **7**, and **12–15** gives:

$$g_v = g_x = g_f - \left(\frac{8}{5}\right)\left(\frac{\lambda_p \rho_S}{E_3 - E_0}\right) - \left(\frac{2}{5}\right)\left(\frac{\lambda_d \rho_S}{E_d - E_0}\right). \qquad [16]$$

$$g_u = g_z = g_f - \left(\frac{4}{5}\right)\left(\frac{\lambda_p \rho_S}{E_1 - E_0}\right)$$
$$- \left(\frac{4}{5}\right)\frac{\lambda_p \rho_S}{E_2 - E_0} - \left(\frac{2}{5}\right)\left(\frac{\lambda_d \rho_S}{E_d - E_0}\right). \qquad [17]$$

when it is assumed that, on the average, one electron of each bonding pair is on the S. With the term in λ_d given by Eq. **11**, with $\rho_S = \rho_{3p} + \rho_{3d} = 0.70 + 0.20$, $g_f = 2.0023$, $E_1 = E_2$, and $\lambda_p = -382$ cm^{-1}, these expressions reduce to:

$$g_v = 1.990 + 550/(E_3 - E_0). \qquad [18]$$

$$g_u = 1.990 + 550/(E_1 - E_0). \qquad [19]$$

With the measured values $g_v = 2.006$, $g_u = 2.214$, these equations give $E_3 - E_0 = 34,000$ cm^{-1} and $E_1 - E_0 = 2400$ cm$^{-1} = E_2 - E_0$. In addition to the other approximations, it is assumed that the spin density of 0.10 on the CH$_2$ group contributes nothing to the g anisotropy. Despite the small energy difference between E_1 or E_2, and E_0, the Boltzmann factor $\exp(-\Delta E/kT)$ is 0.00034 at 300 K, and the calculated spin density in orbital ϕ_1 or ϕ_2 is only 0.0003, not enough to give an observable SH proton splitting, nor a measurable deviation in the axial symmetry of the ^{33}S coupling.

In structure (I), the negative charge is on the S, and there are two electrons in the S orbital forming the S- - -H——O bridge.
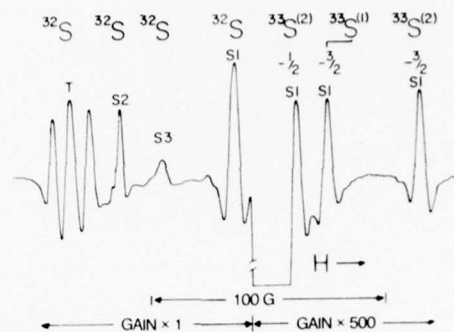

FIG. 3. ESR spectrum of stable disulfide radicals observed at room temperature. In the left-hand part of the spectrum are shown the ^{33}S patterns observed with low amplification. The crystal is oriented with the magnetic field in the direction of the minimum g-value for the S1 radical. A portion of the ^{33}S spectrum for S1 is shown at high gain in the right-hand portion of the spectrum. The spectrum reveals unequal coupling to two sulfur atoms, S$^{(1)}$ and S$^{(2)}$, within the radical.

If the same orbitals are assumed with ϕ_1 forming the SH bond and ϕ_2 having an unshared pair, and if the approximation $E_1 \approx E_2$ is made, then a similar calculation gives g_v the same as before but $g_u = 1.990 + 820/(E_1 - E_0)$. The observed g_u then indicates that $E_1 - E_0 = 3600$ cm^{-1}.

To eliminate unknown parameters in these solutions, we were forced to make rather severe simplifying assumptions. Whatever the nature of hybridization of the orbitals, $E_1 - E_0$ and $E_2 - E_0$ must be small and $E_3 - E_0$ must be large to account for the observed g_v and g_u values. Similar conditions are required for the model proposed by Akasaka (1), who assumed $E_{px} \approx E_{py} \ll E_{pz}$.

In the earlier work (6), we found that the isotropic CH$_2$ proton coupling A in the neutral RCH$_2$S and RCH$_2$SS radicals could be calculated with the relation

$$A = A_0 \rho_S \cos^2 \phi \qquad [20]$$

with $A_0 = 31.5$ G. If one assumes the same HCH angle, 125°, for the present radical as for RCH$_2$S and a $\rho_S = 0.90$, the combined $3p$ and $3d$ density, Eq. **20**, requires a somewhat higher value, $A_0 = 36.6$ G, to account for the observed proton couplings of 22.1 G and 29.4 G. Perhaps this signifies a more effective hyperconjugation by the p-d hybrid orbital, but this conclusion
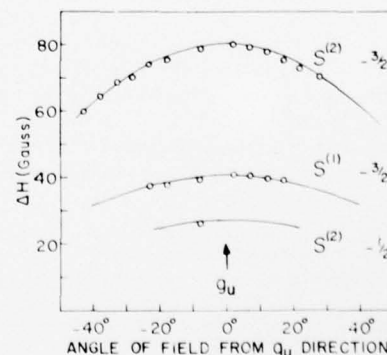

FIG. 4. Plot of the ^{33}S hyperfine splitting versus angle of the external field from the direction of the minimum principal g value for the disulfide radical S1. Circles represent measured splittings from the ^{33}S resonance; the curves are computer fits to the $-\frac{3}{2}$ components for each of the two sulfur sites. The splitting is axially symmetric about the g_u direction.

Table 2. ^{33}S couplings and S spin densities
of the disulfide radical S1

Radical S1		^{33}S coupling (MHz)		S spin density	
		A_f	B	$3s$	$3p$
RCH$_2$S$^{(1)}$S$^{(2)}$	S$^{(1)}$	29.7	23.0	0.011	0.29
	S$^{(2)}$	59.6	44.8	0.022	0.57

is uncertain. Whatever the cause, the CH$_2$ couplings are significantly larger for the current radical than for the RCH$_2$S and RCH$_2$SS radicals.

THE DISULFIDE RADICALS

Fig. 3 shows the ESR spectrum for one orientation of an acetyl cysteine crystal which has been aged for 1 month after irradiation. In the low-gain region there are four distinct signals of sulfur-centered radicals of the normal isotopic species: a triplet indicated by T1 and three singlets indicated by S1, S2, and S3. The principal g values for T1 are 2.003, 2.024, 2.053; for S1, 2.002, 2.025, 2.064; for S2, 2.002, 2.025, 2.054; for S3, 2.003, 2.026, 2.054. They fall into the two sets of g values earlier observed for disulfide radicals (6–9), differing significantly only in the maximum value which is either close to 2.054 or to 2.064. For this reason, all four signals are presumed to arise from disulfide radicals although this structure could be verified by ^{33}S hyperfine structure only for the S1 signal.

The crystal orientation for Fig. 3 is such that the applied magnetic field is along the direction of g_u, the minimum g value for the S1 signal. The signals to the right, observed under high gain, are ^{33}S hyperfine components corresponding to the S1 species. We were able to observe these ^{33}S components over a sufficient range of crystal orientations (see Fig. 4) to obtain the principal values of the coupling as given in Table 2. The two different coupling values for ^{33}S prove the disulfide structure of the radicals as explained in the first paper of this series (6). The spin densities on the two sulfurs obtained from the coupling values are also listed in Table 2.

1. Akasaka, K. (1965) *J. Chem. Phys.* **43**, 1182–1184.
2. Box, H. C., Freund, H. G. & Budzinski, E. E. (1966) *J. Chem. Phys.* **45**, 809–811.
3. Ayyar, R. R. & Srinivasan, R. (1965) *Curr. Sci.* **34**, 449–450.
4. Kayushin, L. P., Krivenko, V. G. & Pulatova, M. K. (1972) *Stud. Biophys.* **33**, no. 1, 59–66.
5. Saxebøl, G. & Herskedal, Ø. (1975) *Radiat. Res.* **62**, 395–405.
6. Hadley, J. H., Jr. & Gordy, W. (1974) *Proc. Natl. Acad. Sci. USA* **71**, 3106–3110.
7. Hadley, J. H., Jr. & Gordy, W. (1974) *Proc. Natl. Acad. Sci. USA* **71**, 4409–4412.
8. Hadley, J. H., Jr. & Gordy, W. (1975) *Proc. Natl. Acad. Sci. USA* **72**, 3486–3490.
9. Hadley, J. H., Jr. (1976) *Bull. Am. Phys. Soc.* **21**, 382.

Electron spin resonance of ^{17}O-labeled protein–peroxide radicals: Zein and edestin

(oxygenated free radicals/electron spin resonance spectra/^{17}O hyperfine structure)

LOUIS J. DIMMEY* AND WALTER GORDY

Department of Physics, Duke University, Durham, North Carolina 27706

ABSTRACT   Hyperfine structure due to ^{17}O has been measured in irradiated zein and edestin after exposure to gaseous oxygen with ^{17}O concentrated to 24%. The observations prove that the free radicals produced by ionizing irradiation under vacuum at 300 K are converted by the oxygen to protein–peroxide free radicals $X—O^{(1)}—O^{(2)}$, with the unpaired electron density in a π-type orbital predominantly on the peroxide group. From the observed couplings, the $2p_\pi$ spin densities on zein–peroxide are found to be 0.29 and 0.45 for $O^{(1)}$ and $O^{(2)}$, respectively; those on edestin–peroxide are 0.26 and 0.48 for $O^{(1)}$ and $O^{(2)}$, respectively.

In the first observations of electron spin resonance (ESR) signals in irradiated proteins (1), a proton hyperfine doublet produced from bone collagen was found to be converted to a singlet when the specimen irradiated in vacuum was exposed to oxygen. It was postulated that that O_2 combined with the free radicals in the irradiated sample to produce a protein–peroxide free radical. Since this initial finding, many examples of this oxygen effect have been observed for other proteins (2) as well as for biochemicals of other types (3). In certain proteins such as zein and edestin, chosen for the present ^{17}O study, the conversion of the proton multiplet to the oxygen singlet is rapid, with complete conversion to the singlet occurring within minutes after exposure of the sample to atmospheric oxygen. In others, most notably silk, the oxygen effect is slow, requiring days of exposure for partial conversion. This slower conversion is believed to result from steric factors that hinder or prevent the molecules of oxygen from reaching the free-radical centers in fibrous proteins such as silk. The oxygen effect is not observed for sulfur-centered radicals produced by irradiation of proteins, probably because molecular oxygen does not combine with the sulfide free radicals.

The earlier studies of the oxygen effect in irradiated proteins were made with ^{16}O, which has no hyperfine structure. Although there seems to be little doubt that the radicals formed upon admission of oxygen are peroxide radicals, the present study of ^{17}O-labeled radicals unquestionably confirms this interpretation and, in addition, provides new information about the electronic structure of the protein–peroxide radicals.

In many irradiated proteins, including edestin and zein, the free-radical site giving the ESR pattern in the absence of oxygen is believed to be the $C_\alpha—R$ group in structure **I**
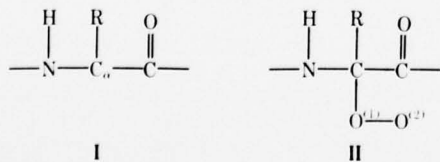
formed by loss of a H from a carbon of the polypeptide chain. For edestin under vacuum, a proton doublet like that for the

$C_\alpha H$ fragment in irradiated polyglycine is formed (2), which indicates that R = H and that the radical is formed in the glycine unit. A similar doublet is observed for evacuated zein, but with a superimposed quartet like that for polyalanine (2). This indicates formation of radical sites in both glycine and alanine (R = CH$_3$) units of zein. Relative intensities of the superimposed patterns indicate that formation in the alanine unit is somewhat less than that in the glycine unit. Both patterns are converted to singlets when normal oxygen (^{16}O$_2$) is admitted to the irradiated sample.

Upon exposure of the irradiated samples to oxygen, peroxide radical **II** is evidently formed. When this occurs, as the present study confirms, the spin density of **I** is effectively transferred to the captured O_2, where its interaction with the protons of the R group is insufficient to produce a resolvable proton splitting. Although ^{16}O has no hyperfine structure, the substituted ^{17}O has nuclear spin $I = 5/2$, which gives rise to a sextet ESR splitting by each of the inequivalent oxygens in peroxide radical **II**.

Previously, ^{17}O hyperfine structure has been observed for randomly oriented peroxide radicals of irradiated polytetrafluoroethylene (4) and for oriented peroxide radicals $C_{10}H_{11}OO$ in single crystals (5). Also, the isotropic component of the ^{17}O hyperfine structure has been observed for some simpler peroxide free radicals in liquid solutions (6, 7). These earlier observations have been helpful to us in our analysis of the ^{17}O hyperfine structure for the protein–peroxide radicals.

EXPERIMENTAL PROCEDURES

A balanced-bridge, X-band ESR spectrometer operated at a frequency of 9000 MHz was used for these measurements. Evacuated tubes made of Spectrosil quartz held the protein powders, which were placed in a ^{60}Co γ-ray source for irradiation at 300 K. Doses were approximately 3×10^5 rads (300 grays). Afterward, the tubes were annealed in a gas/oxygen flame to eliminate any free radicals formed in the quartz.

Exposure of the irradiated samples to normal gaseous oxygen or to ^{17}O concentrated gas was accomplished in this way. The tube was connected to a flask of the oxygen gas, the glassware between them was evacuated, and the flask was immersed in liquid nitrogen. When the valve on the flask was opened, the oxygen at its vapor pressure at 77 K (about 130 torr) flowed into the sample tube. After the sample was disconnected from the flask, it was ready for observation in the spectrometer. Conversion of the radicals formed under vacuum to peroxides required 2–4 hr. The enriched oxygen gas contained 24% ^{17}O atoms.

Abbreviation: ESR, electron spin resonance.
* Present address: School of Engineering, Duke University, Durham, NC 27706.

OBSERVED SPECTRA

Fig. 1 shows a comparison of the second-derivative spectra of irradiated zein after exposure to normal oxygen gas and after similar exposure to gas with 24% substitution of ^{17}O atoms for ^{16}O atoms. The spectrometer amplification for the two curves was approximately the same. The stick diagrams at the base correspond to the theoretically expected ^{17}O hyperfine patterns of the two forms, X—^{16}O—^{17}O and X—^{17}O—^{16}O. Hyperfine components for the less-probable species, X—^{17}O—^{17}O, proved to be too weak for detection. The pattern with the wider span is that for X—^{16}O—^{17}O. Fig. 2 shows the curve obtained for irradiated edestin after exposure to the ^{17}O-substituted gas.

The nature of the ESR signals and of the free radicals formed upon irradiation in the absence of oxygen are described in the Introduction. For both proteins, the primary radicals are believed to have the general structure **I** and the peroxide radicals (secondary) to have structure **II**. The hyperfine structure and g values for these protein–peroxide radicals are explained in the following paragraphs.

HYPERFINE STRUCTURE

The analysis of ESR hyperfine structure for randomly oriented free radicals is now well known (ref. 8, pp. 353–441). The shapes of the observed absorption curves depend on several factors, the most important of which are the anisotropy in the **g** tensor and in the nuclear coupling tensors. In the protein–peroxide
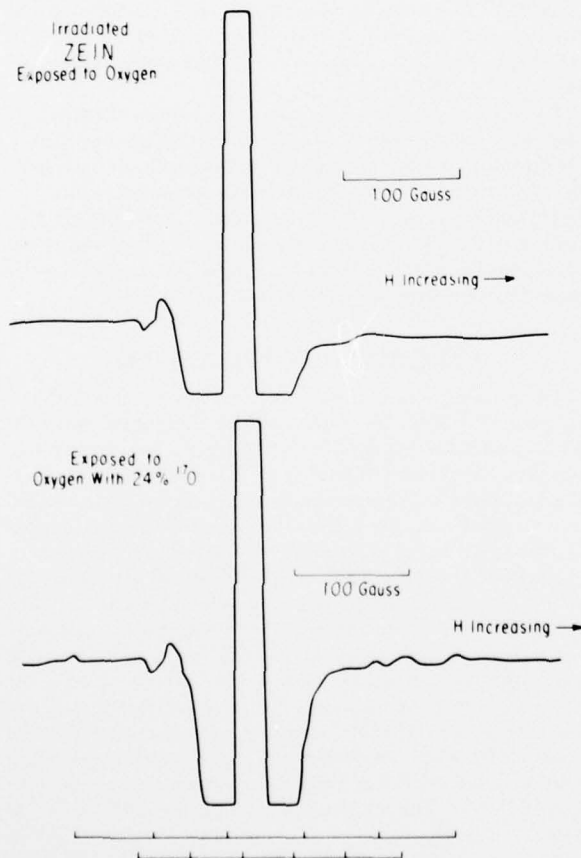

FIG. 2.   Second-derivative ESR spectrum of γ-irradiated edestin after exposure to oxygen gas enriched with 24% ^{17}O.

FIG. 1.   Second-derivative ESR spectrum of γ-irradiated zein after exposure to gaseous $^{16}O_2$ (*Upper*) and after exposure to oxygen gas enriched with 24% ^{17}O (*Lower*).
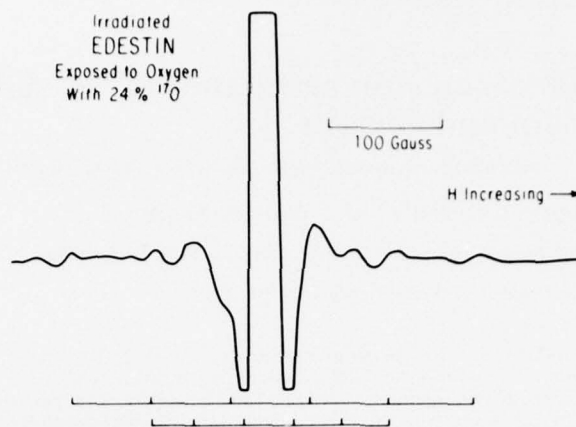
radicals considered here, the isotropic component A_f of the ^{17}O coupling is of comparable magnitude to the anisotropic coupling B and is of like sign. Consequently, the resultant coupling $(A_f - B)$ for the magnetic field of orientations perpendicular to the p_π orbital of the unpaired electron is very small. As a result, the critical absorptions corresponding to the perpendicular-field orientation are not resolvable and are not separable from the strong ^{16}O singlet absorption. To obtain a value for B, one must observe the much weaker critical absorptions corresponding to orientation of the field approximately parallel to the coupling p_π orbital of the ^{17}O atoms.

The nature of the ^{17}O hyperfine spectra is illustrated by the idealized curves of Fig. 3, in which line-broadening factors are neglected except those of the anisotropy in the nuclear coupling and in **g**. Also, for simplification of the diagram, **g** as well as **A** is assumed to be axially symmetric about the directions of the coupling p_π orbital. The weak peaks in the observed derivative curves (Figs. 1 and 2) correspond to the outer terminations of the different ^{17}O component absorptions. If the coupling constant is expressed in magnetic-field units, these outer peaks occur at the critical field values,

$$H_\parallel = h\nu_0/(g_\parallel\beta) + A_\parallel M_I, \qquad [1]$$

where ν_0 is the operating frequency and $g_\parallel = g_u$ is the effective g value for **H** along the coupling p_π orbital, and

$$A_\parallel = A_f + 2B, \qquad [2]$$

where $A_\parallel$ is the effective coupling constant for **H** along the coupling p_π orbital. The much stronger unresolvable inside-component terminations occur at

$$H_\perp = h\nu_0/(g_\perp\beta) + A_\perp M_I, \qquad [3]$$

where $g_\perp$ is the effective g value for **H** imposed in the plane perpendicular to the p_π orbital, and

$$A_\perp = A_f - B. \qquad [4]$$

Although $g_\parallel$ has a fixed value, $g_\perp$ ranges in value from g_e to g_u. However, for simplicity in Fig. 3, g_e was chosen as the particular value for $g_\perp$. The quantum numbers are $M_I = \pm5/2$, $\pm3/2$, $\pm1/2$, corresponding to the spin $I = 5/2$ for ^{17}O. The coupling constants have the same sign and are both negative because the nuclear magnetic moment of ^{17}O is negative.

The fact that the $H_\perp$ components cannot be resolved or separated from the unsubstituted ^{16}O absorption indicates that $A_f \approx B$. With $A_f = B$, the observed component separation of

Biophysics: Dimmey and Gordy
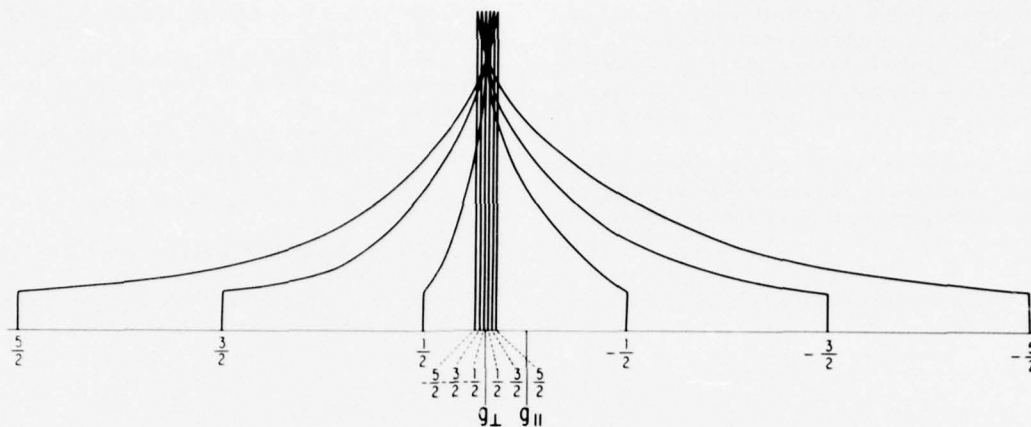
Proc. Natl. Acad. Sci. USA 77 (1980)   345

FIG. 3. Idealized theoretical pattern of ESR hyperfine structure for a coupling ^{17}O of randomly oriented peroxide radicals having axial symmetry in coupling with $A_\perp = A_f - B = 2.5$ G and with $A_\| = -71$ G, as for $^{17}O^{(2)}$ of edestin peroxide. For simplicity, the **g** tensor is also assumed to have axial symmetry about the coupling $2p$ orbital with $g_\| = g_u$ and $g_\perp = g_v$ for edestin. Line-broadening factors other than anisotropies in **g** and **A** are neglected.

71 G for $^{17}O^{(2)}$ in edestin-peroxide gives with Eq. **2** the value $A_f = B = 23.7$ G for the terminal oxygen; and the observed component separation of 42 G for $^{17}O^{(1)}$ gives $A_f = B = 14$ G for the central oxygen. However, we believe that more accurate values for B are obtained with the assumption that $A_f(^{17}O^{(1)}) = 16$ G and $A_f(^{17}O^{(2)}) = 22$ G, as measured for the radicals $(CH_3)_2$ COO and $C_6H_5(CH_3)_2COO$ in liquid solution (7). These values are close to the isotropic coupling observed in diverse peroxide radicals (5–7) in which the O_2 is bonded to a carbon. With these values assumed for A_f in both zein and edestin, the anisotropic coupling constants calculated with Eq. **2** are as listed in Table 1. The couplings $A_\|$ in MHz are related to the component separations in gauss by

$$A_\|(MHz) = 1.40 g_\| \Delta H(G). \qquad [5]$$

PRINCIPAL g VALUES

The principal g values of these protein–peroxide radicals cannot be accurately derived from the randomly oriented radicals, but approximated values have been deduced by the following procedure. The weak peak to the left of the strong central absorption in the unsubstituted ^{16}O peroxides, shown for zein in Fig. 1 *Upper*, evidently corresponds to the maximum g value, g_w. The value determined by this peak is $g_w = 2.044$ for the zein peroxide. The value similarly obtained for the edestin is 2.040. These values are in the range of those derived for the peroxide radical in single-crystal measurements (ref. 8, p. 602). For example, in the $C_{10}H_{11}OO$ radical, $g_w = 2.045$ and 2.039

for the two crystal sites (5). The g_u values are expected from theory to be directed approximately along the O—O bond axis. Peaks corresponding to the intermediate and minimum g values, g_v and g_u, respectively, cannot be separated for the unsubstituted ^{16}O radicals; both of them are evidently within the strong central absorption with the center corresponding to 2.007 for zein and to 2.006 for edestin. However, the minimum value g_u is expected from theory to have the direction of the p_π orbital, that for which the ^{17}O hyperfine components are measured. Thus, if slight second-order shifts are neglected, the g_u value corresponds to the center of the $A_\| M_I$ hyperfine pattern like that shown in Fig. 3. We have assumed that the intermediate values g_v correspond to those for the strong central absorption for the unsubstituted ^{16}O radicals. The unresolved $A_\perp M_I$ pattern is depicted as a closely spaced multiplet centered near g_v in Fig. 3. This multiplet evidently falls under the strong central $^{16}O_2$ absorption. For orientations of the magnetic field along or near g_w, the ^{17}O components are too weak for observation. The approximate g values derived by these procedures and assumptions are listed in Table 2. They are close to the values 2.0026, 2.0065, and 2.038 derived by Che and Tench (4) for the chain radicals —CF_2—$CF(OO)$—CF_2— at 77 K.

CONCLUSIONS

The combined spin densities on $O^{(1)}$ and $O^{(2)}$ derived for edestin and for zein, 0.74, are not unity, as would be expected for an unpaired electron entirely in a π orbital on the two oxygens for which orbital-overlap distortions are neglected. This discrepancy might be interpreted to indicate some spreading of the π orbital of the unpaired electron to the carbon or to another atom of the protein. Also, some reduction in the effective B values and derived p_π spin densities is expected to result from rather large torsional oscillations of the peroxide group about the C—O bond. Such oscillations would reduce the observed maximum coupling below that expected for a static, parallel alignment of the p orbital as was assumed in the derivations. If the entire reduction is attributed to these oscillations and the $2p_\pi$ spin

Table 1. ^{17}O coupling constants for protein peroxides, X—$O^{(1)}$—$O^{(2)}$

Parent protein	Coupling atom	Component separations $\Delta H_\|$(G)	Effective couplings,* MHz $A_f^\ddagger$	B	Spin densities[†] ρ_{2s}	ρ_{2p}
Zein	$^{17}O^{(1)}$	46 ± 2	(−)45	(−)42	0.010	0.29
	$^{17}O^{(2)}$	68 ± 2	(−)62	(−)65	0.013	0.45
Edestin	$^{17}O^{(1)}$	42 ± 2	(−)45	(−)37	0.010	0.26
	$^{17}O^{(2)}$	71 ± 2	(−)62	(−)69	0.013	0.48

* Signs are not measured but are theoretically negative.
[†] Calculated with atomic coupling values $A_{2s} = -4628$ MHz and $B_{2p} = -144$ MHz (ref. 8, pp. 337, 338).
[‡] Values assumed from measurements of liquids (see text).

Table 2. Approximate g values of protein–peroxide radicals

Parent protein	g_u	g_v	g_w
Zein	2.001	2.007	2.044
Edestin	2.002	2.006	2.040

density on the two oxygens is normalized to unity, the indicated $2p_\pi$ spin densities are 0.39 and 0.61 for $O^{(1)}$ and $O^{(2)}$ of zein peroxide and 0.35 and 0.65 for $O^{(1)}$ and $O^{(2)}$ of edestin peroxide. The small $2s$ spin densities are attributed entirely to spin-polarization effects and do not influence the calculations of ρ_{2p}.

These measurements of ^{17}O hyperfine structure verify that the ESR signals produced by exposure of these irradiated proteins to molecular oxygen are due to peroxide radicals, as earlier postulated.

1. Gordy, W., Ard, W. B. & Shields, H. (1955) *Proc. Natl. Acad. Sci. USA* **41**, 983–996.
2. Patten, R. A. & Gordy, W. (1964) *Radiat. Res.* **22**, 29–44.
3. Rexroad, H. N. & Gordy, W. (1959) *Proc. Natl. Acad. Sci. USA* **45**, 256–269.
4. Che, M. & Tench, A. J. (1976) *J. Chem. Phys.* **64**, 2370–2374.
5. Melamud, E., Schlick, S. & Silver, B. L. (1974) *J. Magn. Reson.* **14**, 104–111.
6. Fessenden, R. W. & Schuler, R. H. (1966) *J. Chem. Phys.* **44**, 434–437.
7. Adamic, K., Ingold, K. U. & Morton, J. R. (1970) *J. Am. Chem. Soc.* **92**, 922–923.
8. Gordy, W. (1979) *Theory and Applications of Electron Spin Resonance* (Wiley-Interscience, New York).

DATE
ILMED
—8